People's Democratic Republic of Algeria
Ministry of Higher Education and Scientific Research

National Polytechnic School
Department of Electronic
Laboratory of Communication Devices
and Photovoltaic Conversion

PhD Thesis in Electronic

Presented by:

Zine Elabadine DAHMANE

Entitled:

Contribution to the modeling of Li-ion batteries

Members of jury:

M. S. AIT-CHEIKH	Professor, ENP	President
A. MALEK	Researches Director, CDER	Supervisor
M. HADDADI	Professor, ENP	Co-director
C. LARBES	Professor, ENP	Examiner
A. TALHA	Professor, USTHB	Examiner
A. HADJ ARAB	Researches Director, CDER	Examiner

ENP 2019

Laboratoire de Dispositifs de communication et de Conversion Photovoltaïque (LDCCP),
10 Avenue Hassen BADI, El-Harrach 16200
Alger Algérie

People's Democratic Republic of Algeria
Ministry of Higher Education and Scientific Research

National Polytechnic School
Department of Electronic
Laboratory of Communication Devices
and Photovoltaic Conversion

PhD Thesis in Electronic

Presented by:

Zine Elabadine DAHMANE

Entitled:

Contribution to the modeling of Li-ion batteries

Members of jury:

M. S. AIT-CHEIKH	Professor, ENP	President
A. MALEK	Researches Director, CDER	Supervisor
M. HADDADI	Professor, ENP	Co-director
C. LARBES	Professor, ENP	Examiner
A. TALHA	Professor, USTHB	Examiner
A. HADJ ARAB	Researches Director, CDER	Examiner

ENP 2019

Laboratoire de Dispositifs de communication et de Conversion Photovoltaïque (LDCCP),
10 Avenue Hassen BADI, El-Harrach 16200
Alger Algérie

République Algérienne Démocratique et Populaire
Ministère de l'Enseignement Supérieur et de la Recherche Scientifique

Ecole Nationale Polytechnique
Département d'Electronique
Laboratoire des Dispositifs de Communication
et de Conversion Photovoltaïque

Thèse de Doctorat En Electronique

Option: **Electricité Solaire**

Présentée par :

Zine Elabadine DAHMANE

Intitulée

Contribution à la modélisation des batteries Li-ion

Membres du jury :

M. S. AIT-CHEIKH	Professeur à l'ENP	Président
A. MALEK	Directeur de Recherche au CDER	Directeur de thèse
M. HADDADI	Professeur à l'ENP	Co-directeur de thèse
C. LARBES	Professeur à l'ENP	Examinateur
A. TALHA	Professeur à l'USTHB	Examinateur
A. HADJ ARAB	Directeur de Recherche au CDER	Examinateur

ENP 2019

Laboratoire de Dispositifs de communication et de Conversion Photovoltaïque (LDCCP),
10 Avenue Hassen BADI, El-Harrach 16200
Alger Algérie

ACKNOWLEDGEMENT

This thesis has been conducted at the Laboratory of Communication Devices and Photovoltaic Conversion in the Department of Electronic of Ecole Nationale Polytechnique (ENP) of Algiers.

Firstly, I would like to express my sincere gratitude to my Professors **Ali Malek, Mourad Haddadi**, and **M. S. Ait Cheikh** for the continuous support of my Ph.D study and related research, for their patience, motivation, and immense knowledge. Their guidance helped me in all the time of research and writing of this thesis. I could not have imagined having a better advisors and mentors for my Ph.D study.

Besides my advisors, I would like to thank the rest of my thesis committee: Prof. **Cherif Larbes**, Prof. **A. Talha**, and Dr. **A. hadj Arab**, for their insightful comments and their constructive analysis of the present work.

My sincere thanks also goes to Dr. **Vincent lotentz**, Head of departement at Fraunhofer Institute for Integrated Systems and Device Technology IISB, and Dr. **Erik Schaltz**, Associate Professor at Aalborg University, who provided me an opportunity to join their team as intern, and who gave access to the laboratory and research facilities. Without they precious support it would not be possible to conduct this research.

I thank my fellow labmates in for the stimulating discussions, for the sleepless nights we were working together before deadlines, and for all the fun we have had in the last five years.

Last but not the least, I would like to thank my family: my parents and to my brothers and sisters for supporting me spiritually throughout writing this thesis and my life in general.

ملخص:
يعتبر نموذج البطارية الذي يتنبأ بالأداء الكهربائي بدقة عالية أمرًا حيويًا لتصميم الدوائر للتحكم في استخدام البطارية وتحسين وقت التشغيل والسلامة في الأنظمة الكهربائية مثل السيارة الكهربائية (EV). في هذه الورقة ، تم تطوير نموذج بسيط قائم على أساس الدوائر المكافئة لنمذجة أداء بطاريات الليثيوم أيون المستخدمة في تطبيقات السيارات. تعتمد إستراتيجية النموذج المعتمدة لتوصيف المعلمات الداخلية على تقنيتين رئيسيتين: الأول هو اختبارات التحليل الكهربائي الكهروكيميائي (EIS) ، حيث يتم إعداد دارة مماثلة وفقًا لتصورات اختبار EIS والآخر هو تقنية نبضات التيار ، وهذا الأخير يتم باستخدام ملف تعريف نبضات تيار مقترح. تتم جدولة المعلمات المستخرجة على حالة الشحن ودرجة الحرارة والاتجاه الحالي. توضح المقارنة بين نتائج التجربة والمحاكاة أنه باستخدام معلمات الأداء المستخرجة على النحو الأمثل ، يمكن للنهج المقترح التنبؤ بدقة بأداء البطاريات المختلفة من مختلف الأحجام والقدرات والمواد. في نهاية المطاف ، يمكن استخدام هذا الطراز البسيط من البطاريات كأداة قوية وموثوقة للتنبؤ بأداء البطارية (توتر و شدة كهرباء) في أنظمة إدارة بطارية السيارة بالكهرباء
الكلمات المفتاحية: بطارية ليثيوم أيون ، اختبارات EIS للمركبات الكهربائية ، نمذجة الدوائر الكهربائية ، المقاومة الداخلية.

Résumé :
Un modèle de batterie, prédisant ses performances électriques avec une grande précision, est essentiel pour l'étude, l'investigation et la simulation des circuits conçus. Ce modèle nous permettra ainsi de contrôler son utilisation, améliorer son autonomie et sa sécurité dans les systèmes tels que les véhicules électriques. Dans cette thèse, un modèle basé sur un circuit équivalent relativement simple est développé pour modéliser les performances des batteries lithium-ion utilisées dans les applications automobiles. La stratégie du modèle adoptée pour la caractérisation des paramètres internes repose sur deux techniques principales: (1) les tests de spectroscopie d'impédance électrochimique (EIS), où un circuit comparable est configuré selon les perceptions du test EIS et (2) la technique des impulsions, cette dernière est effectuée en utilisant un profil d'impulsions de courant proposé. Les paramètres extraits sont programmés sur l'état de charge, la température et la direction du courant. La comparaison entre les résultats de l'expérience et ceux de la simulation montre qu'avec les paramètres de performance extraits de manière optimale, l'approche proposée peut prédire, avec précision, les performances de différentes batteries de différentes tailles, leurs capacités et le matériau utilisé. À terme, ce modèle de batterie simple peut servir d'outil robuste et fiable pour prédire les performances I-V des batteries dans les systèmes de gestion de véhicules électriques (BMS).

Mots Clé : Batterie Li-ion, Tests EIS de véhicule électrique, Modélisation de circuits électriques, Résistance interne.

Abstract :
A battery model that predicts the electrical performance with high accuracy is vital for circuit designing to control the battery usage and improve its runtime and safety in electrical systems such as electric vehicle (EV). In this Thesis, a relatively simple equivalent circuit based model is developed for modeling the performance of lithium ion batteries used in automotive applications. The model's strategy adopted for characterization of the internal parameters is based on two main techniques: one is the electrochemical impedance spectroscopy (EIS) tests, where comparable circuit is set up as per EIS test perceptions and the other is the current pulses technique, this latter is carried out using a proposed current pulses profile. The extracted parameters are scheduled on the state-of-charge, temperature, and current direction. The comparison between experiment and simulation results demonstrates that with the optimally extracted performance parameters, the proposed approach can accurately predict the performance of differents batteries of various sizes, capacities, and materials. Eventually, this simple battery model can serve as a robust and reliable tool for predicting the battery's I-V performance in electrified vehicle battery management systems.

Keywords: Li-ion battery; Electric vehicle; EIS tests ; Electrical circuit modelling; Internal resistance.

CONTENTS

LIST OF FIGURES

LIST OF TABLES

GENERAL INTRODUCTION

General Introduction

Batteries are omnipresent in most people's everyday lives. For example, lithium-ion cells are used in mobile phones, smartphones, notebooks or tablets, providing runtimes and applications that were unthinkable ten years ago. But even with the so-called power tools, the lithium-ion cells play an ever-increasing role. Just a few years ago, cordless screwdrivers with NiMH batteries were the only battery-powered tool, and thanks to their high performance, the spectrum has expanded significantly. As an example, circular saws of exotic applications such as robotic lawn mowers are called.

In addition to these consumer applications, the use of lithium-ion cells should also help to control global warming. At the time of printing, a record 410 ppm CO_2 was recorded in Mauna Loa, Hawaii. [1] If a maximum tolerable average temperature increase of 2 K is used compared to the pre-industrial level, then a limit of 450 ppm CO_2 must not be exceeded [2].

Seen against this background, efforts to expand renewable energy sources are all the more important. However, a large part of the energy generated from wind power or solar energy is subject to high volatility, so that storage solutions must be used here. The use of batteries for the central storage of large amounts of energy is advised against by experts [3], but there are already marketable concepts for grid stabilization

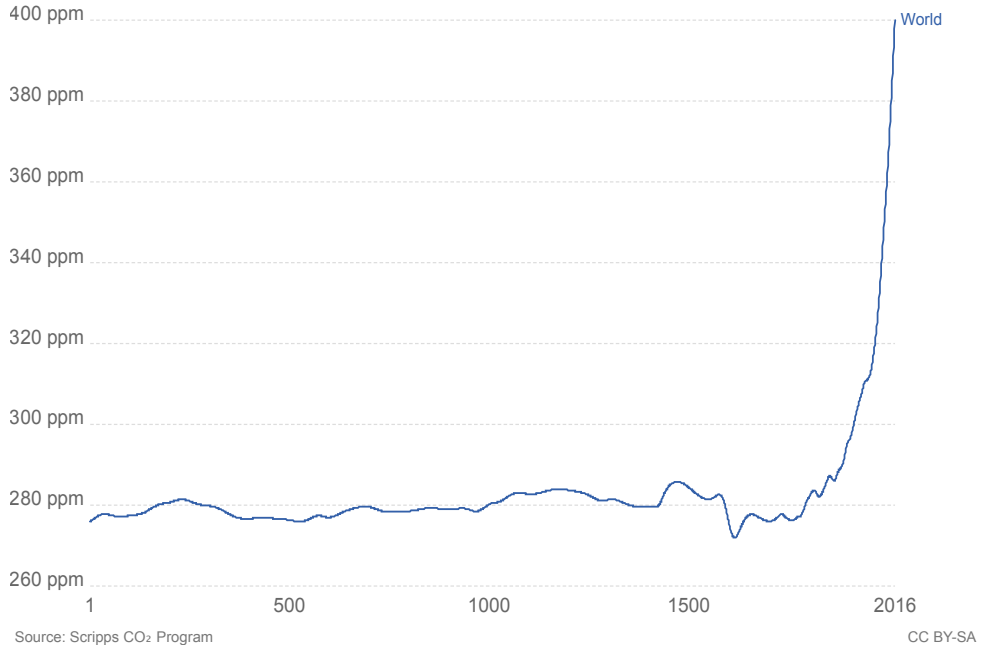

Figure 1: Global average long-term atmospheric concentration of carbon dioxide, measured in parts per million (ppm).

today. The repeated amendment of the law for the priority of renewable energies (EEG) led to a decreasing feed-in tariff and makes self-consumption seem more economically attractive. This and the legislative support [4] will lead to an increasing demand for decentralized battery storage solutions.

A further contribution to the reduction of the CO_2 emission and the fine dust pollution can be made by a progressive electrification of the drive train in the motor vehicle. Even if the internal combustion engine will last for a long time according to the assessment of the automotive industry, the trend towards hybridization is clearly visible. A greater spread of purely electric vehicles could also be furthered by the trend towards megacities. For example, at the beginning of this year, a value of PM 2.5 of 886 $\mu g/m^3$ was measured on the grounds of the American Embassy in Beijing [5], the visibility was clearly limited [6]. The term PM 2.5 covers particles with a diameter of less than 2.5 µm, for which, according to the European Directive 2008/50/EC, an annual average value of 25 $\mu g/m^3$ is given. Even though the eco-balance of an electric vehicle well to wheel by using electricity from fossil fuels contradicts the dream of emission-free mobility, it is possible to relax the situation locally in metropolitan areas

[7]. One form of electro mobility that is already widespread in metropolitan areas of emerging countries today is the use of electric scooters and pedelecs. The use and further development of lithium-ion batteries is thus linked to the major developments and trends of mobility, global warming and megacities and can make a significant contribution to mastering the associated challenges. This makes it all the more important for material developers to provide tools that allow them to characterize the cells comprehensively and create understanding models.

Therefore, the automotive industry has observed a renewed interest in electricity as an automotive propulsion technology in the recent decade [8]. EVs and electrified (hybrid) vehicles are superior to conventional vehicles in the following areas [9, 10]:

1. Compared to an internal combustion engine (ICE) with about 20 % energy efficiency, electric motors convert about 75% of the chemical energy stored in the battery into mechanical energy. Thanks to the regenerative braking system, which allows for energy recovery during braking, the efficiency of the electric traction system is further improved.

2. Electric motors require less maintenance compared to ICEs as they have fewer moving parts. Furthermore, electric motors are able to provide high torque at low speeds; making the multi-speed gearboxes unnecessary for certain EVs.

3. EVs offer a simple powertrain design, zero tailpipe emissions, and high efficiency on a tank-to-wheel basis.

Figure 2: The highest efficiency ICE in the world (left) and a typical permanent magnet synchronous motor (PMSM) for EV application (right).

As shown in Fig. 2, the highest efficiency ICE in the world, Wärtsilä-Sulzer RTA96-C diesel engine, only has a peak efficiency of 57% [11]. The efficiency of a typical vehicle used gasoline engine is lower than 40% [12]. To overcome these shortcomings, the electric drive system based vehicles (EVs) are considered as a feasible solution.

Thesis organization

This thesis is organized as follows,

Chapter 1 is introduction and overvieiw of electrical vehicle than it is followed by chapter 2, which introduces literature review about the fundamentals and modeling of batteries used in electrified vehicle. In addition, the chapter presents a detailed analysis of the load consumption of vehicle. The analysis is based on a simulation model of the vehicle and on field measurements. These information will make it possible to situate the objectives of our work in relation to the current literature in the field of energy modeling and management in electric vehicles. Chapter 3, a battery modeling approach is proposed which can dynamically update the model parameters based on battery temperature and SOC. The model parameters are experimentally extracted for automotive grade cell. The major contribution of the thesis is that the proposed battery model for various battery states of life is computationally efficient and can be utilized in a real-time battery management system. In addition, the chapter presents a detailed analysis of the electrochemical behavior and provides the evaluation and optimization of existing measurement techniques and the development of the new Pulse Fitting process. Utilizing the proposed modeling approach, the impact of battery impedance on performance of EVs under realworld drive-cycles is discussed in Chapter 4.

Finally, a General Conclusion summarizes the thesis, and highlights the main contributions of the research. It also contains recommendations for future works.

CHAPTER 1

INTRODUCTION AND OVERVIEW OF ELECTRICAL VEHICLE

Contents

1.1 Environmental Aspects

There is currently a strong growth in the car fleet, especially in emerging countries, which implies an increase in energy needs. These needs translate into greenhouse gas emissions, which are largely responsible for current and future global climate change [13]. The responses that will be made in the coming years to all these very diverse developments can change the current economic equilibrium.

Most governments of industrialized countries negotiated in December 1997 the Kyoto Protocol, which aims to strengthen their commitments to mitigate global GHG emissions. Thus, the countries pledged to reduce them by at least 5% between 2008 and 2012, compared to 1990 levels. This protocol only targets industrialized countries, with a percentage of 56% of global CO_2 emissions. The emission reduction targets established in Kyoto cover several types of GHGs (Greenhouse gas), starting activities that can cause these effects.

The transportation sector is the largest consumer of fossil energy and therefore represents a significant source of GHG emissions. Fig. 1.1 illustrates the evolution of emissions by economic sector, breaking down transport by world and grouping those of the energy sector industries into one whole [14].

As the road transport sector is the largest contributor to global warming, its share of pollution is estimated at 20% worldwide. Indeed, the impact of road transport plays an important role in these environmental phenomena and most emissions from the transport sector concern road transport with 94% [15]. All these environmental constraints have forced car manufacturers to mention the fuel consumption and the amount of CO_2 emitted per kilometer.

Improving the energy efficiency of vehicles, reducing their emissions and promoting clean electric vehicles remain major challenges.

Following the presentation of the issues related to the context and the environmental aspects of the vehicles, the following section will be dedicated to the discussion on the generalities concerning the organs of electric traction.

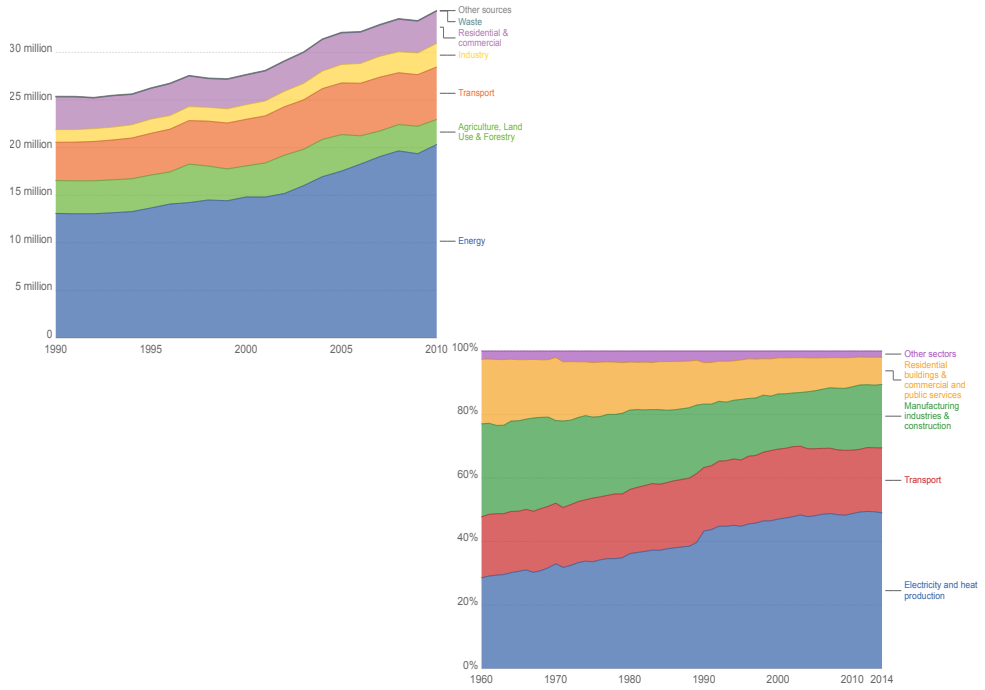

Figure 1.1: (a).Evolution of CO_2 emissions by sector, measured in gigagrams of CO_2 per year. (b).Percentage of CO_2 emissions worldwide by sector.

1.2 Electric vehicles literature review.

1.2.1 Overview of Electrical and Hybrid vehicles

By definition, a hybrid electric vehicle (HEV) is a vehicle in which two different energy sources are integrated, typically a conventional engine (ICE) and an electric motor.

Fig. 1.2 shows the concept of a HEV and the different energy flows flowing through it. For the configuration presented above, we have nine situations in which the two energy sources can meet the demand of the load:

- Energy source 1 alone provides the power demand of the load;
- Energy source 2 alone provides the power demand of the load;
- The two energy sources together supply the demand for power;
- The energy source 2 is charged by the energy source 1;
- The energy source 2 is charged by the load by energy recovery;

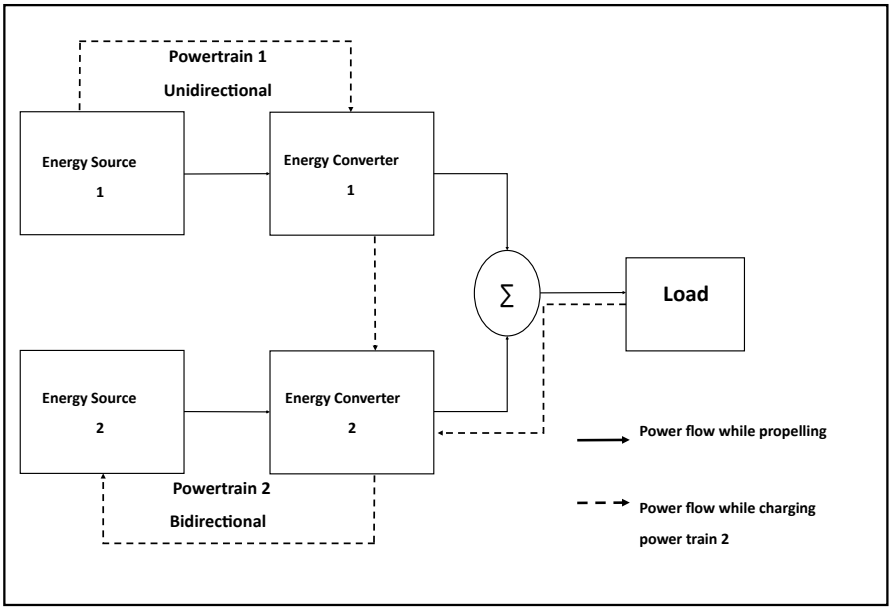

Figure 1.2: Generic concept of a hybrid drivetrain .

- The energy source 1 provides the energy required for the load and at the same time for the second source;
- The energy source 1 supplies the energy for the source 2 and the energy source 2 provides the power demanded by the load;
- The energy source 1 provides the demand for power demanded by the load and the load supplies the energy for the source 2 by recovery.

Most HEVs are equipped with two types of engines. The main purpose of their design is to save energy. Adding an electric motor to a conventional gasoline or diesel engine saves energy in a number of ways. The different ways of combining these components make it possible to define several powertrain architectures.

On the ecological front, electric vehicles (EV) provide an undeniable reduction in pollutant emissions. On the other hand, the reduction of CO_2 emissions remains conditioned by the production of the electricity used for recharging the batteries. Electric vehicles offer lower performance (i.e. autonomy) to thermal vehicles, but meet the needs of users with the advantage of reducing greenhouse gas emissions

and our dependence on hydrocarbons. If their purchase price is currently higher, it could become competitive in the medium term.

1.2.2 Electric vehicle powertrain components

The electric powertrain system is the heart of electric and hybrid vehicles. Its components consist of electric motors, power converters and their controls. The electric motor is used to convert the electrical energy that comes from the source of mechanical energy used to propel the vehicle or vice versa to allow energy recovery during braking. While braking, the mechanical chain becomes partly the source of power, and the main source of energy becomes the receiver. The power converter is then used to power the electric motor within the allowable limits of voltage and current.

For uqeful management of all components that make up the electric propulsion system, the control system provides control signals and references to continue in torque or speed according to the wishes of the driver and the mission. The scheme of operation of the electric propulsion system is shown in Fig. 1.3.

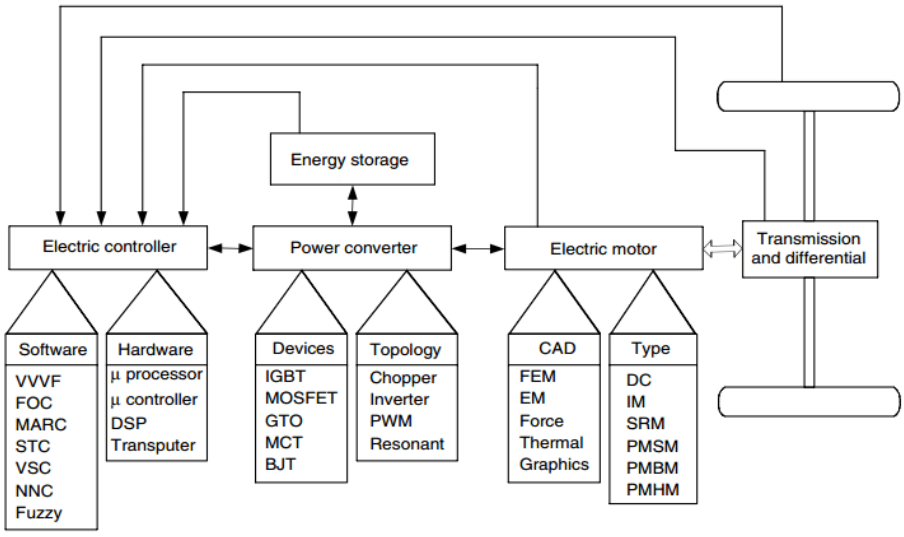

Figure 1.3: Diagram of a typical electric propulsion system.

The choice of electric propulsion systems for the electric and hybrid vehicle depends mainly on three factors, namely the driving cycle, the constraints of the vehicle

and the energy source [9]. The driving cycle is defined as the cycle that includes the acceleration, the maximum speed, the braking and the duration of the different phases. The vehicle's stresses, including volume and weight, depend on the type and mission of the vehicle. The main sources of energy are batteries, supercapacitors, fuel cells, flywheels, etc. The interaction of subsystems and the likely impacts of exogenous factors are of course a high point requiring attention.

1.3 Main architectures of hybrid vehicles

1.3.1 Hybrid electric thermal vehicles

The two main reasons why hybrid concepts are interesting are the saving of energy and the reduction of pollutants. Traditionally, Hybrid Electric Vehicles (HEV) are divided into two major groups: series and parallel. Today, we can classify them into four groups: series hybrid, parallel hybrid, series-parallel hybrid and complex. We will then mention the different topologies of hybrid vehicles [16,17].

1.3.1.1 Series Hybrid

The topology of the hybrid series vehicle is the configuration of the vehicle in which both power sources power a single powertrain that propels the vehicle. In this type of vehicle (Fig. 1.4), the heat engine is mechanically decoupled from the wheels (transmission) and is connected to a generator either on the same shaft or by a mechanical assembly. The main source of energy ensures the recharge of the secondary source of energy and the power supply of the electric motor. When additional energy is needed, for recoveries during overtaking or in coasts for example, it is the secondary source of energy that provides this extra energy. This source can be a diesel engine or gasoline.

The main advantage of this structure comes from the total decoupling between the engine and the mechanical transmission, which makes it possible to operate the engine in its maximum efficiency range or minimum emissions.

On the other hand, the major disadvantage of the hybrid series architecture is its low overall efficiency. In fact, the mechanical energy produced by the heat engine

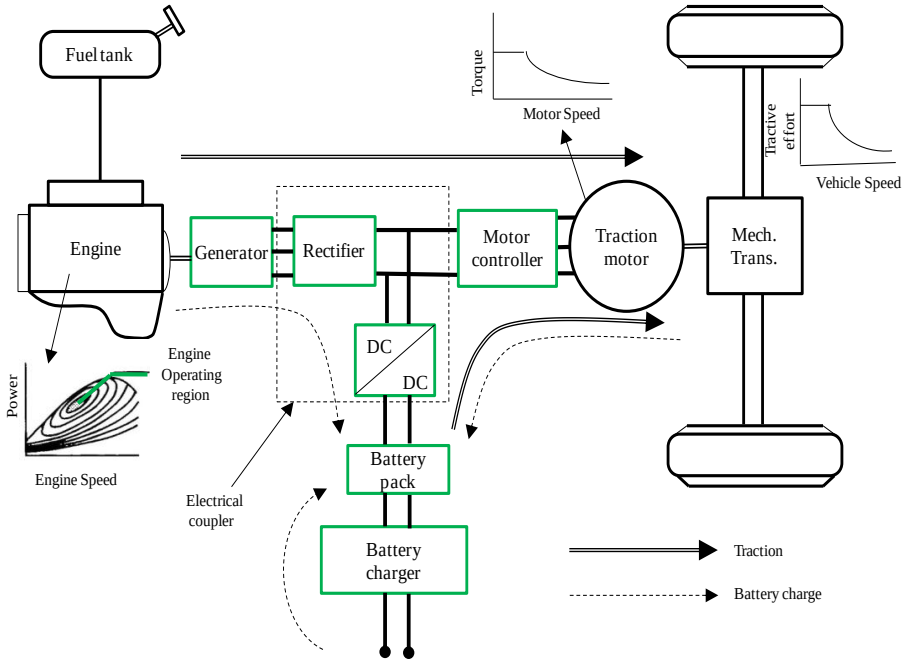

Figure 1.4: Detailed Configuration of Series Hybrid Vehicle.

is then transformed into electrical energy via the generator and then again converted into mechanical energy by the electric motor. Thus, the efficiency cascade of the motor train is quite unfavorable to the reduction of the energy consumed [9].

1.3.1.2 Parallel Hybrid

In the parallel configuration (Fig. 1.5) the two motors, thermal and electric, are directly linked to the transmission and therefore to the wheels. They can participate in the traction of the vehicle in a parallel way because the energy flows from the two energy sources arrive simultaneously to the wheels. Mechanical connections between the shaft of the electric motor and the shaft of the heat engine via a gear box make it possible to ensure the transmission of power to the wheels.

This structure has a better overall performance than the series architecture, because the size of the engine can be reduced. It is for this architecture that we obtain a better fuel economy, with the ability to operate the electric motor and the engine together for strong demands for power.

The major disadvantage is the complexity of the control-command architecture

and the rigid connection between the engine and the wheels [9].

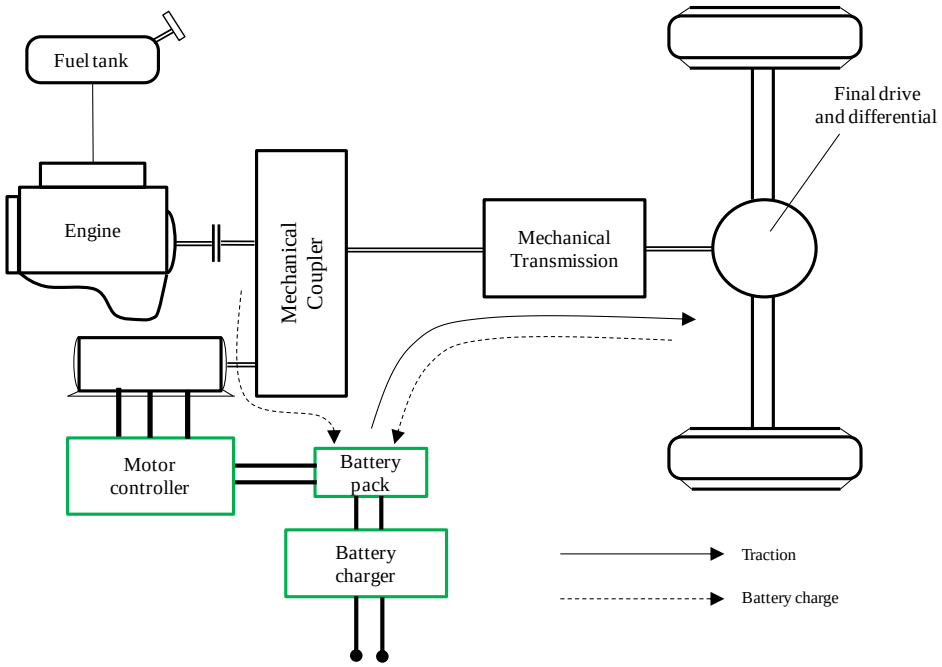

Figure 1.5: Detailed Configuration of Parallel Hybrid Vehicle.

1.3.1.3 Series-parallel Hybrid

This series-parallel architecture, also called "parallel hybrid power bypass", it incorporates an electric motor, a generator and a heat engine (Fig. 1.6). Using efficient power demand management on one side, and provided on the other, it is possible to control the operating speed with maximum efficiency regarding the engine and to share the power between the demands of the vehicle (load) and charging the battery.

The combination of the advantages of the serial configuration and the advantages of the parallel configuration make it possible to take advantage of this configuration.

The series-parallel architecture requires at least two electric motors in addition to the heat engine which makes it expensive and increases the complexity of the control-command structure [9].

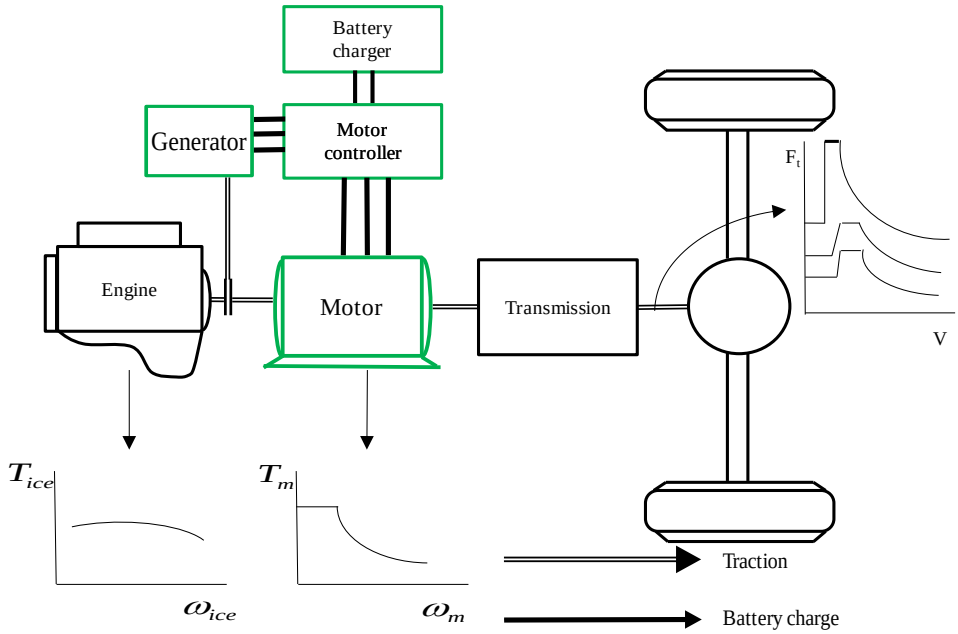

Figure 1.6: Detailed Configuration of Series-parallel Hybrid Vehicle.

1.3.1.4 Complex Hybrid

The complex type architecture (Fig. 1.7) is an architecture composed of three electric motors with an associated power interface and a heat engine. From an energy point of view, this solution is not an ideal solution. Thanks to an efficient management of the powers demanded on one side, and provided on the other, it is possible to control the engine at maximum efficiency, and to share its torque between the demands of the vehicle and the recharge of the engine. The idea is to make some changes in the classical design (series architecture, parallel or series-parallel). One of these approaches is to place a small electric motor (powered by a battery for example) behind the engine and runs it as a starter for the engine and as a generator to charge the battery. In this way it can help provide power for the powertrain in case there is a high demand for power, and be used to recover kinetic energy during vehicle braking [9].

1.3.2 Elctrical Vehicles EVs

Fig. 1.8 shows the block diagram of a typical electric vehicle (VE). In this case, the only source of energy on board is batteries that are recharged using a charging system and

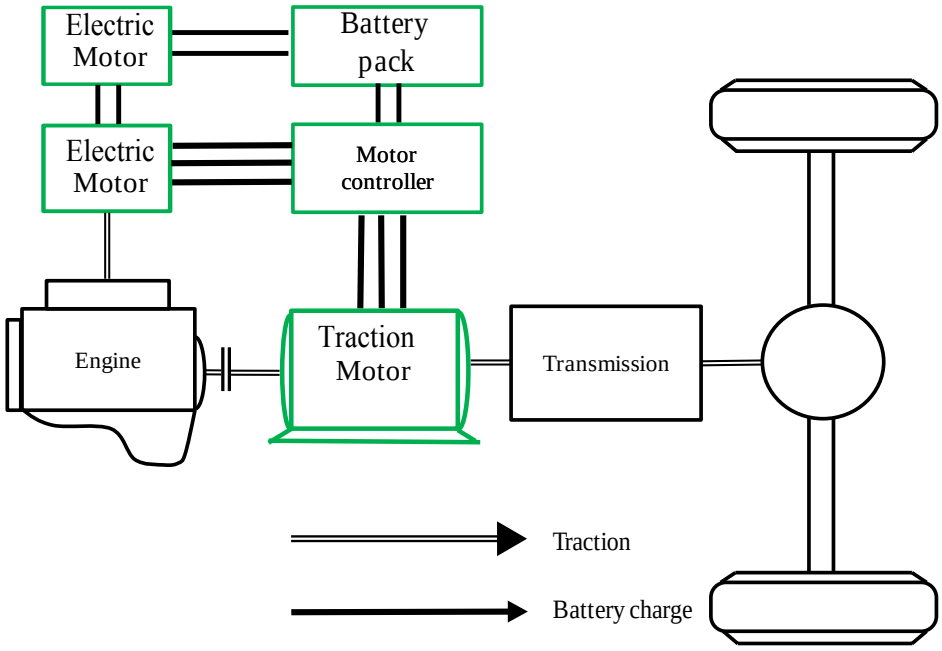

Figure 1.7: Detailed Configuration of Complex Hybrid Vehicle.

often with energy recovery during braking.

The weak point in this type of vehicle concerns the main source of energy (the batteries). The electric battery is the key organ of electric cars. It directly affects the performance and especially the autonomy of the electric-powered car. Indeed, their power density expressed in W/kg is limited and their lifetime is directly related to the constraints that are applied to them. Thus, their charge and discharge current must be limited to ensure a lifetime compatible with a hybrid vehicle. Regarding the charge of the batteries, the solution is to use a weak current for a long time for example the load of the vehicle during the night. A limitation of the discharge current which is a function of the driving cycle, is synonymous with a decrease in the dynamic performance of the vehicle. This is not possible for an electric vehicle with a single source of energy. The current taken from the batteries during acceleration (high power stress) therefore remains important. In many cases in the field of transport, batteries must be sized mainly according to a criterion of power.

In an EV, the braking energy can be theoretically recovered. In this case, the electric motor operates as a generator and re-injects into the batteries the kinetic energy of the

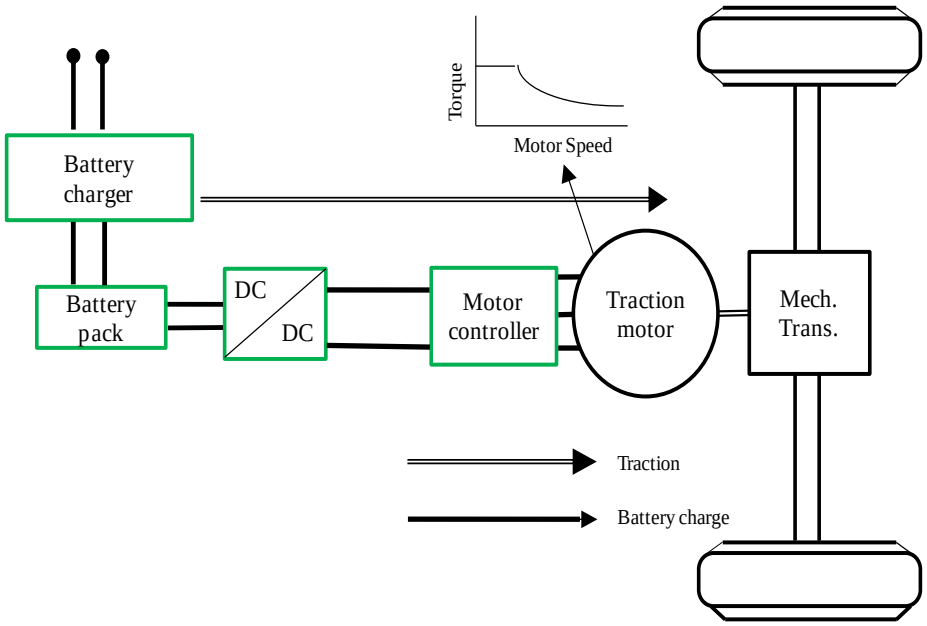

Figure 1.8: General Configuration of a Electric Vehicle .

vehicle converted into electrical energy. For standard type batteries, the maximum charge current is lower than the maximum discharge current. The braking power that can be recovered is directly related to the maximum charging current of the electrical energy storage element; therefore, it happens that we do not recover all the energy of braking. Of course, friction braking is still present.

The main advantage of purely electric propulsion compared to what we have presented before is that the EV does not emit any polluting gases during its use and that the energy on board the vehicle is stored in batteries. The electric vehicle is "clean" at the end user level, i.e it does not emit polluting gases locally. On the other hand, the recycling of used batteries and the production of electricity for recharging must be taken into account. In the worst case, electrical energy is produced from fossil fuel releasing CO_2 into the atmosphere. For an electric vehicle to qualify as "clean", the energy required for charging must be produced by renewable energies (solar, wind, hydro, etc.). In addition to the problem concerning the electrical supply for the charging of the batteries, the main drawbacks with this type of vehicles using batteries are the following:

- The batteries's life is short, especially if the instantaneous power constraints applied to them are important;
- The autonomy that can be achieved with conventional type batteries is limited;
- The maximum charging current of the batteries is low, the charge generally requires several hours and the braking energy can only partially be recovered.

1.4 Problem definition and research objectives

In this thesis, different aspects of Li-ion battery performance and behavior are studied as presented in the following sections.

1.4.1 Battery Performance Modeling

Electrical energy storage (battery) continues to be the greatest challenge to the commercialization of both PHEV and EV models. Beside battery price, range anxiety (fear of getting stranded on the road due to lack of charge) is the main concern expressed by consumers [18]. Range anxiety stems from the fact that the specific energy of the battery packs (0.25 kWh/kg) compared to fossil fuel (13 kWh/kg) is very low. Furthermore, refuelling (recharging) stations are not widely available and the charging time is rather high (depending on the method, full recharge times typically range from 30 minutes to almost 12 hours). With a gasoline car, many people are not at all affected by the range they get as refuelling is quick and easily accessible almost everywhere. Several surveys have been conducted on range anxiety. Accenture [19] conducted a survey, in 13 countries, on consumer preference concerning driving an electrified vehicle in which Chinese participants showed the highest tendency to buy and drive an EV as their future choice, while Dutch participants expressed the lowest interest. However, a higher range means a huge battery size and, consequently, a higher cost vehicle.

A determinant factor on the EV range is the battery management system (BMS). In electrified vehicles, the BMS plays a significant role in the battery and the whole

vehicle performance, efficiency and safety. The BMS is actually required to respond to dynamic power demands dependent on driving behavior, road conditions, and electrical accessories [20]. In addition, the BMS is responsible for cell safety. Therefore, accurate prediction of SOC, propre management of current and temperature, and cell potential balance are BMS's curcial tasks [21]. However, the efficiency of a BMS is highly dependent on the fidelity of the battery model built in the BMS. Furthermore, on board processing power is limited. Therefore, it is imperative to have an accurate model that is sufficiently simple to be operated on board the BMS. Model complexity is dependent on application requirements. High fidelity Li-ion electrochemical models, which were first introduced by Doyle et al[22], are widely used for battery design. Another type of battery model is the equivalent circuit model (ECM). These models are more useful for real-time applications (such as BMSs), in which cost and processing power is strictly limited. An ECM represents the complex electrochemical interactions within a battery as simple circuit components. Components may be added to model observed phenomena and increase accuracy, or may be removed to increase efficiency. ECM circuit elements, such as resistors and capacitors, may also be scaled to account for changes in SOC [23–27], temperature [28–32], aging [33], and C-rate [26], which affect cell performance.

As a contribution to the existing models, this thesis presents a comprehensive ECM developed for commercially available Li-ion cell used in EVs, which, compared to commonly used models, proves to be more efficient in terms of voltage prediction. Such an improvement in voltage prediction can be interpreted as an additional few kilometers to the vehicle range. Also, the proposed ECM's parameters determined by the proposed pulses current method, which, can be used as an alternative to hybrid pulse power characterization (HPPC) tests within a limited error.

1.4.2 Battery Thermal Characterization

Devices with high energy density, such as Li-ion batteries, have the potential for high heat generation and Li-ion batteries are no exception. A single Li-ion polymer cell can undergo a temperature increase of 5 to 20 K at a 1C discharge rate [34], depending on

cell geometry and assembly. Thermal management of the cells in a pack is, therefore, an important issue that must be considered to ensure vehicle safety, performance and cycle life.

Depending on ambient conditions, there may be a need to remove or add heat to the battery in order to maintain the optimal temperature range and distribution. Non-uniform temperature distribution results in low charge and discharge performance and cell unbalancing, over time. Existing thermal management techniques include applying liquids, insulations and phase-changematerials [35]. Essential tools in automotive pack design and thermal management are thermal and performance models. Such models require inputs such as system and operational parameters. Not all of these parameters are easy to directly quantify (e.g. heat effect and transport properties) because their effects cannot be isolated; thus, extensive tests are necessary to yield a clear understanding of heat generation and cell performance [36]. Several papers have been published on this topic so far; some proposing a simple one dimensional(1-D) [31, 37] approach and others with further details by three dimensional(3-D) [38]modeling of the heat generation inside the cell. However, for vehicle simulation and BMS applications, a fast and accurate heat generation model based on a limited number of lab tests may serve as an adequate alternative. In this regard, this thesis contributes to the literature by presenting a simple and accurate modeling approach of Li-ion cell heat generation that can be readily applied for fast simulations and on-board applications.

1.4.3 Battery Degradation

Battery state of health (SOH) has been a hot topic since rechargeable (secondary) batteries were introduced to the industry. To extend the battery lifetime, the focus has been initially on minimizing the power consumption of the devices powered by these batteries. However, such methods would not be adequate, as they ignore important characteristics of the battery source such as the dependency of available capacity on the battery discharge rate and internal temperature, and the cycle aging effect [39]. In recent years, a number of researchers have developed models for battery SOH and

degradation rate based on battery detailed electrochemistry coupled with thermal characteristics [40, 41]. In EV applications, battery SOH is known to be very much dependent on the driving and charging habit; therefore, there is a growing desire to evaluate the path dependence of battery degradation. This is due to the fact that a lab environment is far different from what the battery experiences under real operation in EVs. However, real-life testing is expensive and labor intensive and is associated with a very low level of control, which explains why, so far, it has rarely been the subject of research [42–44].

1.4.4 Auxiliary Loads in EVs

In EVs, the on-board battery provides the power not only for driving but also auxiliary loads such as climate control loads. Therefore, the use of a climate control system (air conditioning (AC) and heating) adds more challenges to the EV design. The primary task of AC is to provide passengers's thermal comfort through maintaining the vehicle cabin temperature and humidity at desired levels. AC is believed to be the accessory that requires the largest quantity of power from the traction source. In conventional and hybrid electric vehicles (HEVs), this power is provided by the engine; however, in EVs, the power has to be extracted from the battery [45, 46]. It is reported that, in an EV, AC may reduce the driving range up to 35%, depending on the AC usage frequency [47]. The loads are more significant when the climate-control systems are used in an initially very hot or very cold cabin at the beginning of a trip. Associated with the range reduction, there would be increased battery degradation for the same distance driven when AC/heating system is operating. Therefore, it is necessary to develop a tool for assessing the climate control system impact on the battery and vehicle performance.

CHAPTER 2

BACKGROUND AND LITERATURE REVIEW(BATTERY AND VEHICLE MODELLING)

Contents

2.1 Introduction

Li-ion batteries have become popular in many applications due to their high energy density which allows them to be used in portable devices. Earlier versions of electrochemical energy storage could not hold enough charge to power the devices in use today while allowing them to remain portable. The first galvanostatic cell was created by Alessandro Volta in 1800 when he stacked zinc and silver disks between a sodium chloride soaked cloth. Advancing from this primary cell, the lead-acid battery became the first rechargeable system when it was created in 1859 by Gaston Plante. [48] While lead-acid batteries were novel at the time, they suffered from low energy density and would fail at meeting the demands of many power and energy hungry electronic devices in today's world. Nickel-Cadmium (Ni-Cd) was proposed as an alternative chemistry in the early 1900's and Nickel Metal Hybdride (NiMH) became prominent in the latter half of the century. Both batteries improved upon the lead-acid battery's energy density and were used in many first generation consumer electronics and hybrid vehicles. But Ni-Cd and NiMH suffered from several deficiencies. Both nickel and cadmium are toxic materials and the cell voltage for both types of batteries is only 1.2V which limits the energy and power density for these chemistries. Searching for a material that could store more energy, lithium metal was investigated because it is a lightweight metal with a high electropositive potential (which leads to high storage densities). [49] When early lithium batteries were introduced, their weight and volume energy densities were about double that of Ni-Cd. [50]

The focus in this chapter will be also on the modeling and designig of the power system of a battery electric vehicle. Less attention will therefore be put on the selection of each component (electricmachines, power electronics, batteries, etc.) of the power system as this is a very big task in itself. This chapter will therefore concentrate on the methodology of the modeling and design process. However, the method presented here is also suitable for other architectures and choice of components.

The chapter is organized as follows. Sections 2-5 provide a literature review about batteries and different elements that compose a battery and its specifications. Section 6 involves various battery models found in recent literature in addition to various

strategies applied for model parameters identification. Section 7-9 outline battery degradation modeling. After these sections, section 10 describes the modeling of the electric vehicle. Lastly, a section gives the conclusion and remarks.

2.2 Battery Elements and Specifications

Battery is an energy storage device that consists of one or more electrochemical cells that produce electrical energy from chemical energy. This chemical energy is stored in its active materials through electrochemical reactions depending on the desired nominal battery voltage and capacity Cells, which are connected in series, parallel or both. The main components of the cell are anode, cathode and separator [51,52].

2.2.1 Anode

Upon the chemical reaction at the anode (oxidation), electrons are released and flowed to the cathode through an external circuit. The important parameters in selecting the anode material are efficiency, high specific capacity, conductivity, stability, ease of fabrication and low cost [53,54].

2.2.2 Cathode

Cathode is the electrode in which reduction (absorbing electrons) takes place. During discharge the positive electrode of the cell is the cathode. During charge the situation reverses and the negative electrode of the cell is the cathode. The cathode is selected based on its voltage and chemical stability over time [51,55].

2.2.3 Electrolyte

Substances that release ions when dissolved in water are called electrolytes; which could include a wide range of acids, bases, and salts, as they all give ions when dissolved in water. The electrolyte completes the cell circuit by transporting the ions.

The electrolyte are desired to be highly conductive, non-reactive (with the electrode materials), stabile in properties at various temperatures, and economical [56].

2.2.4 Separator

A separator is a porous membrane inserted between electrodes of opposite charge. The key function of the separator is to keep the positive and negative electrodes apart to prevent electrical short circuits and, at the same time allow rapid transport of ionic charge carriers needed to complete the circuit. Care must be taken upon selecting the separator material, as it could adversely affect the battery performance (by increasing electrical resistance). Following considerations should be observed when selecting the separator [56, 57]:

- Electrical insulation
- Minimal electrolyte (ionic) resistance
- Mechanical stability
- Chemical resistance to degradation by electrolyte
- Uniform in property and thickness
- Effective in preventing migration of particles

2.3 Battery Gloassary

2.3.1 Battery Management System

Battery management unit (BMU) is the central component of the battery system to ensure a healthy and appropriate usage of the sensitive battery cells. The BMU controls the usage of the battery cells by measuring variables such as voltage, current and temperature of each individual cell in the package. It also calculates important state variables such as SOC and power limits for charge and discharge of the battery. This information along with other signals (such as alarm signals) is sent from the BMU to

the vehicles main computer which consequently is able to control the propulsion of the vehicle in a qualitative manner without damaging the battery package [10].

2.3.2 State of Charge

The state of charge (SOC) indicates the amount of charge in Amp-hours left in the battery. The SOC can be divided into two types: engineering-SOC (e-SOC) and thermodynamic SOC (tSOC) [58]. The e-SOC is the SOC apparent to the user of the battery and is rate dependent; it is the state of the capacity at a certain discharge rate, so different discharge rates will result in a different e-SOC at the same amount of charge in the battery. The t-SOC is the SOC of a battery defined by the thermodynamic properties in the cell and can be determined by the open circuit voltage of the battery; it is the state of the useable capacity in the cell.

2.3.3 Depth of Discharge

A measure of how much energy has been withdrawn from a battery, expressed as a percentage of full capacity. For example, a 100 Ah battery from which $30Ah$ has been withdrawn has undergone a 30% depth of discharge (DOD). Depth of discharge is the inverse of state of charge.

2.3.4 C-rate

The C-rate is a measure for the current of a battery cell and is scaled to the nominal capacity of a cell stated by the manufacturer at reference conditions. The current level that a battery cell can discharge at depends on the capacity of the battery. A current of 1C means that the battery cell is ideally charged or discharged in one hour, $C/2$ in two hours and $2C$ in half an hour. So a current of 0.5C for a cell with nominal capacity of $160Ah$ is equal to $80A$.

2.3.5 Cell Capacity

The useable capacity is theoretically the possible amount of charge that can be discharged from a fully charged cell with an infinitely small current for a given minimum cell voltage, so that the voltage drop over the internal resistance becomes close to zero. The true capacity is the useable capacity under reference temperature and is used as a measure for the capacity fading determination. The 1C capacity is determined with a C-rate of 1C under reference conditions and is generally used to measure the capacity fading [59].

2.3.6 Cycle

Cycle could be defined as a period of discharge followed by a full recharge. EVs, however, experience regenerative braking during operation, which required a change in cycle definition. Some define a cycle as a period of discharge with regenerative braking followed by a full recharge [60] or an amount of energy discharged with regenerative braking followed by the equal amount recharged [59]. A better alternative to measure the usage of a battery is the charge or energy processed in the battery. The ambiguous definition of a cycle is hereby also avoided.

2.3.7 Cell Open Circuit Voltage

By definition, the open-circuit voltage (OCV) is the battery voltage under the equilibrium conditions, i.e. the voltage when no current is flowing in or out of the battery, and, hence no reactions occur inside the battery. OCV is a function of State-of-Charge and is expected to remain the same during the life-time of the battery. Note, however, that other battery characteristics do change with time, e.g. capacity is gradually decreasing as a function of the number of charge-discharge cycles. Because open circuit voltage shows a strong dependence on SOC for most batteries, it can be used as an estimation method.

Because the battery must be at rest (several hours) for an OCV to be determined, it is not practical for real-time or continuous estimation. This poses problems for

monitoring devices (e.g. clocks) where rest state is never realized. Addionally, Li-ion batteries (such as those used in vehicle applications) have tradionatlly shown a "flat" OCV When comapred with lead acide batteries [61, 62], which can lead to difficulty in estimation as demonstrated in Fig. 2.1 and Fig. 2.2.

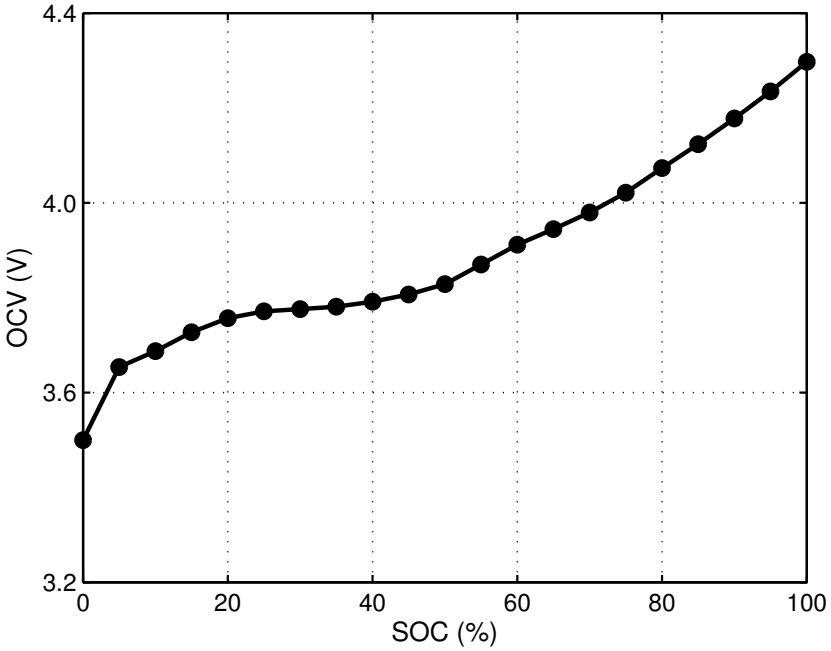

Figure 2.1: Li-ion battery OCV variation against SOC.

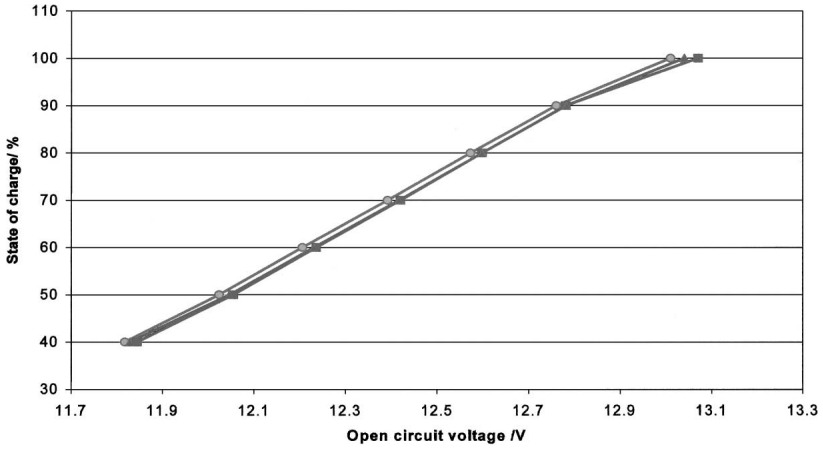

Figure 2.2: Lead acid battery OCV variation against SOC.

2.3.8 Internal Resistance

The internal resistance is sometimes considered as the ohmic resistance of the cell, which is the direct voltage change after application of a current step on a cell in equilibrium [63]. Another definition for the internal resistance is the sum of the ohmic, activation and diffusion polarization resistances [64], which is the largest possible voltage drop in the cell. Nevertheless, the complete voltage drop will result in power dissipation in the form of heat. The voltage drop can be mainly categorized as:

IR drop

IR drop or ohmic drop is due to the current flowing across the internal resistance of the battery.

Activation polarization

Activation polarization refers to the various retarding factors inherent to the kinetics of an electrochemical reaction, like the work function that ions must overcome at the junction between the electrodes and the electrolyte.

Concentration polarization

Concentration polarization takes into account the resistance faced by the mass transfer (e.g. diffusion) process by which ions are transported across the electrolyte from one electrode to another. Fig. 2.3 depicts the typical polarization curve of a battery with the contributions of all three of the above factors shown as a function of the current drawn from the cell. Since, these factors are current-dependent, the voltage drop caused by them usually increases with increasing output current. The internal resistance of a battery is dependent on temperature, SOC and C-rate. Depending on the measurement method, different values for the internal resistance can be found [65]. This is caused by the time constants associated with the activation and diffusion polarization resistances; whether the battery electrodes are in equilibrium or not is also important in determining the value of the internal resistance.

State of health

The state of health (SOH) indicates the state of the battery between the beginning of life (BOL) and end of life (EOL) in percentages. The EOL of a battery is reached when the battery cannot perform according to the minimum requirements. For EVs this

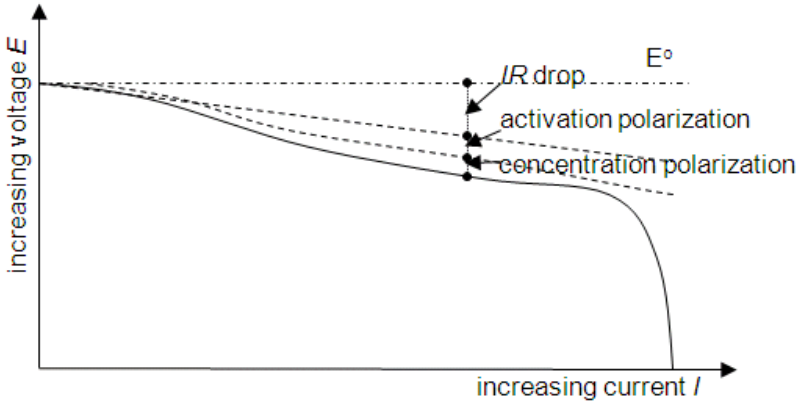

Figure 2.3: Typical polarization of a battery.

is defined by the battery manufacturers when one of the following conditions is met [66]:

- The capacity of a battery under reference conditions has dropped to 80% compared to the rated capacity under reference conditions. This is known as capacity fading.
- The maximum power delivered by the battery under reference conditions has dropped to 80% compared to the rated power under reference conditions. This is known as power fading.

Batteries in BEVs are normally oversized to have sufficient driving range, so the maximum power drawn from the BEV is much lower than the maximum power rating of the battery, therefore in BEVs generally the capacity fading criteria is taken as the SOH indicator.

2.4 Electric Vehicles Battery Types

The batteries can either be of high energy density type or high power density type. Energy density is the amount of energy with regards to kg or liters. Power density provides a good measure on how much energy can be released due to discharge at a

given time with regards to kg or liters. A high energy density battery is useful in applications where a longer driving distance is desired e.g. in a PHEV, which is intended to be driven on pure electricity for longer distances. A high power density battery is useful in an application where a short but intensive power pulse is required; e.g. in an ordinary HEV as the electric motor often only assists the combustion engine in short periods [67]. The first electric vehicles (EVs) developed in the nineties used lead-acid batteries. The range was around 100 kilometers, but since lead-acid batteries have a low energy density, the weight of the vehicle was high; therefore other chemistries were used in the years after [67]. Due to the higher power and energy density and improved cycle life, EVs started to use nickel metal hydrate (NiMH).Today NiMH batteries are still used in hybrid electric vehicles (HEV) and plug-in hybrid electric vehicles (PHEV) for their low cost per Watt. But, due to high self-discharge, limited SOC operation range and low energy density, these batteries are unsuitable for EVs. ZEBRA or molten salt batteries are also used in EVs. These batteries have a low cost and high safety, but because of high operating temperature (270-350$^{\circ}C$) and low power density they are not very popular in EV applications [68]. Table 2-1 presents characteristics of different battery types used in EVs. Fig. 2.4 also shows the Ragone plot for possible options.

Table 2.1: Characteristics of battery types used in EVs [9].

Characteristic	Lead Acid	NiMH	ZEBRA	Li-ion
Nominal voltage	2 V	1.2 V	2.58 V	2.5 V/ 3.3 V/ 3.6 V
Specific energy	30-45 Wh/kg	30-80 Wh/kg	90-100 Wh/kg	90-220 Wh/kg
Energy density	60-75 Wh/L	140-300 Wh/L	160 Wh/L	280-400 Wh/L
Specific power	180 Wh/kg	250-1000 Wh/kg	150 Wh/kg	600-3400 Wh/kg
Cycle life	500-800	500-1000	1000	100-8000
Self-discharge	2-4%/ month	20-30%/ month	0%/ month	2-5%/ month
Temperature range	-20-60 °C	-20-60 °C	270-350 °C	-20-60 °C
Relative costs	Low	Moderate	Low	High

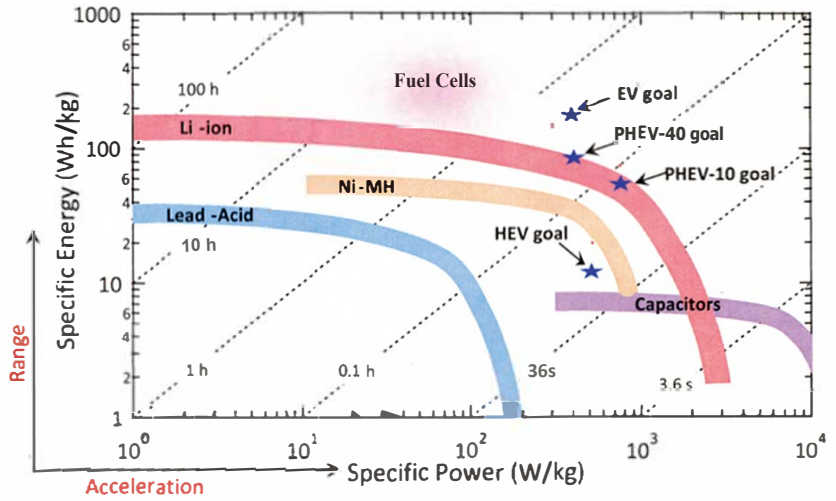

Figure 2.4: The Ragone plot of various cell types capable of meeting the requirements for EV applications.

Today, Li-ion battery is considered as the first choice for EVs, because it is superior in energy density, power density, and low self-discharge and high cycle life. The disadvantages of Li-ion batteries are also the high cost and safty issues. the term 'Li-ion' include a number of different chemistries; Table 2-2 shows some of the chemistries under development in EVs. Also, in Fig. 2.5 a comparison is given between the best EV suitable Li-ion batteries.

Table 2.2: Examples of different Li-ion batteries used in EVs [4].

Developer	Chemistry	Vehicle	Year
A123	Doped Lithium	Fisker-Karma	2010
	nanophosphate	Vue-PHEV	2009
Panasonic	Lithium nickel cobalt	Toyota-PHEV	2010
JCI-Saft	Aluminum oxide	S400-HEV	2009
Hitachi	Lithium cobalt oxide	GM-HEV	2010
Altair Nanotechnologies	Lithium titanate spinel	Phoenix Electric	2008
EnerDel	Lithium manganese Titanate	Think	2009
Compact (LG)	Manganese spinel	Volt-EV	2010
NEC		Nissan-EV	2010

As an example, Lithium-iron-phosphate (LiFePO4/LFP) does not experience thermal runaway and has almost no fire hazards, since no oxygen is released at high temperatures [69]. LiFePO4 cells have the lowest costs per Ah and kW [70], good life span, good power capabilities and are extremely safe, but they have low specific energy and poor performance at low temperatures.

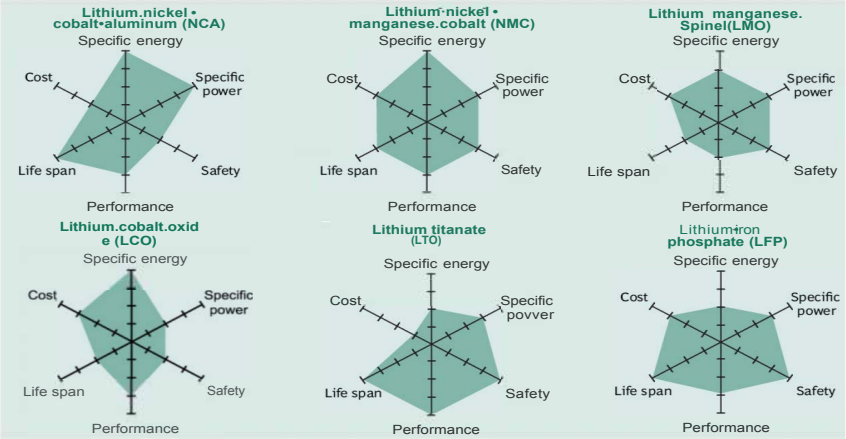

Figure 2.5: Comparison of suitable Li-ions for EV. The more the colored shape extends along a given axis, the better the performance in that direction.

2.5 Li-ion Cell Operation

A battery cell converts chemical energy to electrical energy. This is done by oxidation at one electrode and reduction at the other electrode. Li-ion battery cells utilize lithium ions to store and provide energy. A Li-ion battery cell consists of two electrodes, cathode and anode, with a separator in between, and current collectors on each side of the electrodes. The anode is usually made out of graphite or a metal oxide. The cathode is made of a composite material and defines the name of the Li-ion battery cell. The electrolyte can be liquid, polymer or solid. The separator is porous to enable the transport of lithium ions. It prevents the cell from short-circuiting and thermal runaway [71]. During discharge the lithium ions diffuse from the anode to the cathode through the electrolyte. The lithium ions will intercalate into the cathode, causing the cathode to become more positive. Due to the potential difference between

the cathode and anode, an electric current will flow through the external circuit, supplying power to the load. During charging the opposite effect occurs. The current will cause the lithium ions to deintercalate from cathode and diffuse to the anode. At the anode intercalation of the lithium ions occur, charging the battery. These processes are shown in Fig. 2.6 for a Li-ion cell.

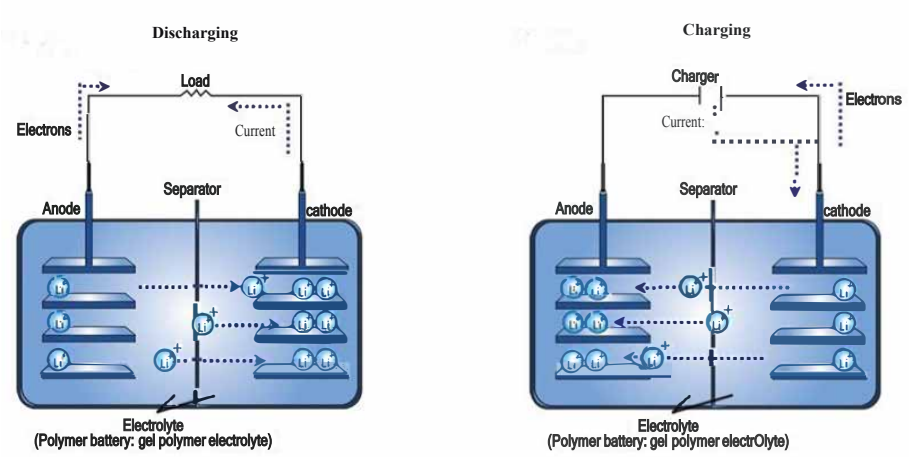

Figure 2.6: Charge and discharge process in Li-ion batteryy.

Li-ion cells are manufactured in various types of cell formats and geometries. Some of them are illustrated in Fig. 2.7[72].

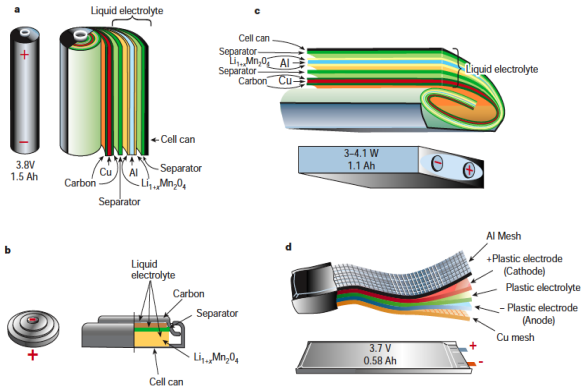

Figure 2.7: Different Lithium-Ion cell configurations: a) cylindrical, b) coin, c) prismatic, d) pouch.

2.6 Battery Models

A major obstacle in PHEV commercialization is the high cost of the battery pack. To address this issue, different solutions such as energy density improvements, reduction of material cost, etc. could be considered. To come up with an optimal solution, one approach is to develop battery models. Battery modeling, in fact, provides information on battery charging/discharging and transient behavior and health status of the battery (battery degradation) as a function of different stress factors (temperature, discharge rate, etc.). EV designer use battery models for sizing the required battery and predict the battery performance. Battery models are also used for on-line self-learning performance and SOC estimation in BMS [73–75]. Common battery models used in the automotive applications are reviewed in the following sections.

2.6.1 Electrochemical Models

Battery modeling based on electrochemical equations provides a deep understanding of the physical and chemical process inside the battery and makes it useful when designing a cell, but high computational time makes these models improper for applications with high dynamics. The first electrochemical modeling approach to porous electrodes with battery applications was presented by Newman and Tiedemann in 1975 [76]. In the porous electrode theory, the electrode is treated as a superposition between the electrolytic solution and solid matrix, the matrix itself is modeled as microscopic spherical particles where lithium ions diffuse and react on the sphere surface. This approach was expanded to include two composite models and a separator by Fuller et al. in 1994 [77]. This model was later adapted for Ni-MH batteries [78], and then Li-ion batteries.

2.6.2 Equivalent Circuit Models

Equivalent circuit-based modeling (ECM) is suitable for automotive real time applications (such as BMS design), since it does not need deep understanding of electrochemistry of the cell and at the same time it is well capable of simulating the battery

dynamics. ECMs simulate the battery as a circuit often composed of resistors, capacitors, and other elements. There is a wide selection of models depending with tradeoffs of accuracy and time required. A large capacitor or ideal voltage source is selected to represent the open-circuit voltage (OCV), with the remainder of the circuit representing battery internal resistance and dynamic effects (e.g. terminal voltage relaxation). Generally, each observed phenomena is modeled with an individual circuit component. For example, the bulk electrolyte resistance is represented with a simple resistor, R_0. To keep the model simple, similar phenomena (e.g. concentration and electrochemical polarization effects) could be grouped, although this decreases model accuracy. Resistances of other components such as electrodes and separator are additive, and included in R_0. Other phenomena including the polarization effect of the battery are usually represented by capacitors and resistors in parallel. In addition, diffusion effects are represented by a Warburg element. In the following, common ECMs used in EV applications are presented.

Simple Resistance (R_{int}) Model

the R_{int} model as shown in Fig. 2.8 is the simplest equivalent circuit battery model. It includes an ideal voltage source and resistance R_0. R_0 is usually defined as a function of SOC and temperature and operation modes (charge, discharge) calculated from HPPC tests [79].

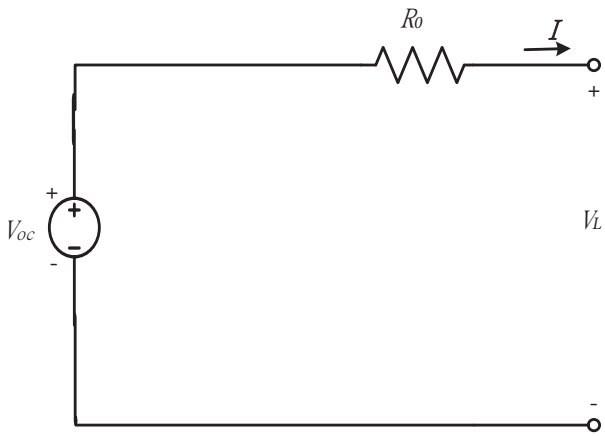

Figure 2.8: R_{int} model equivalent circuit diagram.

RC Model

The resistor capacitor (RC) model shown in Fig. 2.9, consists of three resistors and two capacitors. R_t , R_e, and R_c represent the resistance across the terminal, bulk solution, and surface respectvely. C_b represents the battery's ability to chemically store charge. C_c, which has a small vlaue, represents battery surface effects [79].

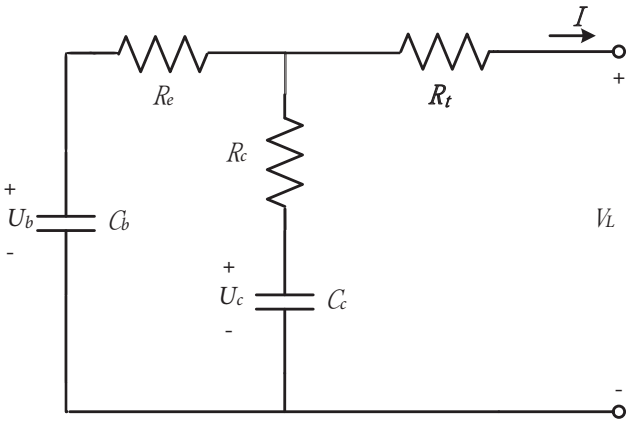

Figure 2.9: RC model equivalent circuit diagram.

Thevenin Model

Thevenin Model circuit structure is shown in Fig. 2.10. E_0 describes the battery's open circuit voltage. R_0 describes battery's internal resistance. $I(t)$ is the battery's charge or discharge current and $V(t)$ is the battery's terminal voltage. the RC circuit describes the battery polarization [80] .

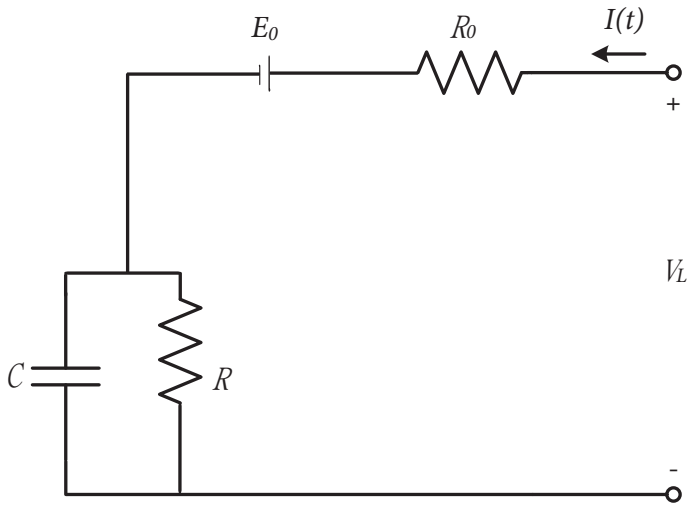

Figure 2.10: Thevenin model equivalent circuit diagram.

DP Model

Although a single RC component is capable of modeling polarization (like Thevenin), but, it becomes less accurate at the end of charge or discharge. The DP model shown in Fig. 2.11 improves the polarization characteristics by simulating the concentration and electrochemical polarization effects separately. R_{pa} and R_{pc} represent electrochemical and concentration polarization respectively. C_{pa} and C_{pc} characterize the transient response during power transfer for electrochemical and concentration polarization respectively [79].

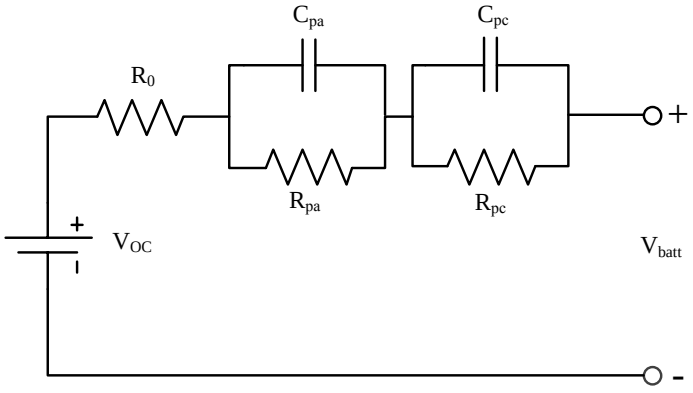

Figure 2.11: DP model equivalent circuit diagram.

EDP Model

The expanded dual polarization (EDP) is shown in Fig. 2.12. The model components and their corresponding EIS features are also shown in Fig. 2.13. R_0 corresponds to the cell bulk resistance (conductivity of the electrolyte, separator, and electrodes). C_{pa} and R_{pa} correspond to the semi-circle at high frequencies representing the SEI layer resistance. C_{pc} and R_{pc} correspond to the semi-circle at medium frequencies representing the faradic charge-transfer resistance and double-layer capacitance. Also, the Warburg element corresponds to the low frequencies representing the diffusional effects of lithium ion between the active material and electrolyte, (straight line at the very end in Fig. 2.13) [29]. The combination of R_3 and W are refred to as "faradic impedance", reflecting kinetics of the cell relations.

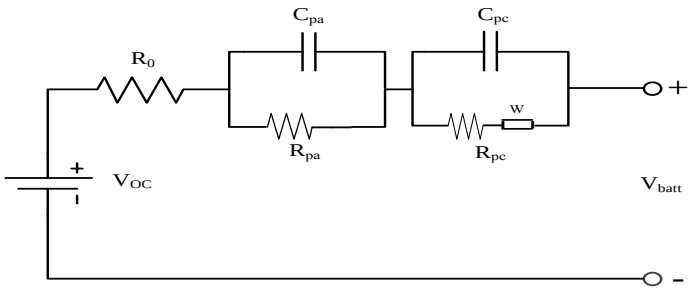

Figure 2.12: Expanded DP model equivalent circuit diagram.

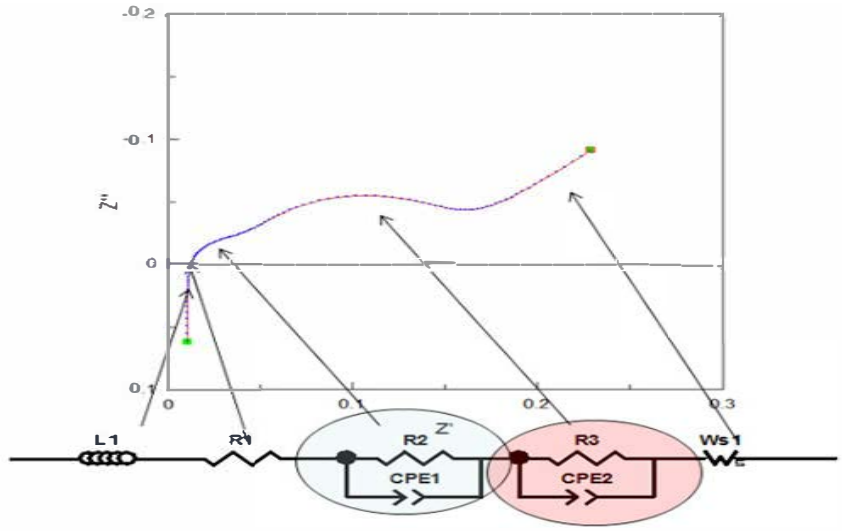

Figure 2.13: EDP model components correlated with EIS results.

2.7 Battery Degradation Modeling

Modeling of degradation is mainly based on the aging experiments and measurements and the complexity of the model depends on the number of stress factors and degradation mechanisms to be incorporated in the modeling. It is worth to mention that each battery type experiences a specific degradation mechanism and not all stress factors have similar impact on different battery chemistries.

To date, assessment and understanding of battery performance in EVs primarily relies on lab testing. Similar to standard driving schedule tests and analyses, these tests and duty cycle analyses have constraints in their validity to real-life operation. A main issue in both cases is that even under specific driving cycles or duty cycles; energy consumption strongly depends on uncontrolled ambient operating conditions. On the other hand, conducting drive cycle analysis using trip data collected from real-life vehicle operation is a challenging task [81]. Although quite helpful in evaluating battery state of health (SOH), very limited effort has been put into field testing with detailed data collection and analysis, mainly because such testing is costly and virtually no control [58].

2.8 Degradation Mechanisms of Li-ion Cells

The other aspect of batteries as traction sources is the battery durability and life which is of much concern in PHEVs. As the battery ages, it becomes less able to store and supply energy. The former is known as capacity fade and latter as power fad. Knowledge about battery durability is also of much importance from the customer point of view, i.e. knowing how far the battery will operate properly over a reasonable period without needing a replacement and additional costs. Of course, it strongly depends on the operating conditions and the environment that the battery is exposed to.

In PHEV applications, the battery lifetime by convention is defined as the time period that the battery loses 20% of its initial capacity [80]. Batteries are designed for 8-10 years of service. However, battery lifetime is affected by several factors. High

power imposed on the battery during acceleration and braking, which could be up to ten times higher than the average power demand, as well as driving behavior, extreme ambient temperature and charging habit all are known to be significant factors on the battery state of health (SOH). To improve the battery performance and lifetime prediction models these effects should be carefully taken into account [81]. Also thermal heating of the cell can significantly reduce the lifetime of a battery.

Li-ion cells undergo degradation in terms of capacity and power capability as result of continuous usage and also during the storage time. The performance degradation during cycling occurs much faster than storage under the same conditions. In the following, normal and accelerated degradation mechanisms for cycling and storage will be described.

2.8.1 Degradation under Storage (i.e. Calendar Aging)

Even under storage status, the active anode material is exposed to the electrolyte through the porous SEI layer, and side reactions enhance this SEI layer. High SOCs or high temperatures result in more severe capacity fading and resistance growth (power fading) in the cell as well. Therefore, to slow down the electrochemical processes and improve battery life, Li-ion cells need to be stored under optimal conditions (40% SOC and 15°C [82]). This will allow Li-ion cell last many times longer than one stored at 100% charge, particularly at high temperature.

2.8.2 Degradation during Cycling

Capacity fading primarily occurs on the electrode/electrolyte interphase under influence of intercalation and deintercalation of lithium ions. Ideally, loss of lithium ions and active material are the only mechanisms that degrade a Li-ion cell. But, in practice, other degradation mechanisms accelerate the capacity fading. Power fading is also coupled to capacity fading. The growth of the SEI layer results in the internal impedance rise of the battery cell and the deformation of the electrodes in a lower conductivity. As a result the power fading occurs due to the loss of active material.

Capacity fading can be divided into four stage as shown in Fig. 2.14. During stage "A", on the interphase of the anode with the electrolyte of the separator a Solide Electrolyte Interphase (SEI) film will form as a side reaction; this results in the fast decrease of capacity. This stage does not last for many cycles because as the cell is cycled more, the side reaction rate will gradually decay [83]. A schematic of a Li-ion cell with SEI layer is given in Fig. 2.15.

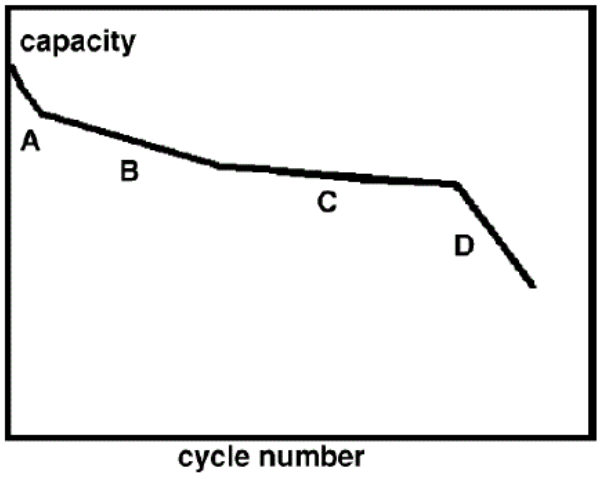

Figure 2.14: The general shape for capacity versus cycle number.

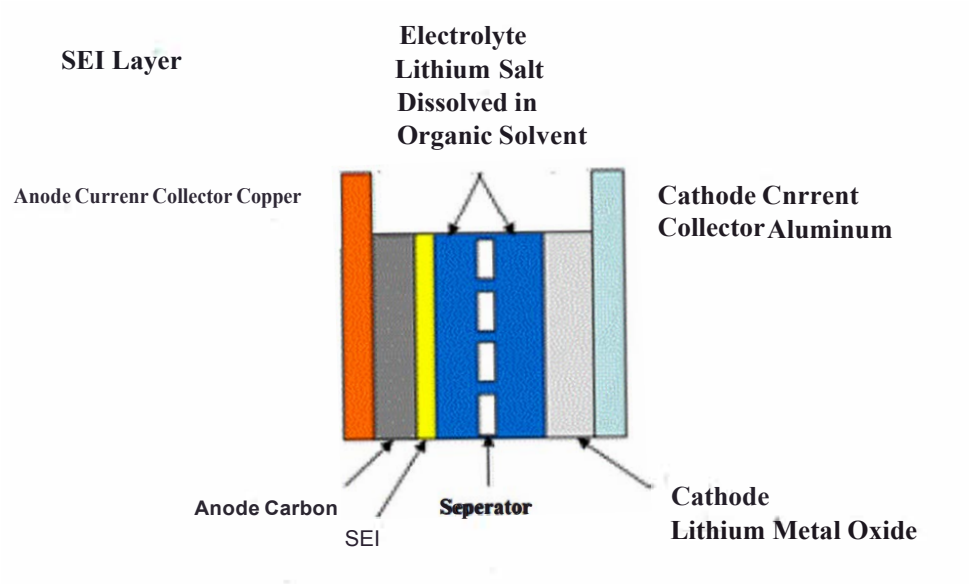

Figure 2.15: Schematic of SEI film layer in Li-ion battery.

In the stage B, anode is the limiting electrode [83]. Due to the SEI film layer formed on the anode, less active material is available and less lithium ions are intercalated into the anode during charging. As a result the loss rate of lithium ions will be slower, and the SEI layer protects the anode from reduction reactions with the electrolyte. During continuous intercalation and deintercalation the SEI layer cracks and more active material will be exposed. This will cause more side reactions and the SEI layer will continue to grow, leading to a less porous SEI layer and loss of lithium ions.

In stage C, the degradation rate of the active cathode material is higher than the loss of lithium ions. On the cathode/electrolyte interphase layer similar to the SEI layer is formed, which is named the Solid Permeable Interphase (SPI) [84]. This layer will also grow due to cycling and limit the active cathode material. The anode is however still the limiting electrode in this stage, as there is still more active cathode material available than lithium ions.

In stage D, due to the high degradation rate of the cathode, the cathode becomes the limiting electrode. Less active cathode material is available than the amount of cycleable lithiumions [83]. Not all the lithiumions that were intercalated into the anode during charging can be intercalated into the cathode during discharge. Hence, more and more lithium ions are stuck inside the anode. The cathode will be fully intercalated during discharge, which raises the active cathode material loss rate. These added effects cause an accelerated capacity fading and the capacity will rapidly decrease.

The severity of these stages is not the same for different types of Li-ion cells. For example, for LiFePO4, the main capacity fading mechanism cells is the loss of lithium ions by the lithium ion consuming SEI film later formation, which also results in a loss of active anode material [83]. Loss of cathode material happens at a lower rate for LiFePO4 cells, since neither cycling nor temperature change enhances the formation of the SPI layer [84]. This causes LiFePO4 cells to have a much higher cycling life compared to other chemistries.

2.9 Accelerated Degradation during Cycling

Stress factors like extreme temperatures, large C-rates and high SOC have negative impact on the cell capacity and cause accelerated degradation. In the following each of these stress factors will be described.

Depth of Discharge

The cycle life of a cell is strongly dependent on the DOD. Fig. 2.16 [85] shows typical curve of cycle number against the DOD. The deeper the discharge, the more intercalation and deintercalation takes place in the electrodes. The loss of lithium ions and active electrode material is higher for larger DOD cycles. At high DODs, additional degradation mechanisms can occur resulting in decomposition and dissolution of cathode material and capacity fading [86]. DOD has no influence on the capacity fading of LiFePO4 cells, but the charge or energy processed is the determining factor [85].

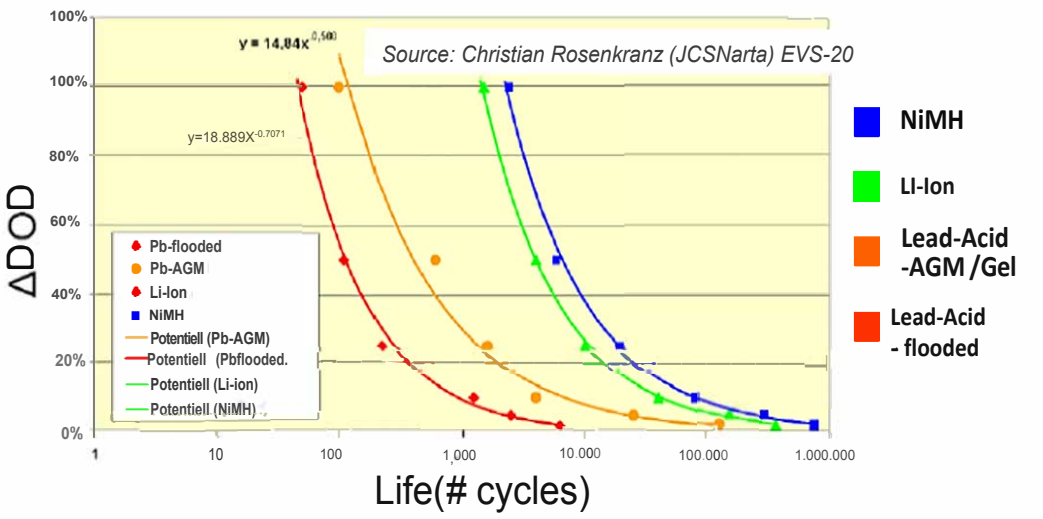

Figure 2.16: Cycle life vs.ΔDOD curve for different battery cell.

C-rate

High currents generate more heat and cause the temperature of the cell to rise invoking the high temperature degradation mechanisms. High currents also cause local over potential of the electrodes; it means that the maximum voltage for the cell is reached at an earlier stage at certain areas of the cell. High C-rates will also cause the

SEI layer on the anode to crack faster. More active anode material is exposed and the SEI layer will restore itself, reducing lithium ions from the battery cell process. High C-rates will furthermore cause additional strain on the electrode materials, resulting in increased deformation and loss of active material [86]. These effects will all result in capacity and power fading.

Temperature

Li-ion cells have an optimal temperature operating range (Fig. 2.17 [87]); outside this range the battery cell undergoes severe loss of capacity. High and low temperatures have different effect on the battery life.

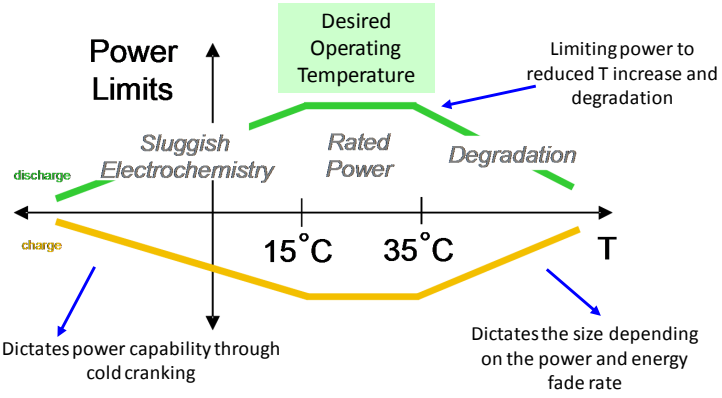

Figure 2.17: Example-Battery cell's temperature range for optimal cycle life.

At low temperature, due to the higher activation energy needed for the chemical reactions and lower ion diffusion; there will be a loss of capacity and deliverable power. However, when the temperature is restored to nominal level, the capacity and power capabilities will be recovered. Under normal discharge, low temperature on its own does not have any permanent influence on capacity fading, but during charging, lithium plating is likely to happen because the intercalation rate at the anode is inherently slower than the deintercalation rate [88].

High temperature, in the long term, may cause severe damages to the cell. As is shown in Fig. 2.18 increasing temperatures results in higher capacity fading. Due to high temperatures the SEI layer will slowly break down and dissolve into the electrolyte. The active material of the anode will be partly exposed to the electrolyte

again, causing the side reactions. The damaged SEI layer will be restored due to the side reactions or a precipitation of the dissolved SEI particles will take place. Also parts of the cathode can dissolve into the electrolyte and incorporated into the SEI layer. As a result the intercalation at the anode will be more difficult and the ionic conductivity will be lowered. The same degradation mechanism happens at the cathode side with the SPI layer. Another degradation mechanism is the deformation of the anode and cathode. Detailed discussion of high temperature effect is available in [86].

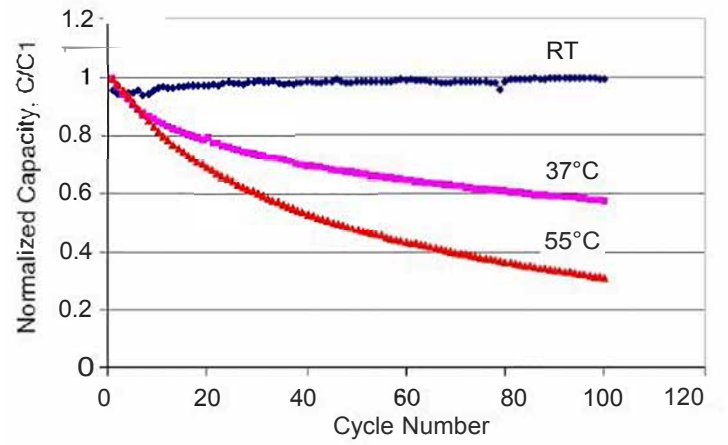

Figure 2.18: The accelerated capacity fading due to high temperatures.

State of Charge

At higher SOC battery cell is more reactive, which will accelerate degradation of the cell. At high SOC the anode will be highly energized and self-discharge will also be higher and the SEI layer will grow faster. Furthermore, electrolyte oxidation occurs at high SOC, leading to impedance increase. These effects result in capacity and power fading. During storage for a long time, high SOC will have more profound effect. In case of overcharge or over discharge, other degradation mechanisms come into play:

Overcharge

When the cell is charged over the specified voltage, a small increase in capacity is initially obtained, but the cycle life is strongly reduced. This effect is stronger as the end of charge voltage increases. During overcharge electrical energy is pumped into the battery, but more intercalation can hardly take place. This will be represented

by a sharp increase of internal resistance and the temperature [27]. Decomposition of the binder and electrolyte, forming insoluble products, blocking the pores of the electrodes, and causing gas generation subsequently may take place [89].

Over discharge

When the cell is discharged under the specified cut-off voltage, two degradation mechanisms severely damage the cell. 1- Corrosion of the copper current collectors on the anode side of the cell and dissolution into the electrolyte resulting in loss of contact with anode and power fade [90]. 2- Decomposition of the SEI layer on the anode. The high anode potential will cause dissolution of the SEI layer. Upon recharge the exposed active material will cause side reactions to restore the SEI layer and reducing lithium ions, causing capacity fading [83].

2.10 Vehicle Modeling

Many different architectures of an electric vehicle exist [91] as there are many possibilities, e.g. , 1 to 4 electric machines, DC or AC machines, gear box/no gear box, high or low battery voltage, one or three phase charging, etc. However, in this thesis the architecture in Fig. 2.19 is chosen [67].

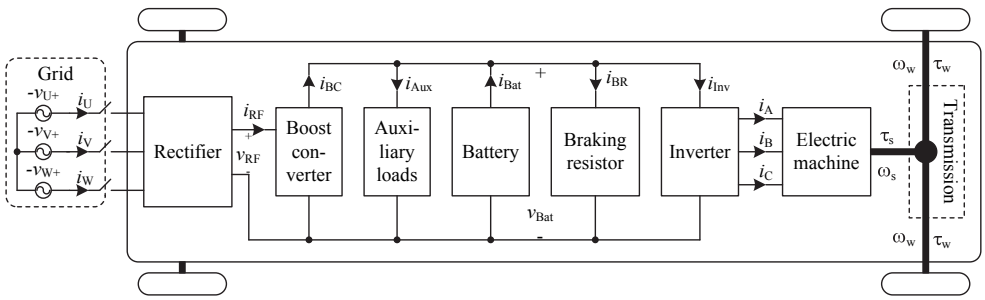

Figure 2.19: Architecture of the battery electric vehicle.

2.10.1 force model

The forces which the electric machine of the vehicle must overcome are the forces due to gravity, wind, rolling resistance, and inertial effect. These forces can also be seen in

Fig. 2.20 where the forces acting on the vehicle are shown.

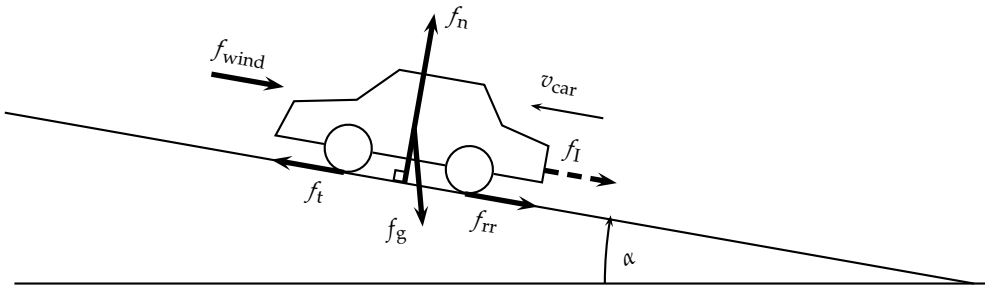

Figure 2.20: Free body diagram of the forces (thick arrows) acting on the car.

The traction force of a vehicle can be described by the following two equations [67]:

$$f_t = \underbrace{M_{car}\,\dot{v}_{car}}_{f_I} + \underbrace{M_{car}\,g}_{f_g}\sin(\alpha) + \text{sign}\,(v_{car})\,\overbrace{\underbrace{M_{car}\,g\,\cos(\alpha)}_{f_{rr}}}^{f_n}\,c_{rr}$$
$$+\text{sign}\,(v_{car}+v_{wind})\,\underbrace{\frac{1}{2}\,\rho_{air}\,C_{drag}\,A_{front}\,(v_{car}+v_{wind})^2}_{f_{wind}} \tag{2.1}$$

$$c_{rr} = 0.01\left(1+\frac{3.6}{100}\,v_{car}\right), \tag{2.2}$$

where: 3.492ptf_t [N] Traction force of the vehicle

f_I	[N]	Inertial force of the vehicle
f_g	[N]	Gravitational force of the vehicle
f_{rr}	[N]	Rolling resistance force of the wheels
f_n	[N]	Normal force of the vehicle
f_{wind}	[N]	Force due to wind resistance
M_{car}	[kg]	Mass of the vehicle
α	[rad]	Angle of the driving surface
$\dot{v}_{car}$	[m^2/s]	Acceleration of the vehicle
v_{car}	[m]	Velocity of the vehicle
$g = 9.81$	[m^2/s]	Free fall acceleration
$\rho_{air} = 1.2041$	[kg/m^3]	Air density of dry air at 20°C

c_{rr}	$[-]$	Tire rolling resistance coefficient
C_{drag}	$[-]$	Aerodynamic drag coefficient
A_{front}	$[m^2]$	Front area
v_{wind}	$[m/s]$	Headwind speed

2.10.2 Auxiliary loads

The main purpose of the battery is to provide power for the wheels. However, a modern car have also other loads which the battery should supply. These loads are either due to safety, e.g., light, wipers, horn, etc. and/or comfort, e.g., radio, heating, air conditioning, etc. These loads are not constant, e.g., the power consumption of the climate system strongly depend on the surrounding temperature. It is reported that, in an EV, AC may reduce the driving range up to 35%, depending on the AC usage frequency [47]. The loads are more significant when the climate-control systems are used in an initially very hot or very cold cabin at the beginning of a trip. Associated with the range reduction, there would be increased battery degradation for the same distance driven when AC/heating system is operating Even though some average values are suggested which can be seen in Table 2.3. From the table it may be understood that the total average power consumption is $p_{\text{Aux}} = 850W$ [67].

Table 2.3: Average power level of the auxiliary loads of the vehicle.

Radio	50 W
Heating Ventilation Air Condition (HVAC)	500 W
Lights	300 W
Total	850 W

2.10.3 Duty cycle and driving cycle

In the analysis of the driving and charging data, terminologies such as drive cycle, duty cycle, and driving pattern are frequently used. A drivecycle refers to a history of driving, typically represented by a speed versus time curve. A dutycycle refers to a

history of power usage of a device, typically depicted by a power versus time curve. A driving pattern is used to describe a driving condition, taking into account both road condition (e.g, road type) and driving behavior. Also, the duration between two successive stop is called driving pulse or micro trip which is represented in Fig. 2.21. Among popular standard drive cycles used in vehicle design and development are, urban dynamometer driving schedule (UDDS), US06 and highway fuel economy test cycle (HWFET), which represent city driving, aggressive driving (high speeds and accelerations) and highway driving respectively [90].

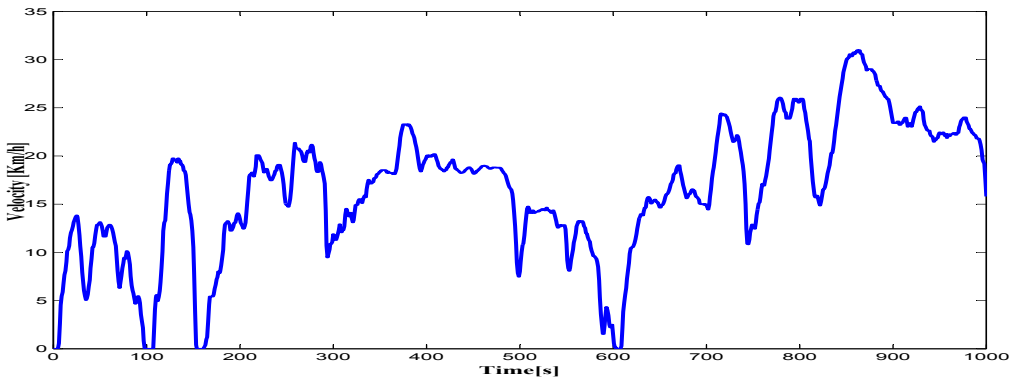

Figure 2.21: Schematic of a driving cycle broken down into a series of sequential isolated "driving pulses" or "micro trip".

In Fig. 2.22 the velocity plot is shown for the New European Driving Cycle (NEDC) which is a widely used driving cycle for certification of vehicles in Europe.

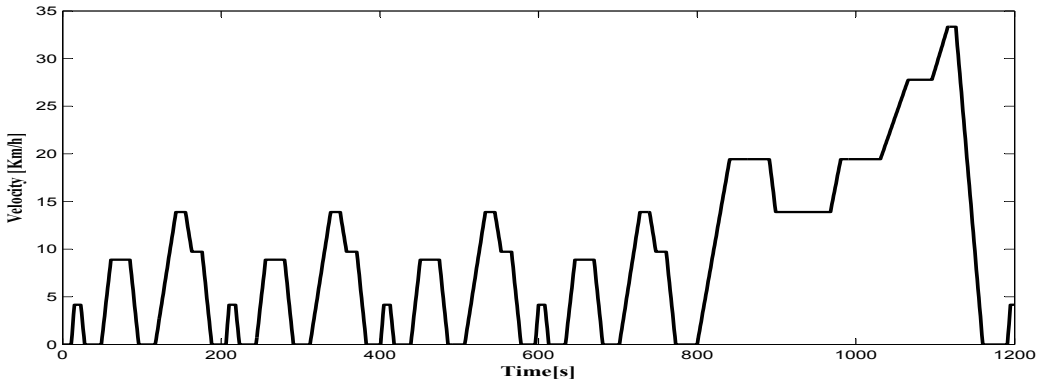

Figure 2.22: Velocity plot for the NEDC.

2.11 Conclusion

This chapter provides a summary of published literature on battery modeling, model parameters identification and extraction, and state of charge and state of health estimation. It is specifically intended for batteries used for energy storage in electric and hybrid vehicles. Moreover, temperature's effect on Li-ion batteries performance is discussed. The right conditions for decreasing capacity fading for storing batteries are discussed. The capacity fading increases by keeping batteries at high SOC or high temperature. A schematic overview on aging mechanisms for lithium-ion cathode materials is also provided.

The modeling of an electric vehicle has been presented. Matlab/Simulink based simulation models have been developed based on force traction equation.

CHAPTER 3

PROPOSED MODEL DEVELOPMENT AND PARAMETERS EXTRACTION.

Contents

3.1 Introduction

The focus of this chapter is on proposing a battery model suitable for vehicle modeling purposes. In the first part, thermal characterization and a thermal ramp model developed for prismatic lithium iron phosphate cell (LFP) is presented. In the second part, a dynamic model of a cell performance based on two techniques, Electrochemical Impedance Spectroscopy (EIS) and a current pulses tests conducted on a similar cell is proposed and validated.

In this work, we focus on getting the advantages from each method. Hence, the proposal model is a blend of the electrical circuit battery model and the impedance-based model [92]. The electrochemical impedance spectroscopy is capable of estimating the thermal behavior and non-linear phenomena [93]. Therefore, the proposed model can accurately capture the dynamic electro-thermal and non-linear behaviors for any operating conditions.

The battery cells chosen for the experimental testbed presented in this chapter are 30 Ah, LiFePO4 prismatic cells manufactured by GP Betteries. These prismatic cells offer high energy density, safety, and improved cycle life. They are also easier to assemble in battery packs compared to pouch cells. Some of the important specifications of the LiFePO4 battery cells, provided by the manufacturer, are summarized in Table 3.1

Table 3.1: The battery cell parameters

Nominal capacity	30Ah
Nominal voltage	3.2V
Max. discharging current	300A
Upper voltage limit	3.65V
Weight	1.1kg

3.2 Thermal Characterization

Depending on ambient conditions, there may be a need to remove or add heat to the battery in order to maintain the optimal temperature range and distribution. Non-uniform temperature distribution results in low charge and discharge performance and cell unbalancing over time. Existing thermal management techniques include applying liquids, insulations and phase-change-materials [36]. Essential tools in automotive pack design and thermal management are thermal and performance models. Such models require inputs such as system and operational parameters. Not all of these parameters are easy to directly quantify (e.g. heat effect and transport properties) because their effects cannot be isolated; thus extensive tests are necessary to yield a clear understanding of heat generation and cell performance [35]. However, a simple model based on a limited number of lab tests may serve as an adequate alternative. In this section, the heat generation and temperature distribution over the cell surface in a commercial EV presmatic cells are evaluated through detailed thermal performance tests. The main objective is to provide a baseline performance model that can be modified to account for ageing in later studies. It should be noted that cycling required for testing will age the cell (affecting subsequent test behavior).

3.3 Model Developement

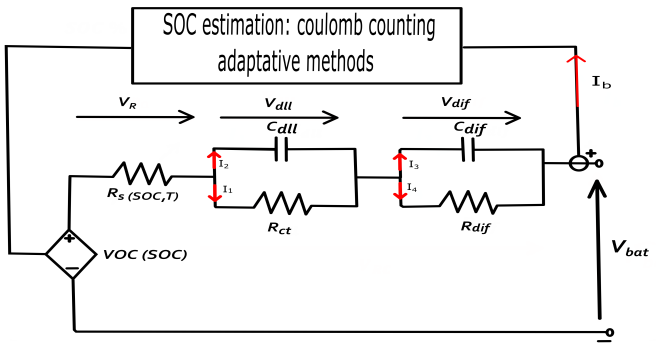

Figure 3.1: Li-ion battery cell equivalent circuit.

As shown in Fig. 3.1, the circuit is mainly composed of voltage-controlled voltage source to represent the cell open-circuit voltage V_{OC}, which depends on SOC and effects by temperature, a serial resistance R_s depends on SOC, temperature T and current sign, which causes the instantaneous drop voltage V_R when step load applied to battery and R_{dll}, C_{dll}, R_{dif}, C_{dif} are responsible for transient response, which depend on the SOC, the temperature, and environment conditions.

The cell terminal voltage V_{bat} can be determined due to the cell open circuit voltage, voltage drop caused by the serial resistance and transient voltage (V_{dll} and V_{dif}), so the terminal voltage can be described by the following equation:

$$V_{bat} = \quad V_{OC}(SOC) - V_R - V_{dll} - V_{dif} \tag{3.1}$$

$$\tag{3.2}$$

Where V_R;

$$V_R = \quad R_s * i_b$$

The SOC cell can be expressed as [94]:

$$SOC = 100. \quad \left(SOC_{int} - \int \frac{\eta \left(I_d - I_{sd} \right)}{Q_n} dt \right) \tag{3.3}$$

Where η is Coulombic efficiency, Q_n the nominal capacity of a cell, I_{sd} is the self-discharge current, I_d is draining current and SOC_{int} is the initial value of SOC.

Theoretically, the self-discharge of battery depends on the temperature and cycle number, in addition, the Li-ion has an ultra-low self-discharge rate. Therefore, the phenomenon can be simplified, or even ignored, without suffering any significant errors. Additionally, the Coulombic efficiency of lithium-ion battery can be considered one $\eta \approx 1$ [95], the equation simplified to:

$$SOC = \quad 100. \left(SOC_{int} - \int \frac{I_b}{Q_n} dt \right) \tag{3.4}$$

Considering a time interval $t_0 < t < t_1$ in which a constant current is drained from battery $i_{cell} = I$ and for the remaining of period $t_1 < t < t_2$ the current $i_{cell} = 0$.

Therefore, the voltages and currents which describe the characteristics of the R_{ct}, C_{dll}, R_{dif}, C_{dif} circuit is shown in Fig. 3.1 are expressed by following:

$$V_{dll} = \frac{\int I_2 \quad dt}{C_{dll}} = \quad R_{ct} * I_1 \tag{3.5}$$

$$V_{dif} = \frac{\int I_4 \quad dt}{C_{dif}} = \quad R_{dif} * I_4 \tag{3.6}$$

From Equation. 3.5 and Equation. 3.6:

$$V_{dll} = \begin{cases} R_{ct} * i(t)_{cell} \left(1 - e^{-\frac{t-t_0}{\tau_{dll}}}\right) & t_0 < t < t_1 \\ v(t_1)_{dll} * e^{-\frac{t_1-t_2}{\tau_{dll}}} & t_1 < t < t_2 \end{cases} \tag{3.7}$$

$$V_{dif} = \begin{cases} R_{dif} * i(t)_{cell} \left(1 - e^{-\frac{t-t_0}{\tau_{dif}}}\right) & t_0 < t < t_1 \\ v(t_1)_{dif} * e^{-\frac{t_1-t_2}{\tau_{dif}}} & t_1 < t < t_2 \end{cases} \tag{3.8}$$

Where $\tau_{dif} = R_{dif} * C_{dif}$ and $\tau_{dll} = R_{ct} * C_{dll}$ are long and short-time constants respectively.

Theoretically, the open-circuit voltage is usually measured as the steady state open-circuit terminal voltage at different SOC points. However, these measurements can take days to reach each point. Nevertheless, in light of extrapolation and averaging procedures we can ascertain the true OCV. In general, the open-circuit voltage is a function of SOC and operating temperature (cell heat generation and environmental temperature). Hence, it is important to include the non-linear relation between SOC and OCV. In this work, the non-linear relation is estimated by:

$$\begin{aligned} V_{OC}\,(SOC) \quad &= \quad x_1 \times exp(\text{-}x_2 \times SOC) + x_3 \times SOC^3 \\ &\quad + x_4 \times SOC^2 x_5 \times \ SOC + x_6 \end{aligned} \tag{3.9}$$

Where $x_{1...6}$ are parameters estimated to make the battery model fits the real battery behavior because this voltage can not be identical for all batteries, even if they were fabricated from the same materials.

In fact, the Li-ion battery internal resistance is divided into two fold. The first one is polarization resistance and second is ohmic resistance. The polarization resistance depends on electrochemical reaction, counting the resistance created by electrochemical polarization and the concentration polarization. The ohmic resistance consists of electrolytes resistance, separators resistance, electrode material resistance and contact resistance of different components. In addition, the term inner resistance must be considered with caution since it is not a simple ohmic resistance and relies on estimation methodology for its determination, on a state of charge SOC and on the battery temperature, further, it influenced by battery materials, fabricating processes, battery structure, and geometrical electrode. Moreover, the internal resistance cannot be measured directly, it only determined by measuring battery voltage and current. Taking into account all these conditions, an original non-linear relation developed in our laboratory to describe the evolution of internal resistance versus temperature T, SOC, and current sign.

$$R_s(SOC, T, I) = (a * T + b) * e^{(-|I| * SOC)} + c \tag{3.10}$$

Where T is the temperature in Kelvin. The parameters a, b, and c are determined using the least-squares curve fitting method and they are experimentally determined and explained in the next sections.

In order to identify the parameters of battery proposed model and to comprehend their electrical behavior at steady-state and in transient operation, numerous battery characterization tests are used in the literature [96]. In general, these tests involve identification of the open circuit voltage OCV, capacity Q_n, internal or ohmic resistance R_s and RC circuit network. Among battery characterization tests commonly used in a field of battery modeling, there are basically two methods [96]: current pulses tests at different temperatures and electrochemical impedance spectroscopy EIS tests, the experimental procedure of both techniques will be explained in the next sections.

3.4 Model Formulation

In order to analyse the effect of a varying discharging current at different temperatures on cell energy capability. The RC blocks model with numerical parameter estimation scheme using tests on LFP cells under different operating conditions was implemented using MATLAB, Simulink and Simscape. The tests performed on LFP cells revealed the dependencies of the model parameter (OCV, series resistance and RC block) on temperature and SOC. These dependencies were implemented into the model as a two-dimensional lookup tables and functions (by using the previous equations 4.1, 4.3) that determine the values of each circuit elements during the simulation stage at three different temperatures ($40°C$, $25°C$, $10°C$, $0°C$) and different SOC (100%, 90%, 80%, 50%, 20%, 10%). Since we want to analyze the energy and power capability of the cell at fixed temperature, the thermal effects of the convective heat exchange between the cell and the environment are not considered and the input temperature of the battery is constant over the charge/discharge cycle.

Fig. 3.2 shows the Simulink blocks used for the simulation. The input parameters of the simulation, charging/discharging current and temperature. Based on the SOC, current and temperature at time t, the cell model is able to set the impedance parameter values (lookup tables) necessary to calculate the dynamic of the battery and gives the output values, which will act as inputs for the following iteration.

3.5 Experimental setup

The thermodynamics of Li-ion cells is complicated due to the complexity and diversity of materials involved. To obtain a reliable prediction of the temperature profile, the total heat generation must be evaluated. Therefore, the temperature variation and heat dissipation of cells under a variety of loading conditions must be measured to provide a baseline for simple but high fidelity models of batteries at higher scales (module, pack).

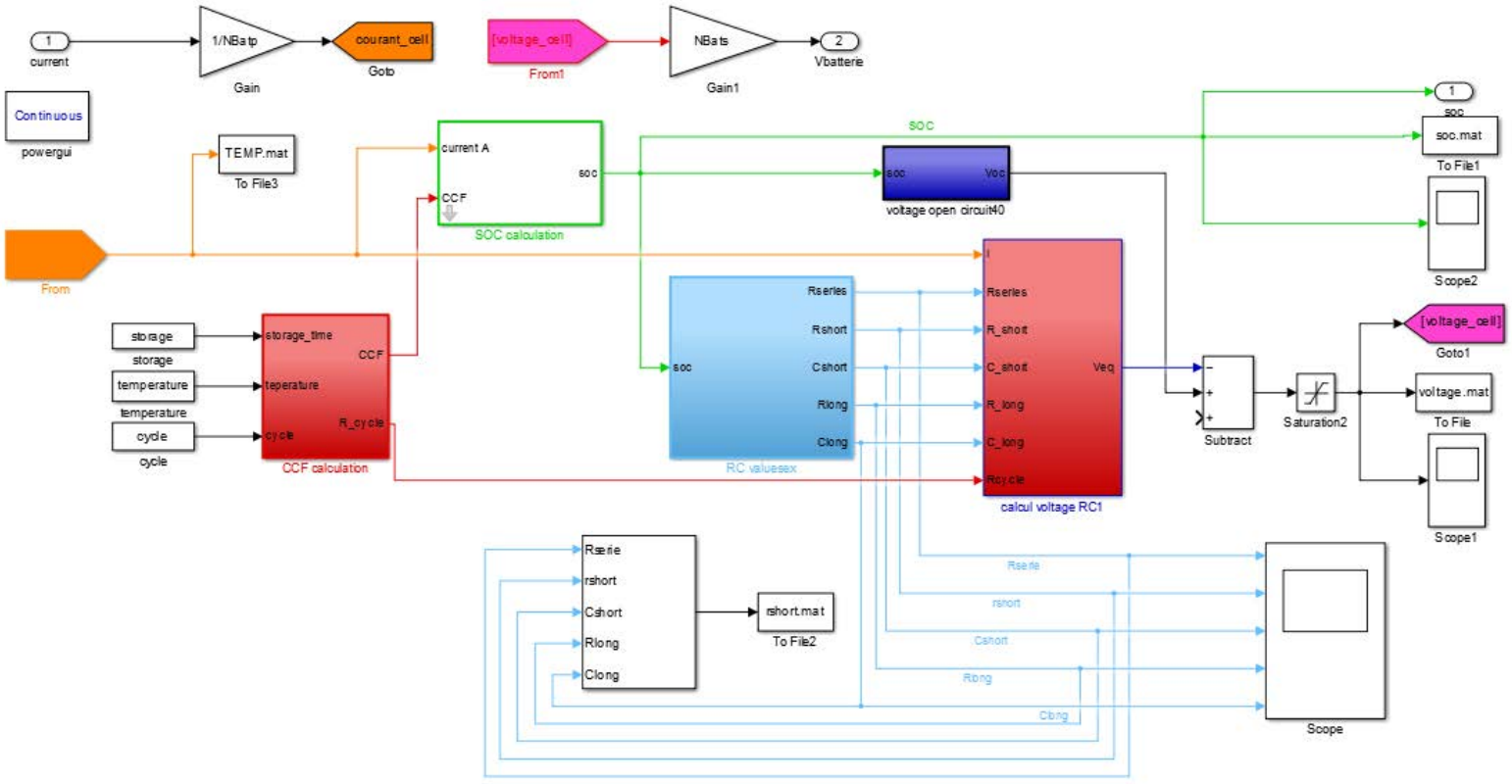

Figure 3.2: Simulink scheme of the battery cell with charging/discharging interface.

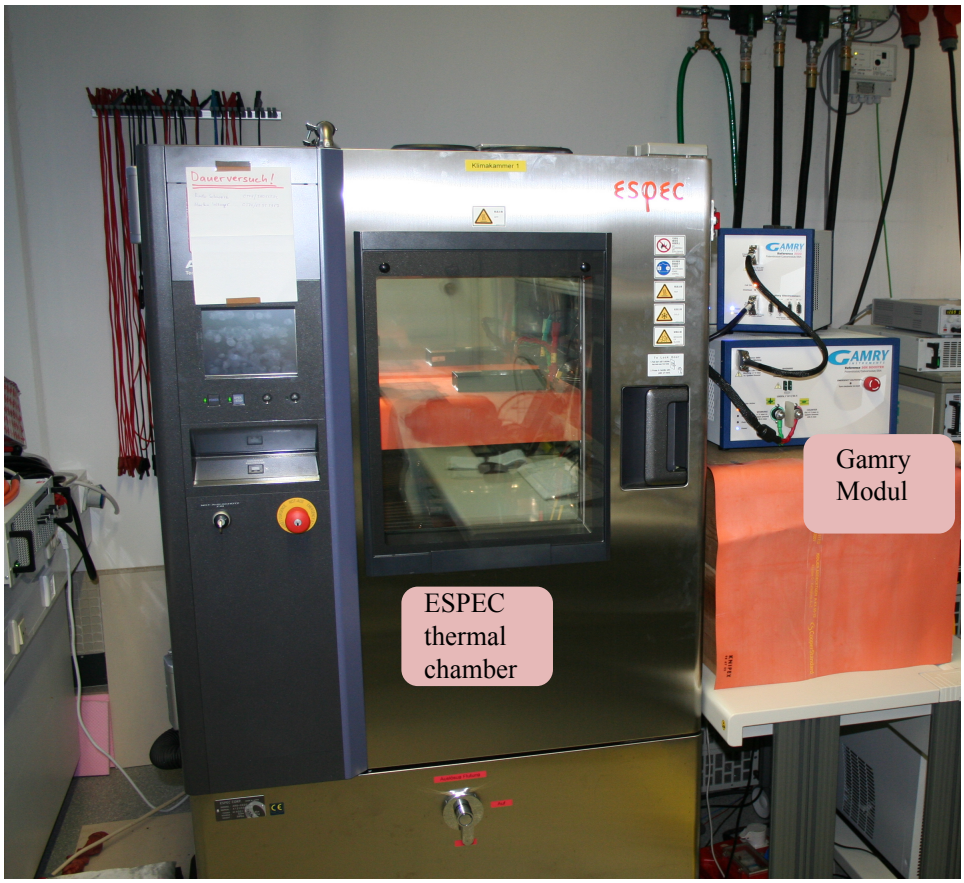

Figure 3.3: Battery cycling test bench.

The configuration of the battery test bench is shown in Fig. 3.3. where we use battery test equipment, GAMRY 3000/30K booster potentiostat/galvanostat to charge / discharge cell with a maximum voltage of 20V and a maximum current of 30A and provides the EIS measurement.

Temperature test chamber (ESPEC,), which was used to maintain the desired cell temperature, also we used a prismatic Li-ion cell 30Ah (LFP-G). This type of cell is designed for high power and lifetime demands. The current-voltage data was logged every second or every change greater than 1 mV. The system directly tracks the charge and discharge capacity based on automatic integration of the current-time data.

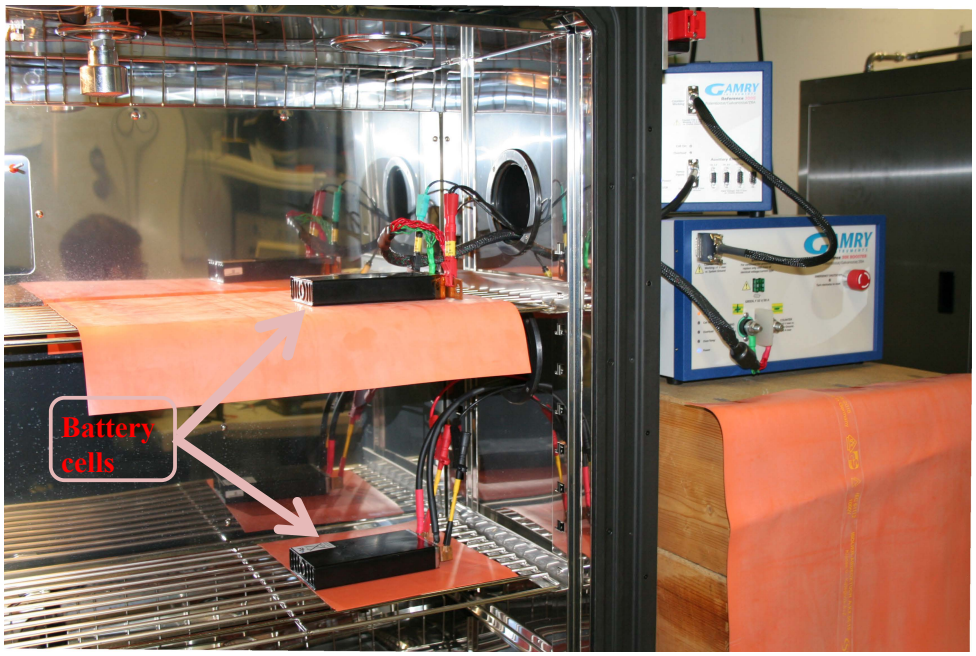

Figure 3.4: Battery setup in thermal chamber.

Figuers 3.3 and 3.4 depict the cell test setup inside thermal chamber.

3.5.1 CHARACTERIZATION

The characterization tests that will be run on individual battery cells are chosen among the enhanced tests proposed in [4]. It should, however, be noted that charge and discharge current magnitudes for these tests are modified due to limitations on the power supply and electronic load ratings. These tests cover the majority of general characterization experiments required for battery system development.

In this study, a series of tests have been carried out to explore the temperature influence and to collect a maximum of data from two points of view:

- The electrochemical view, using the EIS measurements (frequency domain).
- The electrical view, using the current pulse test (time domain).

To achieve our aims a measurements plan was proposed. Before, start any measurement a capacity test has been done, after a complete discharge including constant current discharge at 15A (CC, 0.5) until reaching the cut-off voltage 2V, followed by constant voltage discharge (CV) till the current became less than 1 A, now we are sure that the cell is completely empty. Next is the full charge step which contains a CC charge at 15A till reaching the 3.65V, then charged the cell at a constant voltage until the current was lower than 1.5A(CC/10). After, this necessary step(capacity test), the current pulse test and EIS were conducted at $40°C$, $25°C$, $10°C$, $0°C$ for different values of SOC, In the following the different process of measurements:

1. From 2 to 4 hours rest period after adjusting the temperature to ensure that the cell reached the desired temperature (thermal equilibrium).
2. Full charge CC/CV (capacity test).
3. The cell discharged to the predetermined SOC with C/2 rate.
4. 30 to 60 minutes rest period (potential equilibrium).
5. EIS measurements.

Electrochemical Impedance Spectroscopy (EIS) is an effective electrochemical test tool to analyze the kinetic process of battery. The operating principle of EIS is setof sinusoidal current, which is generated from the EIS equipment and injected into Li-ion battery. Voltage response of the battery is recorded to calculate the battery impedance. The typical frequency range of the EIS test is from mHz to kHz, which associates with different time-scale reaction stages in the battery.

In our case, EIS is done using GAMRY- 3000/30K galvanostatic, at different SOCs (100%, 90%, 80%, 50%, 20%, 10%). The EIS measurements are performed with $\pm 10mV$

perturbation amplitude in the range from 100 kHz to 10 mHz, at a resolution of 10 per decade.

3.5.2 Charge/Discharge Signals

The characterization tests are initialized with a charge/discharge cycle of 1C, which corresponds to (27-30A). Figures 3.5 and 3.6 show the evolution of battery signals during this charge/discharge, respectively.

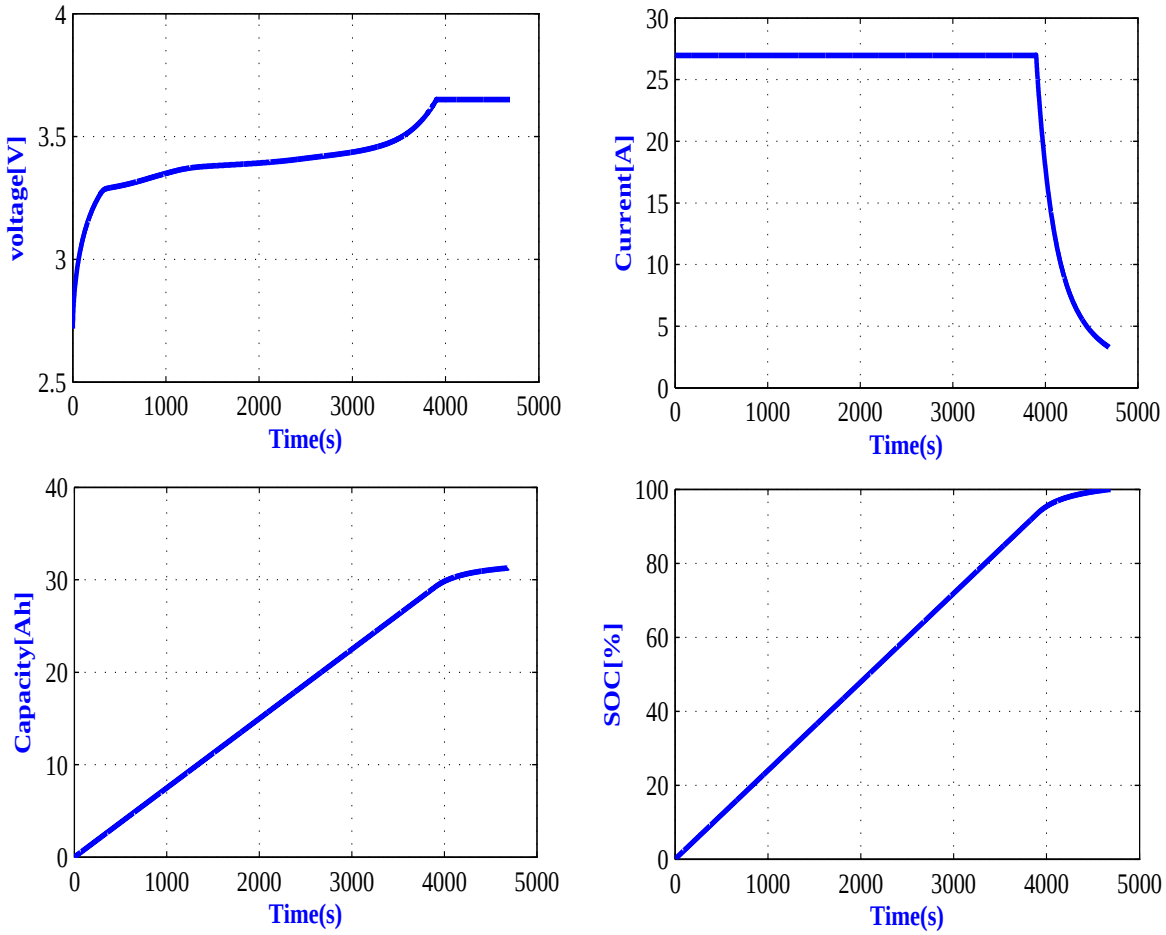

Figure 3.5: Battery charge profile.

Battery charging is performed in constant current constant voltage (CCCV) regime. This is a common battery charging scenario in which a constant current is applied to the battery until its voltage reaches a specified upper limit (in this case 3.65 V). At this voltage limit, the battery will be kept at a constant voltage until its current decays to

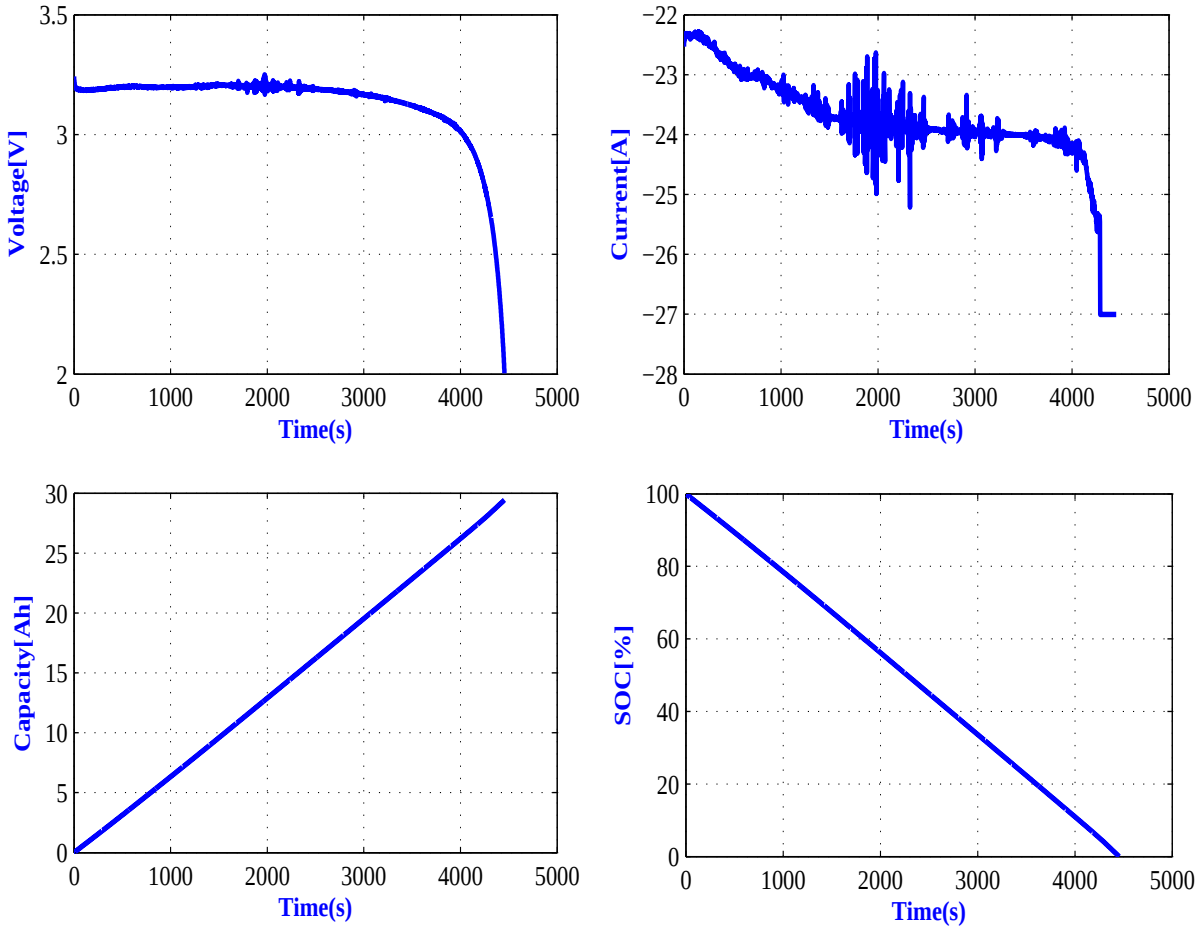

Figure 3.6: Battery discharge profile.

zero. Charge and discharge profiles are terminated according to upper/lower voltage limits prescribed by the manufacturer. As can be seen in Figures 3.5 and 3.6, despite the fact that the cells have a 30 Ah capacity, this nominal capacity cannot be achieved during charge/discharge. The reason for this can be attributed to either inaccurate upper/lower voltage limits in the protection subsystem or incorrect battery nominal capacity. These results magnify the need for characterization tests before any battery system development. Determination of exact battery capacity will be studied in the next subsection. On the other hand, choosing appropriate protection limits for the battery is discussed in the protection system subsection. The rest of the characterization tests are described below.

3.5.3 Static Capacity Test.

The capacity test procedure consists of discharging the cell with constant current until the voltage equals its minimum value, which is 2.0V; followed by 30 min relaxation time. The second step is to supply the empty discharged cell, with constant current corresponding to 1C-rate (30 Ah), until the cell voltage achieves the maximal value. Then, the voltage is regulated at the maximum of cell voltage which is 3.65 V until the charging current equals to 1C-rate/10. At this time, the cell is fully charged. Four tests are carried out with four values of temperature T corresponding to $40°C$, $25°C$, $10°C$, $0°C$. Figure 3.7 illustrate battery voltage, current, SOC, and capacity evolution during these charge/discharge tests.

The capacity Q_n is easy to determine using the equation 3.11, where the I_b is the charge/discharge current. The results are shown in Fig. 3.7. In comparison with the nominal capacity indicated by constructor at 1 C-rate, the measured capacity is perfectly the same.

$$Q_n = \left(\int I_b.dt \right) / 3600 \tag{3.11}$$

After the calculation of the battery capacity, a brief explanation of the proposed profile is given and an associated laboratory procedure is described in the following subsection. The cell is allowed to rest for approximately half an hour before the parameters extraction.

3.5.4 Pulses Current Proposed Profile

Previously, the battery is completely discharge and fully charged in order to determine the capacity. Then the battery tester is programmed to discharged the battery by applying current steps in sequential steps of 5% SoC, considering a 30 min relaxation time between two consecutive pulses, The rest period is intended to let the battery reach thermal and electrochemical equilibrium (the equilibrium is reached when the terminal battery voltage variation is less than 0.2%). At the end of rest step, the Open-circuit voltage V_{oc} is measured. the battery voltage is restricted from reach

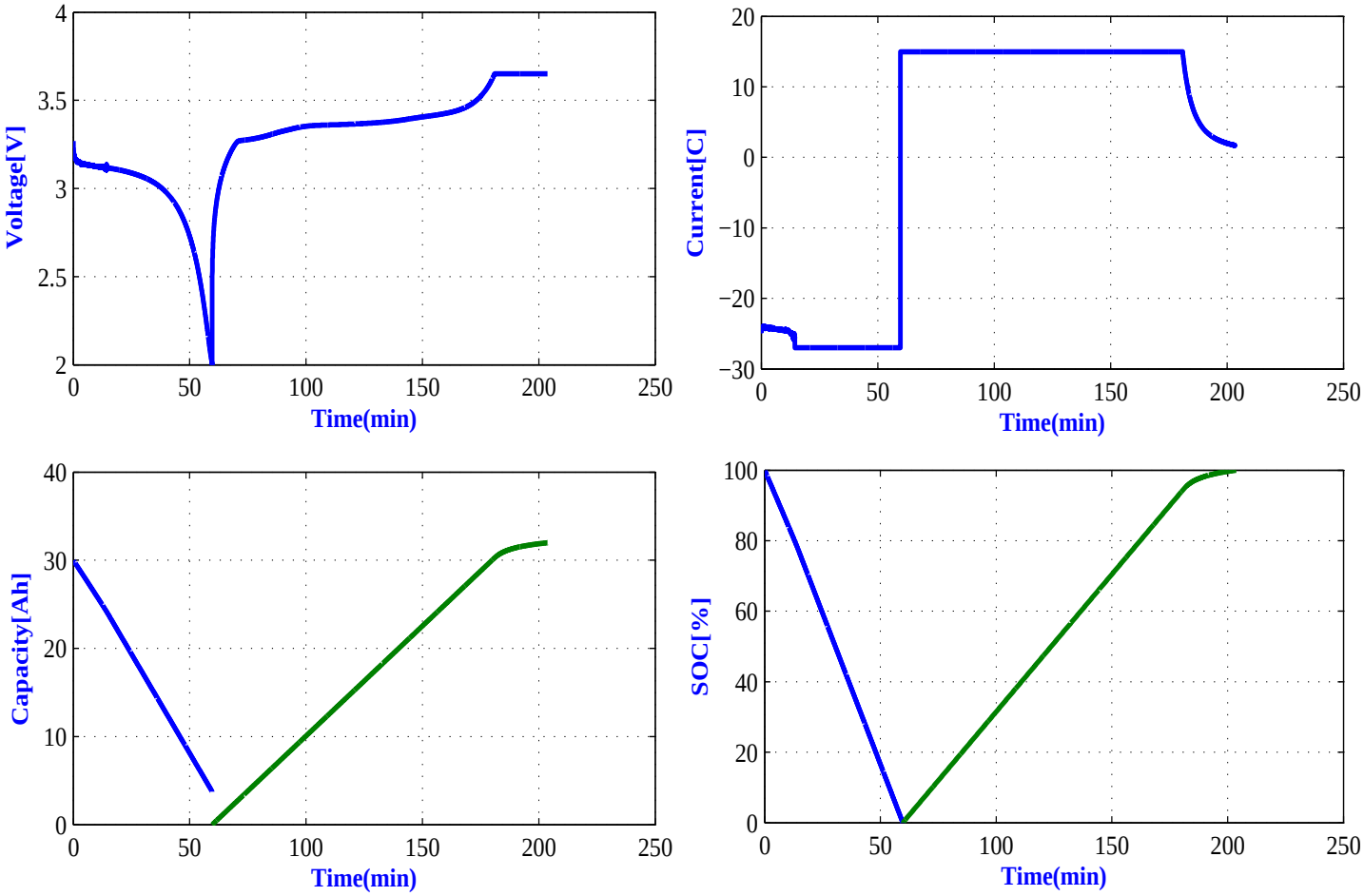

Figure 3.7: Voltage, current, SOC and capacity evolution during capacity determination.

below the cut-off voltage (2V in this case) in order to avoid the permanent damage of battery, as suggested by the battery manufacturer. The tests are conducted at different temperatures: *40°C*, *25°C*, *10°C*, *0°C*.

the current values for the pulses current profile experimentsc are taken as: 6 A continuous discharge current to remove 5% of SOC, 25 A pulse discharge current. The current values are shown in Figure 3.8.

Overall, the pulses current profile procedure is comprised of twenty repetitions of the profile shown in Figure 3.9, separated by a 5% DOD constant current discharges at a 1/5C rate. After two pulses discharge the constant current discharge is followed by an 30 min rest period. This procedure is continued until 100% DOD is achieved, Figure 3.9 shows a complete profile test sequence (where the 30 min rest is shifted).

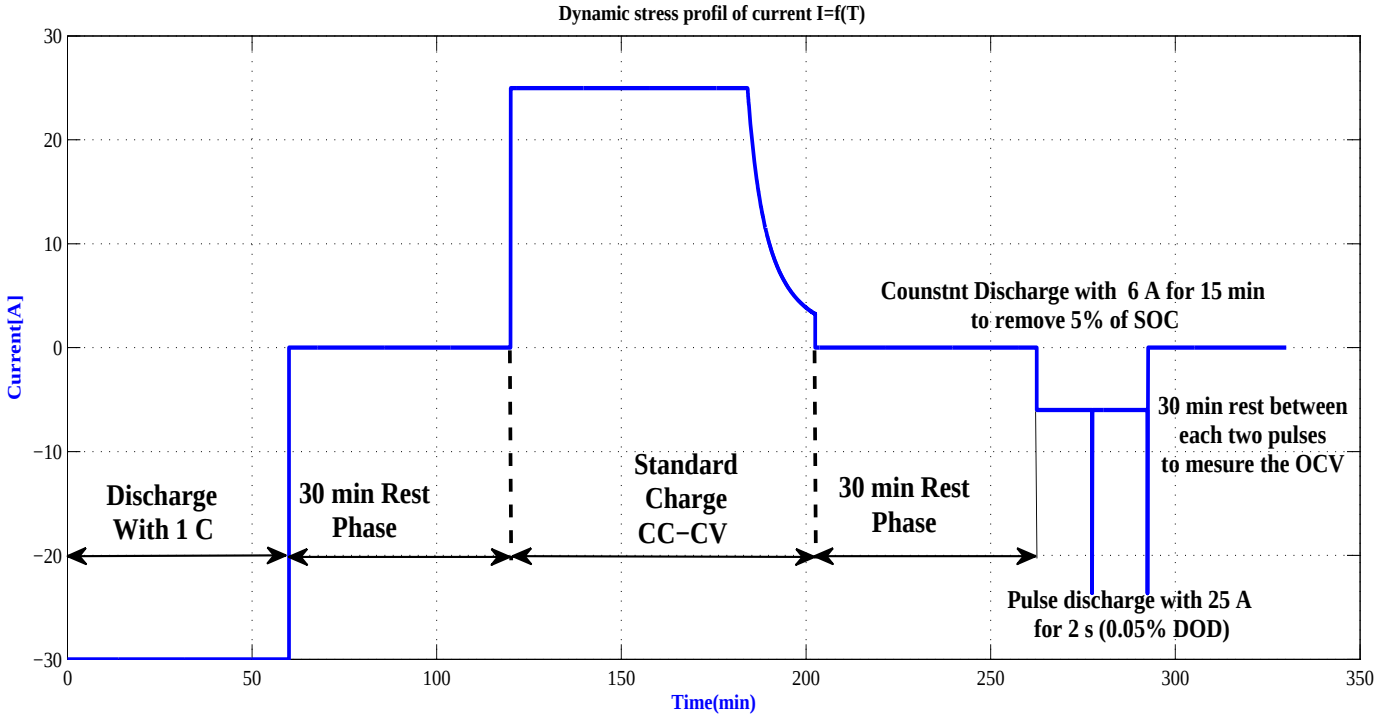

Figure 3.8: The proposed pusles current profile.

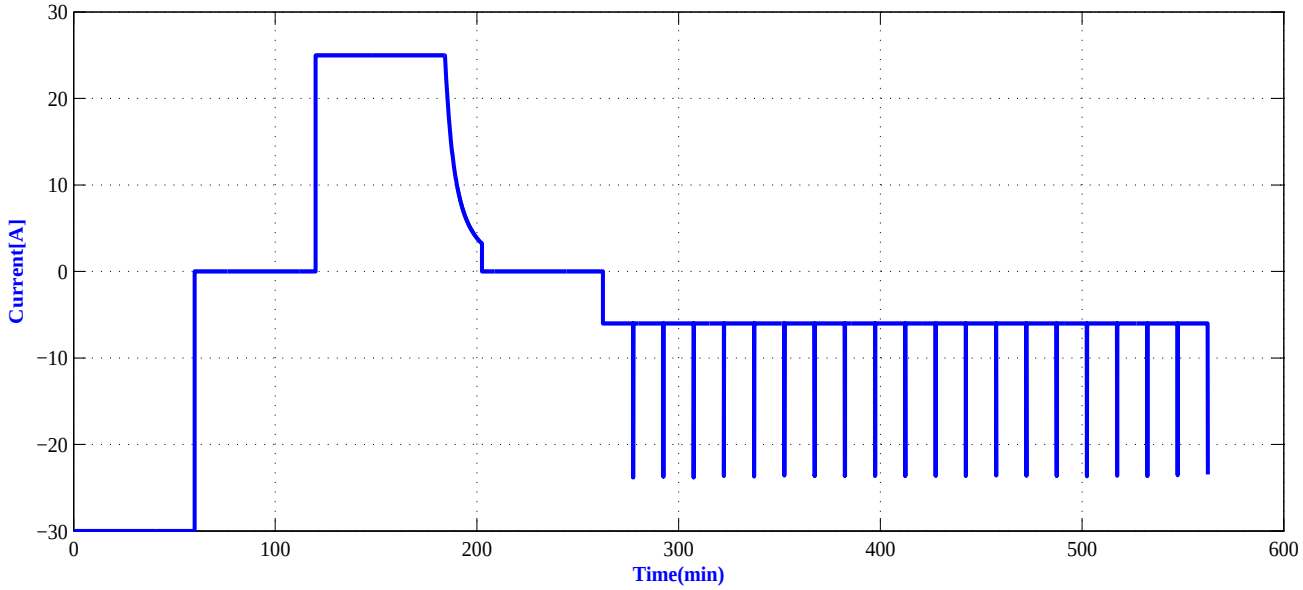

Figure 3.9: Complete pulses current profile test sequence.

For illustrative purposes, exemplary experimental data from pulses current characterization test are displayed in Fig. 3.10 and Fig. 3.11, Besides, the determination of internal resistance and the Open-Circuit voltage vs SOC characteristics. The pro-

posed power pulses may be deemed to be representative of typical EVs and HEVs pack power demands.

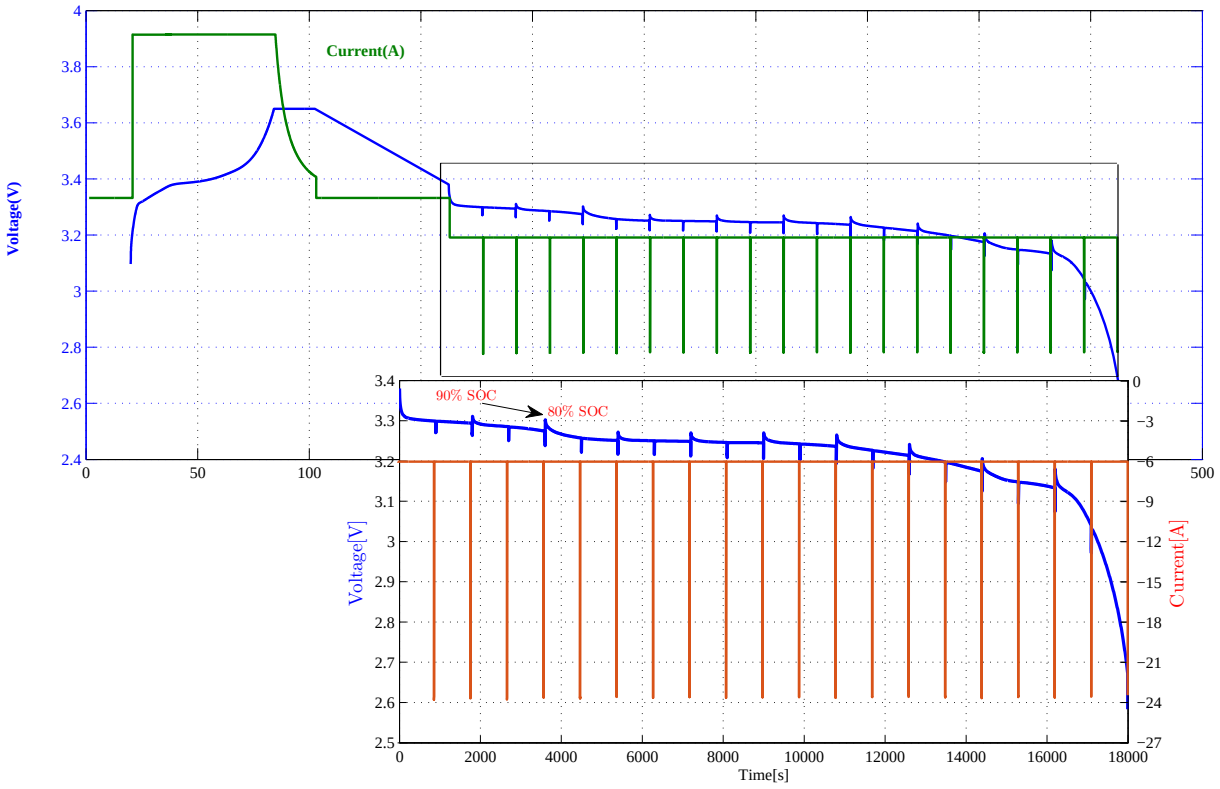

Figure 3.10: Pulses current profil with the terminal voltage variation.

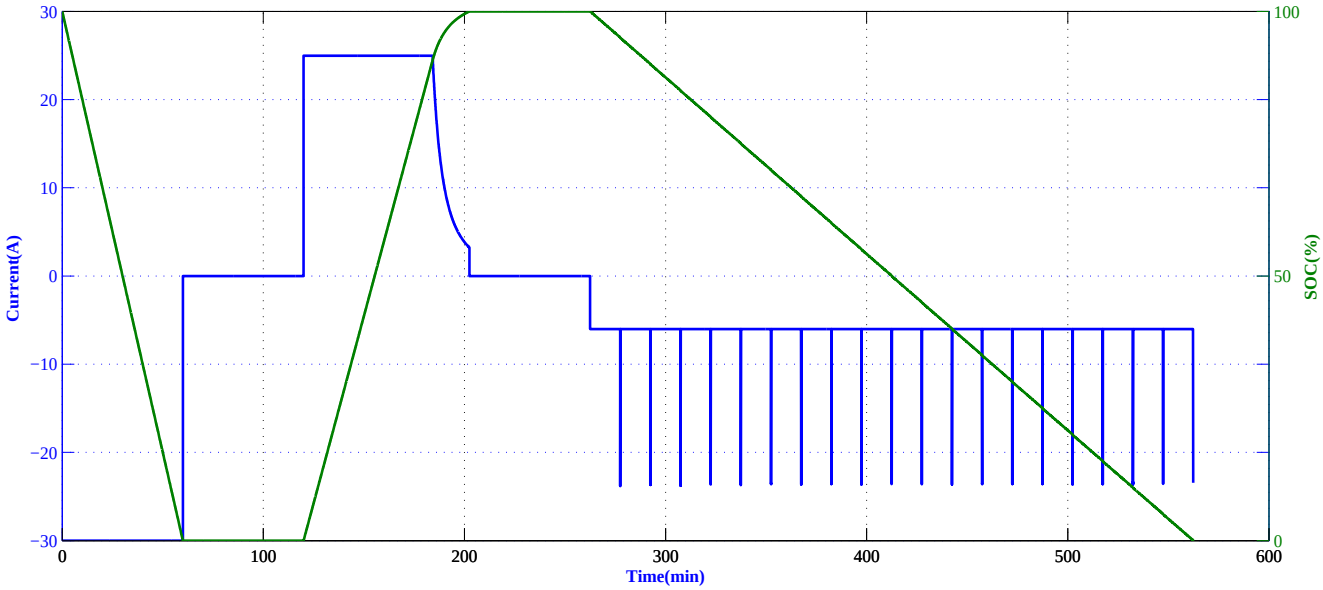

Figure 3.11: Pulses current profil with SOC variation.

3.5.5 Open-Circuit Voltage Test.

Open-circuit voltage tests are comprised of ten repetitions of constant current, fixed discharge intervals. As an example, starting with a fully charged battery, it is discharged with a current of 1/5C until it reaches 90% SOC. After a rest period of about half an hour, the battery is discharged again with the same current until it reaches 80% SOC. A similar rest period is then included. These dischargerest sequences are repeated until the battery SOC reaches 10%. Figure 3.12 shows the first open-circuit voltage test that starts from SOC = 100%.

Open-circuit voltage tests are mainly used to determine the exact relationship between battery SOC and open-circuit voltage. The rest periods in these tests are included in order to allow the battery terminal voltage to reach its equilibrium point so that it can be considered as the battery open-circuit voltage. Typical evolution of Open-Circuit Voltage versus the state of charge is illustrated in Fig. 3.12 at different temperatures

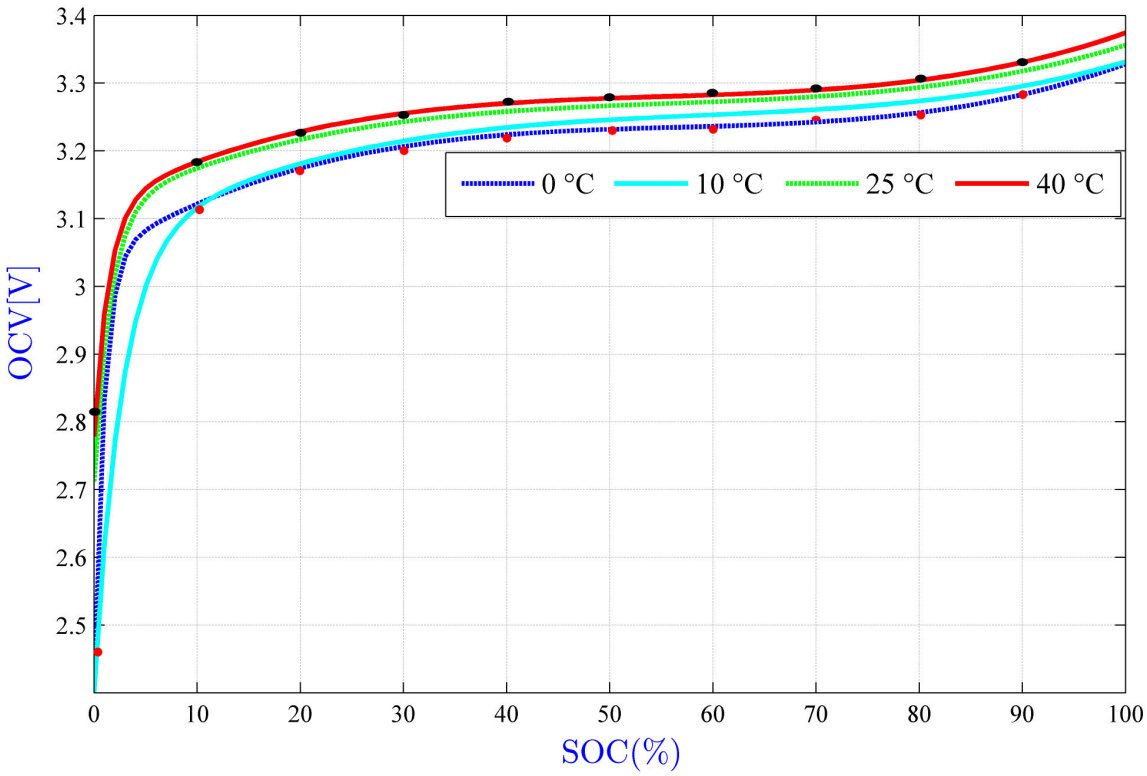

Figure 3.12: OCV-SOC relationship.

The test results can also be used to identify model parameters such as internal resistance and resistor-capacitor (RC) networks values. Figure 3.13 demonstrates battery open-circuit voltage and internal resistance extraction methode.

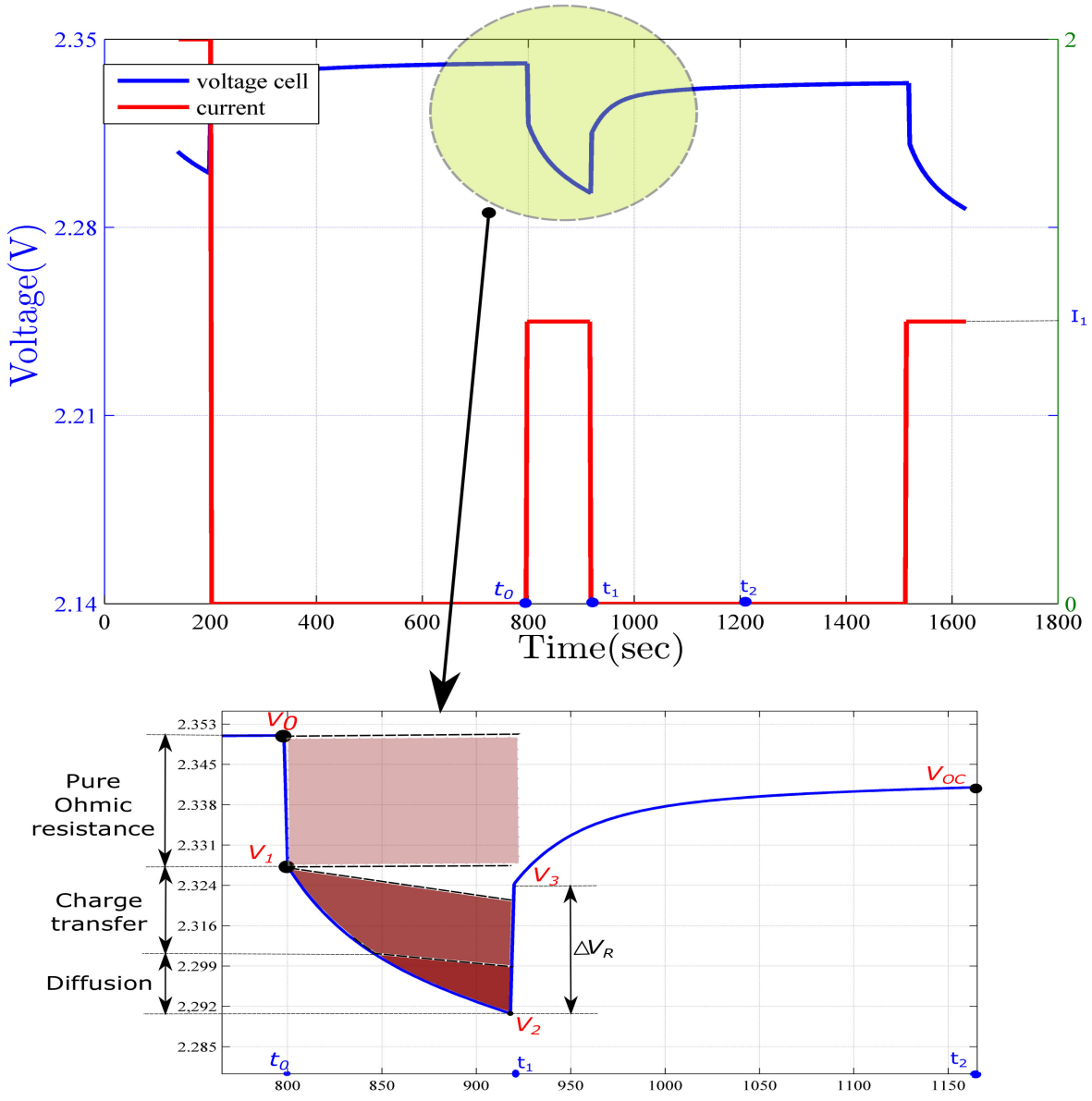

Figure 3.13: Typical curve of evolution of current and voltage under pulsed-current discharge for resistance determination.

3.5.6 Fast Charge/Discharge Aging (Life) Tests

Aging test using well-defined charging/discharging cycles at elevated temperature ($25^{\circ}C$) and high C-rates have been conducted. This accelerated test was conducted to track changes in battery electrochemical model parameters. These tests were conducted 24 hours a day and 7 days a week over a period of 6 months. The test procedure is as follows:

A) Fully charge the battery in a Constant Current Constant Voltage (CCCV) mode until maximum voltage (3.6V).

B) Fully discharge the battery at constant current (CC) mode with 1C-rate until the voltage hits the minimum voltage (2V).

C) All cycler current accumulators are reset to zero. At this moment, the battery is at zero state of charge (SOC).

D) Charge the battery to 90% SOC.

E) Discharge the battery at 10 C-rate until the battery hits the minimum voltage (2V)

F) Allow for voltage relaxation for 5 minutes.

G) Charge the battery at 4C-rate for 20 minutes. If the battery hits the maximum voltage, CCCV charge mode is maintained.

H) Repeat the procedure from D to G for approximately 200 cycles (till capacity hits 80%).

3.6 Conclusion

In this chapter, an electrical battery modelling approach is proposed, where the model parameters are dynamically updated based on cell temperature and SOC variations. A modelling example of a commercialized Li-Ion battery is presented. The model parameters are extracted based on impedance and pulse current characterization.

After a detailed description of design considerations and system development, battery characterization and modeling were studied.

CHAPTER 4

BATTERY CHARACTERIZATION THROUGH FIELD TESTS

Contents

4.1 Introduction

In this Chapter the battery implementation into a vehicle model and how different charging/driving conditions may affect battery efficiency is assessed. First a brief introduction of the vehicle model used is given, and then battery efficiencies in different charging and driving conditions are evaluated.

4.2 Vehicle Model

In this section the model, which describes the longitudinal dynamic effects of the vehicle is introduced. This is important because in the considered Simulink simulation the forces acting on the vehicle for a specific driving cycle are the inputs to the powertrain of the vehicle, and thus, they represent the load on the battery system.

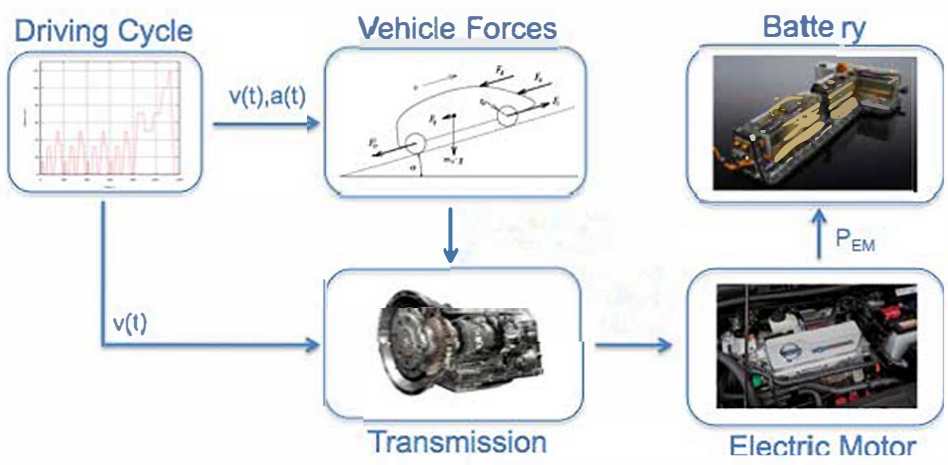

Figure 4.1: Vehicle model schematization.

In our simulation approach, the input variables are the speed , and the acceleration a, of the vehicle. The wind velocity (assumed to be zero), and θ is the roadway gradient (also assumed to be 0). Using these conversions we can take any of the normal velocity drive cycles and convert them to power cycles. Figure 4.2 shows the Simulink blocks used for the simulation. The vehicle and roadway parameters used to convert vehicle velocity into power are shown in Table 4.1.

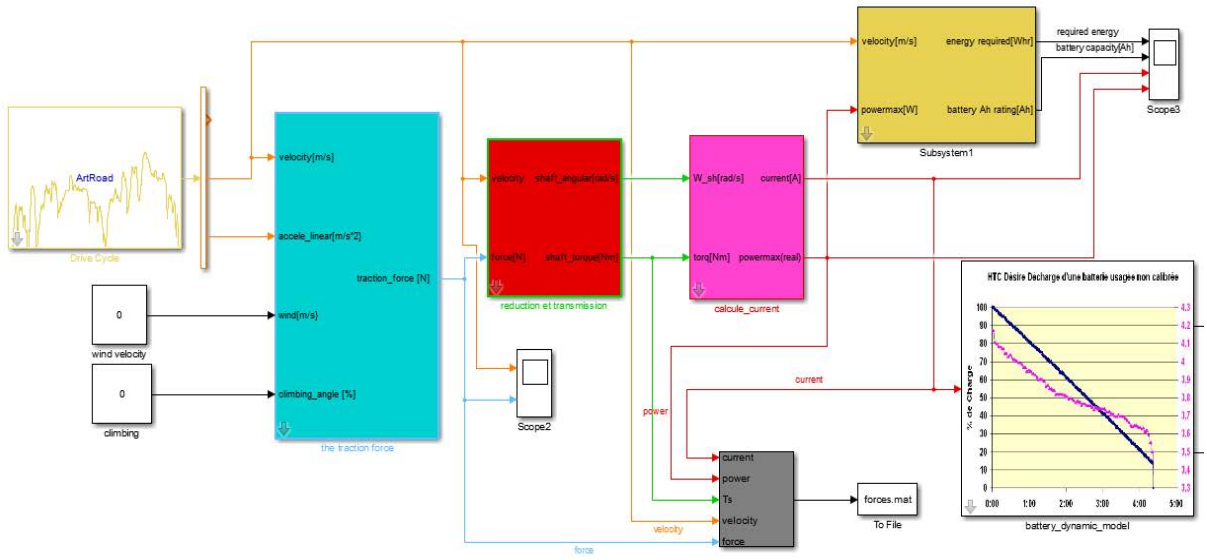

Figure 4.2: Simulink scheme of vehicle model with battery model intergration.

Table 4.1: Parameters used for converting velocity profiles into power profiles for use in electric batteries

Mass of the vehicle	1500 k
Air density	1.20 kg/m^3
Tire rolling resistance coefficient	0.01
Frontal Area	1.9 m^2
coefficient	0.3

4.3 Current Generation

In order to generate the current profiles needed for experimentation, the electric vehicle battery model has been implimanted with the Vehicle model. The model has been simulated using SimScape in Matlab environment in order to obtain the current profile from the velocity profile. Loading conditions such as heating and air conditioning have been ignored in this study. The simulation model, as shown in Figure 4.2, consists of a vehicle dynamic model, DC electric motor, DC-DC convertor, and lithium-Ion battery pack.

Three benchmark driving schedules have been used in the simulation; namely, an Artemis Urban Driving Schedule (ArtUrban), a light duty drive cycle for rural road (ArtRoad), and a High fuel Economy Test (ArtMw150). Even though the driving behaviour of an average driver may likely vary, these driving cycles have been widely used in both industrial and academic settings to simulate various driving patterns.

Table 4.2: Characteristics of ArtUrban, ArtRoad, and ArtMw150 Driving Schedules,

	Length[s]	Distance [m]	Av speed [km/h]
ArtUrban	993	4874	17.7
ArtRoad	1068	17275	57.5
ArtMw150	1092	29547	99.6

The ArtUrban driving cycle represents a city driving condition, the ArtUban cycle was originally used for light duty fossil-fueled vehicle testing. It has been developed to imitate average speed, idle time, and number of stops that the average driver performs in practice. For electric vehicles, the profile has been extensively used to estimate the driving range in miles per full charge [97]. The ArtRoad cycle is a high acceleration, aggressive driving cycle, and the ArtMw150 represents a highway driving conditions with speeds below 80 Km/h, The three aforementioned driving cycles are as shown in Figure 4.3 below. An exclusive summary of these driving cycle characteristics such as distance, time, and average speeds is as shown in Table 4.2, [97].

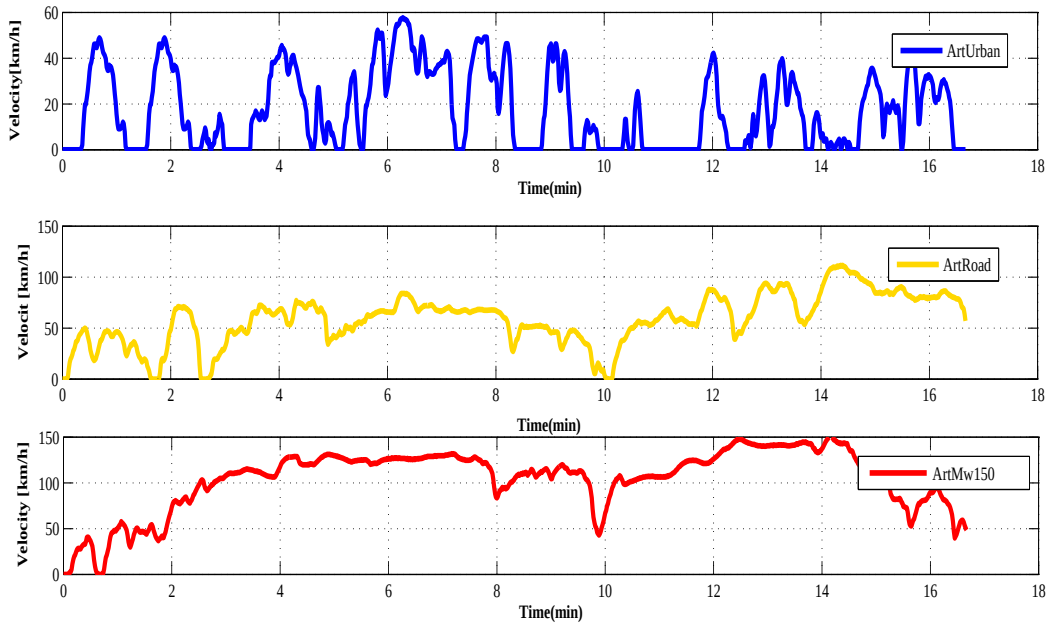

Figure 4.3: Velocity Profiles for the ArtUrban (upper figure), ArtRoad (middle), and ArtMw150 (lower) Cycles.

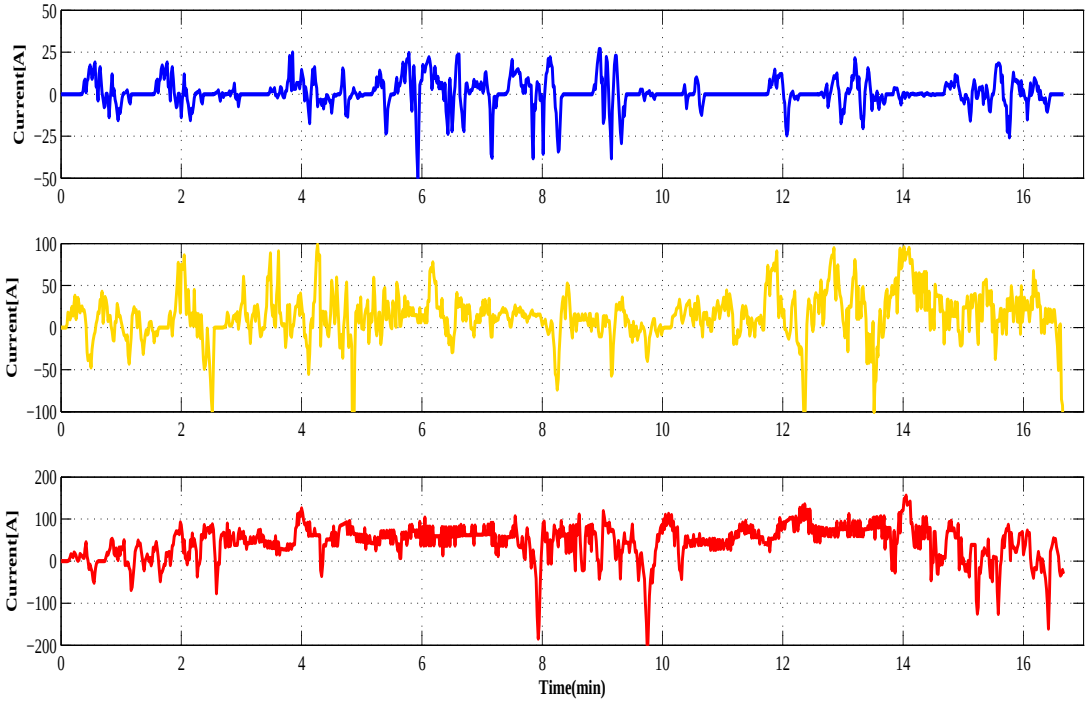

Figure 4.4: The pack current Profiles for the ArtUrban (upper figure), ArtRoad (middle), and ArtMw150 (lower) Cycles.

The pack current profiles from these driving cycles are as shown in Figure 4.4. Since the ArtMw150 and ArtRoad driving cycles are aggressives driving cycles, the current demand by the motor is quite high compared to current profiles from the ArtUrban cycle.

Current profiles have been scaled down to the cell level and used for model parameters fitting. The pack consists of 40 cells connected in series for voltage buildup and 14 cells connected in parallel. Cell balancing has been ignored in this study.

4.4 Simulation Results and Discussions

Using the model introduced in the previous section, we performed the simulation at different temperature and discharge current for the battery cell.

4.4.1 Extraction Parameters Results

A benchmark has been used for data fitting. Experimental data from LiFePO4 cells have been collected and fitted to the battery proposed model. Even though the proposed model has fewer parameters compared to the fullorder model, model parameters are still difficult to identify.

4.4.1.1 Estimation of the Battery OCV and Internal Resistance

Typical evolution of Open-Circuit Voltage versus the state of charge is illustrated in Fig. 4.5 at different temperatures. These curves were extracted based on the proposed current profile.where dots represent the last voltage value of the rest period (with no load) and the continuous lines are the fitted curves. It is remarkable that there is a slight voltage change in the fitted cureves due to the battery equilibrium state. These voltage changes are relativel insignificant and can be neglected. Experiment results desribe that the OCV is strongly depended upon the state-of-charge, while being largely independent of temperature. As it can be observed in Fig. 4.5 a relatively small variation of the OCV for a large SOC with varity temperatures. The OCV-SOC

strong dependent and nonlinear relationship can be approached by a mathematical equation 4.1.

$$\begin{aligned} V_{OC}(SoC) &= \text{-}0.3395 \times exp(\text{-}0.7088 \times SoC) \\ &\quad + 0.91e\text{-}05 \times SOC^3 + \text{-}0.000134 \times SoC^2 \\ &\quad + 0.007871 \times SoC + 3.118 \end{aligned} \tag{4.1}$$

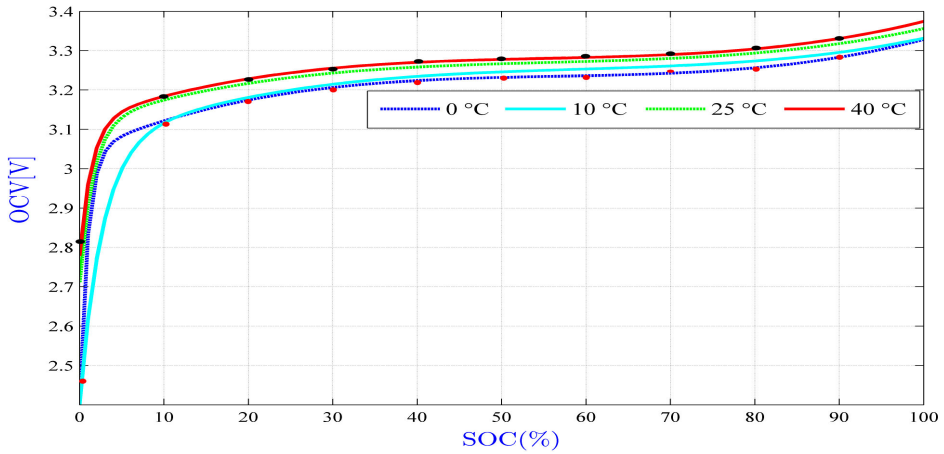

Figure 4.5: Open-Circuit Voltage (OCV) versus (SOC) at various temperatures.

Once the OCV is determined, the internal resistance of the battery pack can be estimated from equation 4.2

$$R_s = \frac{V_0 - V_1}{I} \tag{4.2}$$

The resistive values are calculated utilizing the least square error curve fitting method, such that the equation 4.3 matches the measured battery impedance shown in Fig. 4.6. The curves of resistive values at four different temperatures are provided in Figure 4.8.

As the impedance of the battery is measured at different SOCs (see Fig. 4.7), the resistive and capacitive values are extracted at these SOCs.

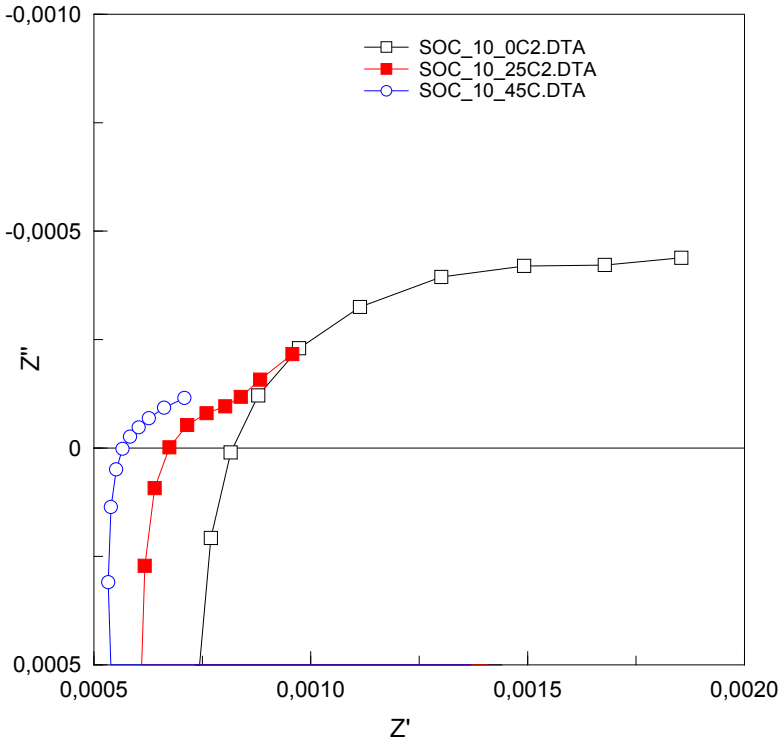

Figure 4.6: Measured Nyquist curve for cell impendence.

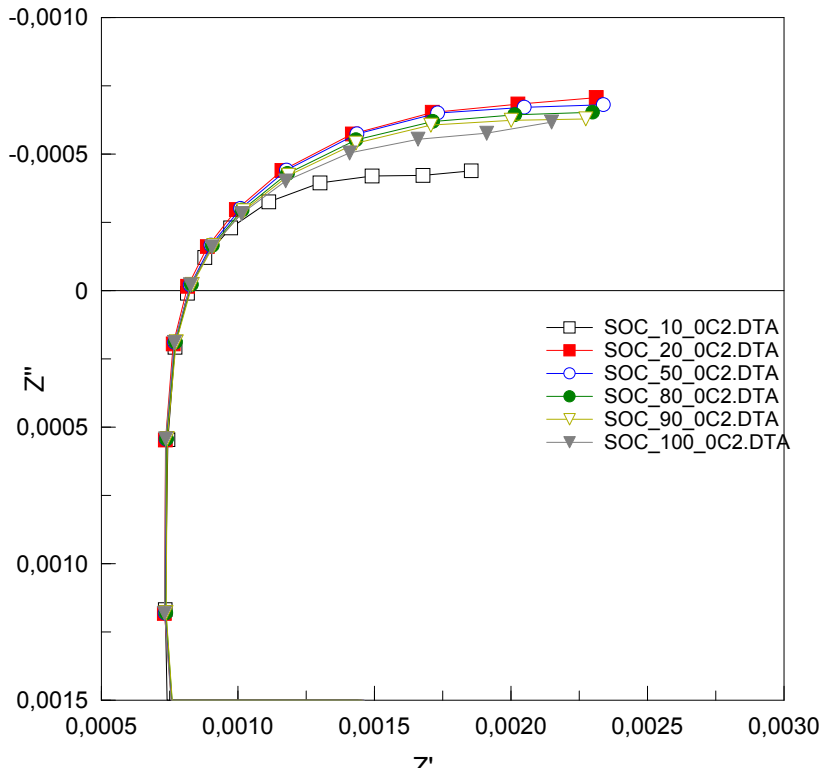

Figure 4.7: Experimental Nyquist curves for the cell impendenceat different SOCs .

the internal cell impedance consists of one ohmic resistance and two parallel RC pairs. As mentioned above, all of these components are function of SOC and strongly dependent on it. Figure 4.8 shows experimental value found for these components at different SOCs.

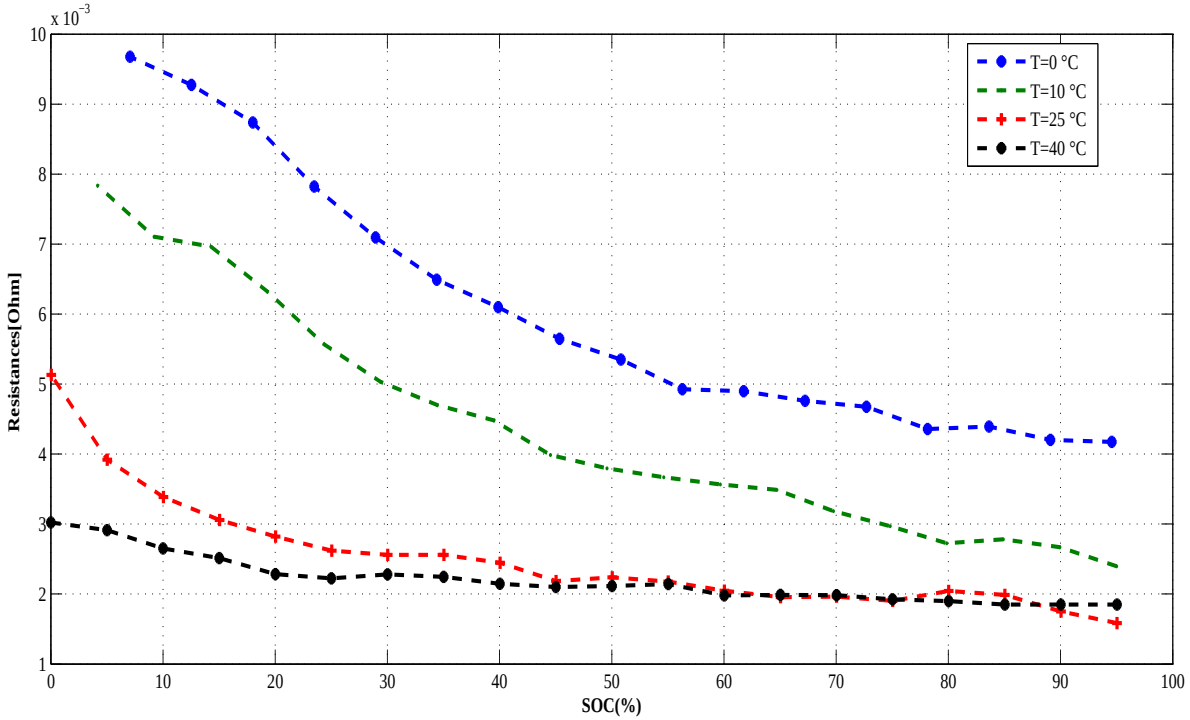

Figure 4.8: Experimental measures for internal resistance at different temperatures.

It can been seen that all these components vary as SOC changes and they are not constant over the SOC range.Therefore, having accurate SOC during testing is essential for modeling parameters to obtain a meaningful battery model. For our experiments, coulomb counting method is used to monitor SOC along with tests.

Modelling of these components for the new cell will be based on the fitting functions. Using data from experiment, the following empirical equation is obtained for serial resistance:

$$R_s(SOC, T, I) = (a * T + b) * e^{(-|I| * SOC)} + c \tag{4.3}$$

where [a b c]= [-0.0001693 0.05418 0.003257]. Fig. 4.9 presents fitted curve to values exported from experiment for the R_s.

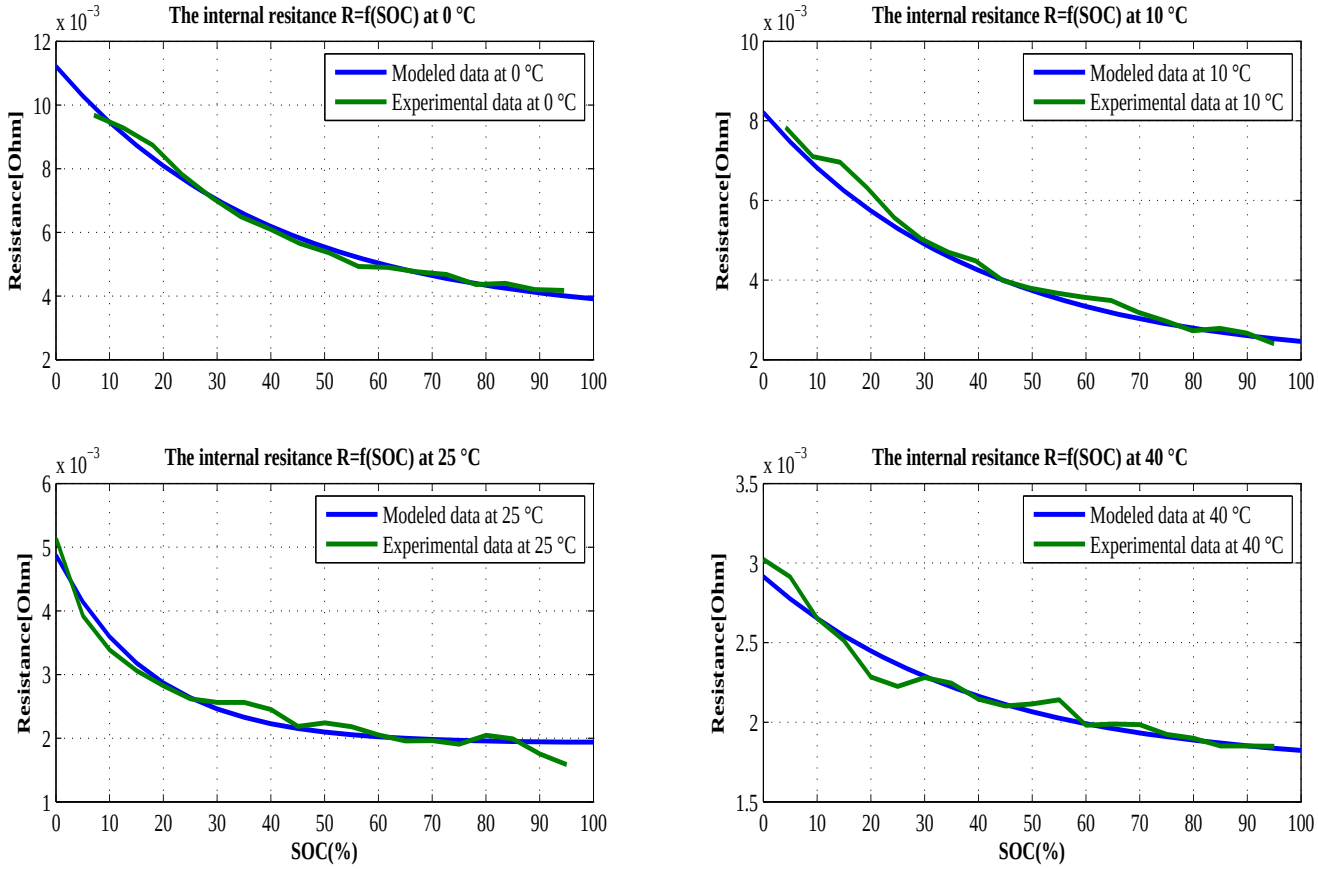

Figure 4.9: Comparison between experimentation and simulation results of R_s versus (SOC) at different temperaturess.

The internal resistance shows a significant temperature dependence. The ohmic resistance Rs increases when temperature and state-of-charge decrease. For example, when SOC is between 50% and 100%, R_s at $40°C$ equals the half of R_s at $10°C$ and R_s at $0°C$ is twice R_s at $10°C$.

The percentage error between simulations and experimentations are explained in Figure 4.10. it shows that error has the average of 5%.

The accuracy can be increased by modelling electrical components by higher order polynomials. One more option for increasing the accuracy is using more parallel RCs in the model. However, it would complicate the model and increase its estimation time and we wouldn't able to estimate SOC and voltage in real time. As mentioned before, C-rate dependency in our modelling is neglected since flowing current is less than 1C and it doesn't affect voltage or internal parameters estimation.

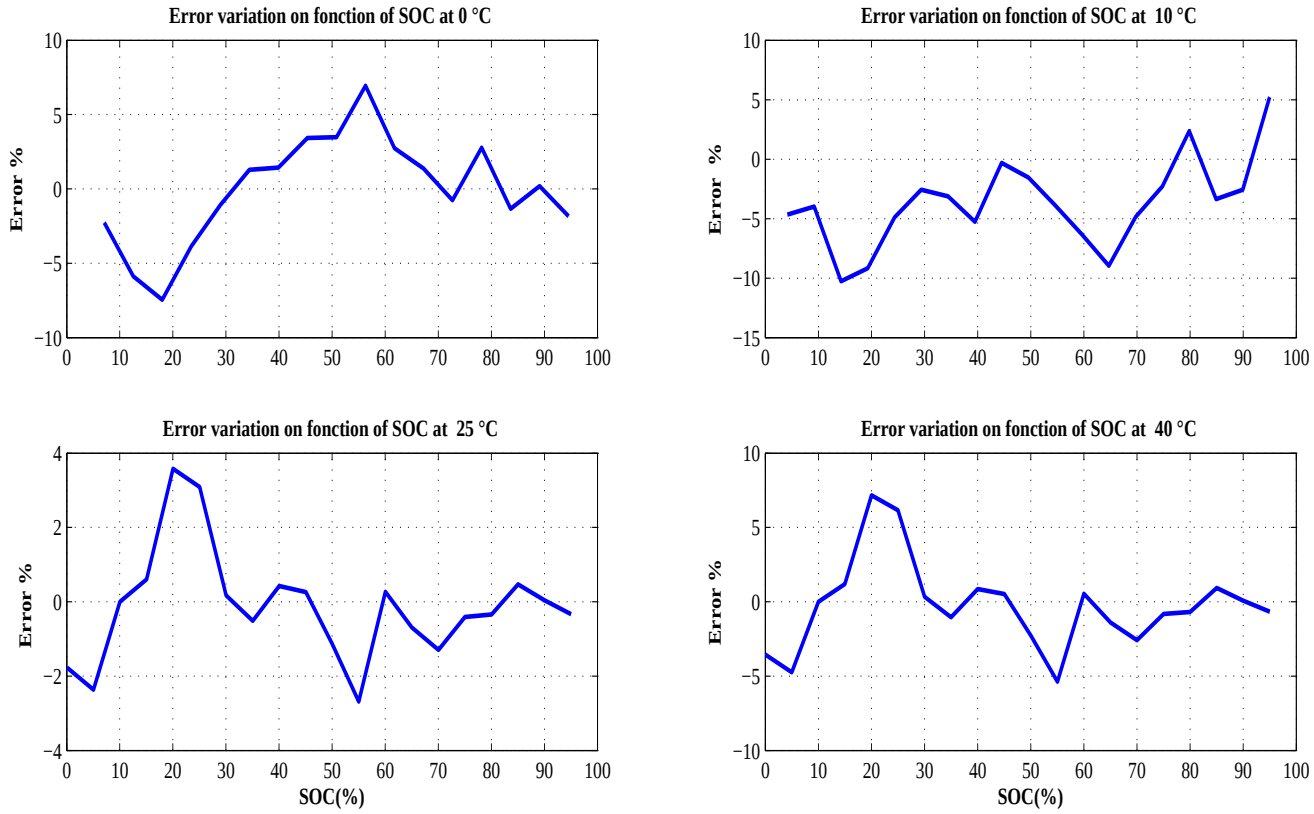

Figure 4.10: Relative error between experimentation and simulation results of R_s.

4.4.2 Model Validation

To validate the proposed modeling approach, the battery discharge curve and the battery behaviour under the urban drive-cycle are simulated and experimentally verified. The cycler system discussed in section 4.3 was utilized to perform the experimental tests.

An individual cells test has been conducted within laboratory conditions, cell's voltages and temperatures are recorded. The cell loaded with various current rates as (1C, 0.5C) at differents temperature. Figure 4.11 illustrates the results of this test. The comparative results show that there is a close agreement between simulation and experiment results. Whereas the maximum error is 0.02V at the ending of discharge due to the quick drop caused by internal resistance.

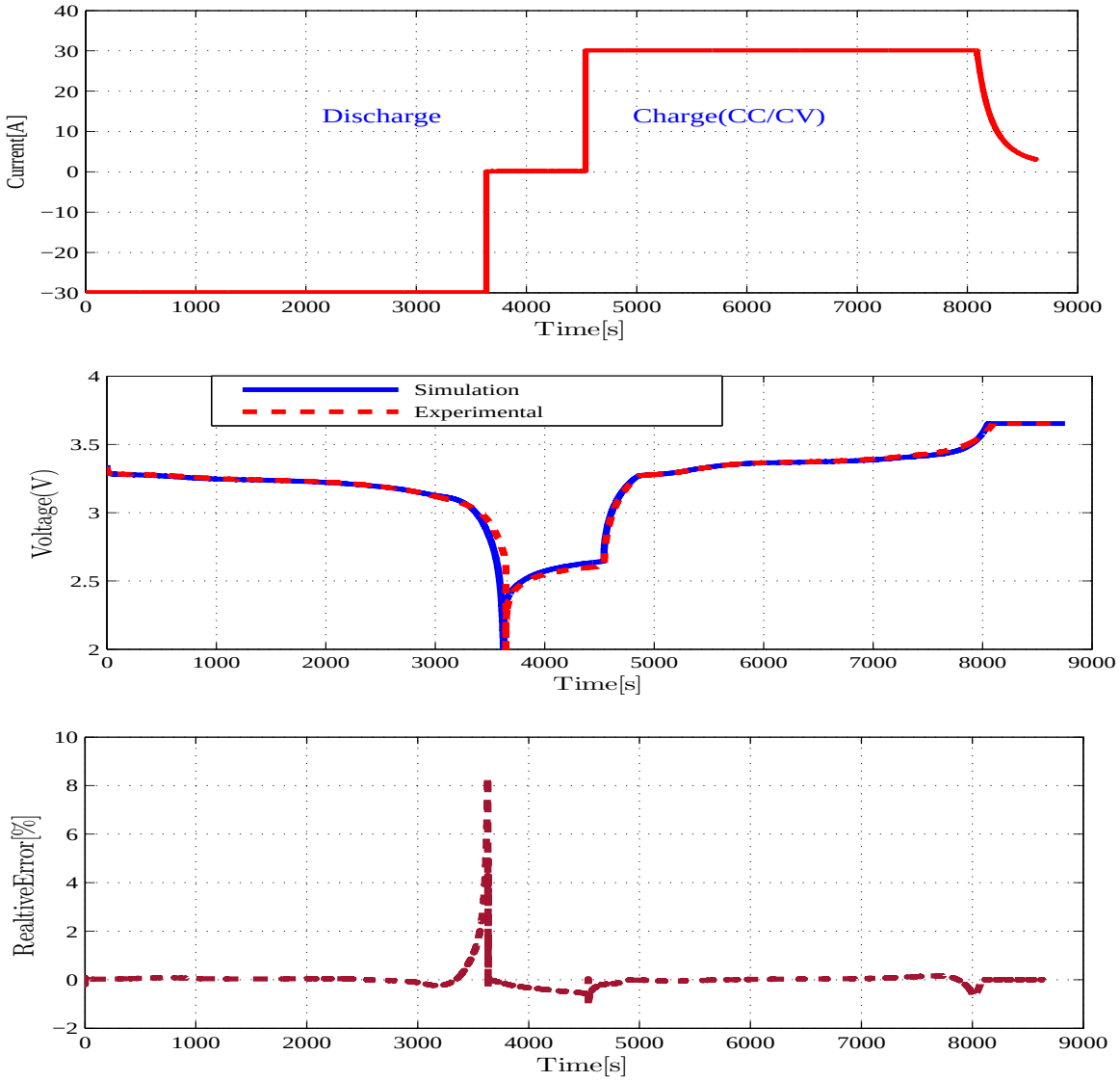

Figure 4.11: simulation and experimental voltage response of Li-ion battery with 1C rate current profile.

The current profile gained from the ArtUrban drive-cycle is applied to the vehicle model, the Figure 4.12 shows the evolution of voltage cell on the function of time. As seen in this figure, the results are relatively indicative. Especially, for high currents a more accurate simulation is gained with the proposed approach. This could be due to a better consideration of the current dependence on the internal resistance.

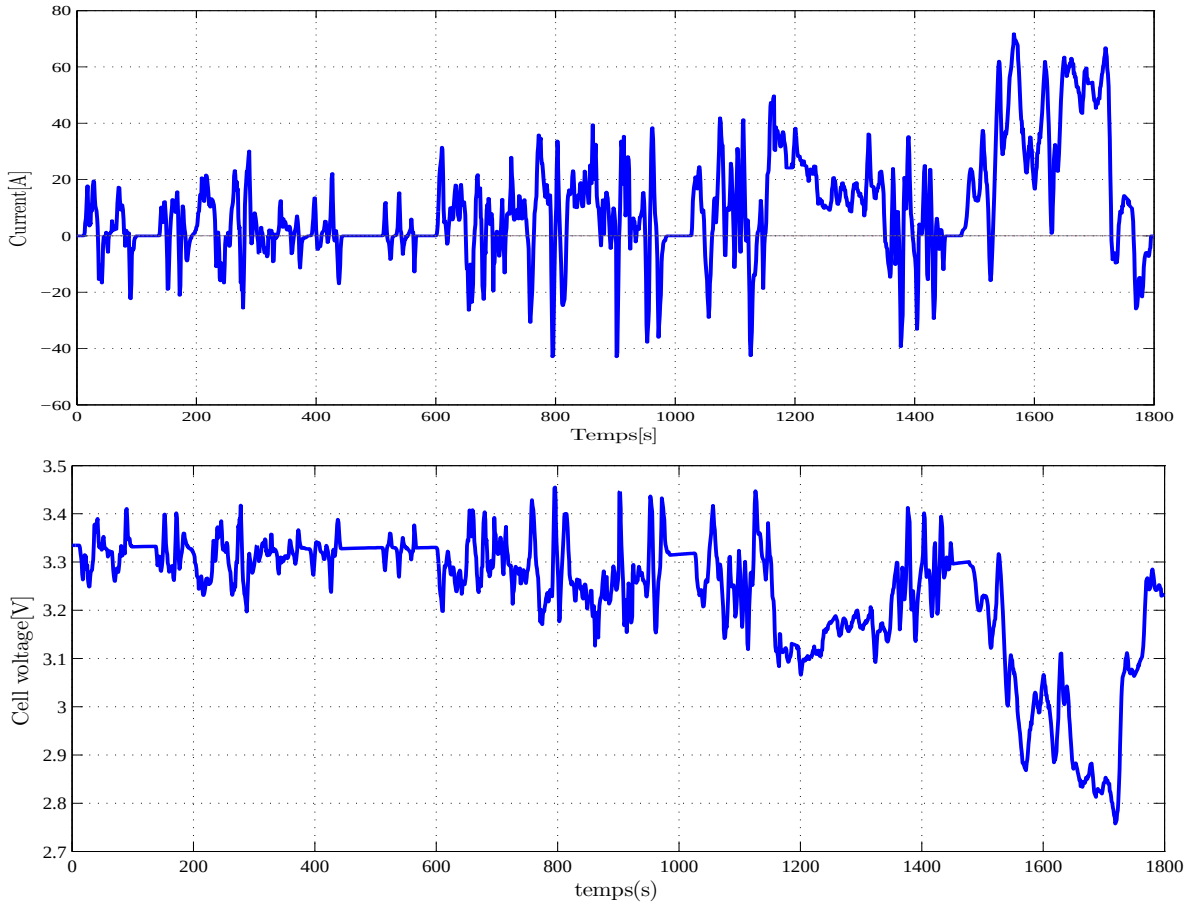

Figure 4.12: Simulated current profile and terminal voltage of cell for the urban drive-cycle.

4.5 Conclusion

This chapter has shown that, depending on state of charge (SOC) and temperature, a lithium-ion cell will show a different open circuit voltage and thus a different static behavior. On a commercial iron phosphate / graphite cell various methods for its characterization were evaluated (constant current, relaxation measurement and cyclic voltammetry).

Battery terminal voltage and current have been identified to be the two main parameters to define battery performance and they are strongly affected by the internal resistance, which depends on battery chemistry and operating conditions such as temperature, SOC and consumer usage. In order to assess these parameters battery and electric vehicle simulation models have been used.

GENERAL CONCLUSION

General Conclusion

In this thesis, an accurate and simple electrical battery model for predicting the lithium-ion batteries behavior is successfully developed based on experimental observations at various battery states of charge and temperatures under the current pulses and the electrochemical impedance spectroscopy (EIS) tests. Which is shown that this model can predict well the battery's electrical performance during various tests process including the drive cycles of electrified vehicles. In addition, a novel rapid and simple impulses current profile was proposed and explained in order to extract the electric parameters of the cell's model. The results demonstrate the serviceability of this proposed current profile for internal resistance identification and can be confirmed, Moreover, it has been shown, using experimental data that the values of the battery inner resistance measured by current pulse characterization technique are sensitive to the specifications of the methodology applied and to factors like temperature, in good agreement with previous results from the literature.

The model was validated using a single ArtUrabn drive cycle and a several individual tests, which is shown an acceptable terminal voltage response indicating a good tradeoff between the accuracy and the complexity of the proposed model. In total, this simple battery model can be used as a real-time model in electrified vehicle battery management systems.

This research has considered the particular requirements of performance modeling for lithium-ion battery. An accurate and simple current pulse characterization profile is successfully developed, to effectively perform the extraction of parameters required for modeling the electrical behavior of a battery. It is noted from the simulation and the correlation with the laboratory test result the serviceability of this pulse current profile for inner resistance.

Since the internal resistance is essentially a representation of electrochemical reactions and transport processes inside the battery, it is strongly affected by the temperature and the state of charge of the battery. The effects of these parameters on the internal resistance have been also evaluated.

Proposed Future Work

The presented study provides a simple electrical battery model for predicting the lithium-ion batteries behavior. There are a number of potential extensions and recommendations that could be considered for future research:

Entropy measurement

The battery model does not include the effect of entropy. It would be interesting if the entropic heat is added which can improve the temperature prediction. In general, the entropy measurement requires a very long period of testing because this measurement must be conducted in an equilibrium state.

Investigation for battery with different chemistry and form factor

In this study, only the Lithium-iron-phosphate battery is used for the assessment of current profile. The study could be expanded by conducting a test with different types of battery chemistry and battery with different form factor. The variations of these testing could therefore benefit the electric car maker especially in the areas of building a better battery pack. Combining the methodology presented in this thesis

with more test data would create an engineering design rule specifically to address the concern of the cell to cell non-uniformities which is one of key problem for the BMS.

BIBLIOGRAPHY

[1] Scripps institution of oceanography: Scripps co2 program - atmospheric co2., http://scrippsco2.ucsd.edu/data/atmospheric_co2/ (2019).

[2] M. Meinshausen, et al., What does a 2 c target mean for greenhouse gas concentrations? a brief analysis based on multi-gas emission pathways and several climate sensitivity uncertainty estimates, Avoiding dangerous climate change 270.

[3] U. Bünger, Energiespeicher in Stromversorgungssystemen mit hohem Anteil erneuerbarer Energieträger: Bedeutung, Stand der Technik, Handlungsbedarf; ETG Task Force Energiespeicher, VDE, 2009.

[4] M. Stadler, M. Kloess, M. Groissböck, G. Cardoso, R. Sharma, M. C. Bozchalui, C. Marnay, Electric storage in california's commercial buildings, Applied Energy 104 (2013) 711–722.

[5] U.s embassy beijing, china: U.s embassy beijing air quality monitor., http://www.stateair.net/web/post/1/1.html (2015).

[6] China daily: Dense fog shrouds beijing., http://www.chinadaily.com.cn/photo/2013-01/12/content_16108546.htm (2013).

[7] S. Schickram, Z. Till, M. Lienkamp, Auslegung von elektrischen fahrzeugkonzepten für megacities in asien, ATZ-Automobiltechnische Zeitschrift 115 (2) (2013) 126–130.

[8] D. Howell, Fiscal year 2013 annual progress report for energy storage r&d, US Department of Energy, Office of Energy Efficiency and Renewable Energy, Vehicle Technologies Office (2013) 2.

[9] M. Ehsani, Y. Gao, S. Longo, K. Ebrahimi, Modern electric, hybrid electric, and fuel cell vehicles, CRC press, 2018.

[10] S. Dhameja, Electric vehicle battery systems, Elsevier, 2001.

[11] Wärtsilä corporation., https://www.wartsila.com/ (May 2018).

[12] C. Mi, M. A. Masrur, Hybrid electric vehicles: principles and applications with practical perspectives, John Wiley & Sons, 2017.

[13] A. Colette, Case studies on climate change and World Heritage, UNESCO Publishing, 2013.

[14] Z. Liu, D. Guan, W. Wei, S. J. Davis, P. Ciais, J. Bai, S. Peng, Q. Zhang, K. Hubacek, G. Marland, et al., Reduced carbon emission estimates from fossil fuel combustion and cement production in china, Nature 524 (7565) (2015) 335.

[15] L. Battistelli, F. Ciccarelli, D. Lauria, D. Proto, Optimal design of dc electrified railway stationary storage system, in: Clean Electrical Power, 2009 International Conference on, IEEE, 2009, pp. 739–745.

[16] A. Emadi, K. Rajashekara, S. S. Williamson, S. M. Lukic, Topological overview of hybrid electric and fuel cell vehicular power system architectures and configurations, IEEE Transactions on Vehicular Technology 54 (3) (2005) 763–770.

[17] N. Kim, S. Cha, H. Peng, Optimal control of hybrid electric vehicles based on pontryagin's minimum principle, IEEE Transactions on Control Systems Technology 19 (5) (2011) 1279–1287.

[18] D. Kodjak, Consumer acceptance of electric vehicles in the us, USA: The International Council for Clean Transportation.

[19] S. Bronchard, M. McGuinness, C. Narich, M. Noom, C. Raut, M. Schutz, M. Stark, P. Ubbink, M. Viglino, A. Vos, Plug-in electric vehicles: Changing perceptions, hedging bets, Source:(Accessed 16 May 2017).

[20] B. Pattipati, C. Sankavaram, K. Pattipati, System identification and estimation framework for pivotal automotive battery management system characteristics, IEEE Transactions on Systems, Man, and Cybernetics, Part C (Applications and Reviews) 41 (6) (2011) 869–884.

[21] Y. Xing, E. W. Ma, K. L. Tsui, M. Pecht, Battery management systems in electric and hybrid vehicles, Energies 4 (11) (2011) 1840–1857.

[22] M. Doyle, T. F. Fuller, J. Newman, Modeling of galvanostatic charge and discharge of the lithium/polymer/insertion cell, Journal of the Electrochemical Society 140 (6) (1993) 1526–1533.

[23] X. Hu, S. Li, H. Peng, A comparative study of equivalent circuit models for li-ion batteries, Journal of Power Sources 198 (2012) 359–367.

[24] B. Martin, A dynamic battery model considering the effects of the temperature and capacity fading (2012).

[25] H. Zhang, M.-Y. Chow, Comprehensive dynamic battery modeling for phev applications, in: Power and Energy Society General Meeting, 2010 IEEE, IEEE, 2010, pp. 1–6.

[26] J. Zhang, S. Ci, H. Sharif, M. Alahmad, An enhanced circuit-based model for single-cell battery, in: Applied Power Electronics Conference and Exposition (APEC), 2010 Twenty-Fifth Annual IEEE, IEEE, 2010, pp. 672–675.

[27] D. Z. Elabadine, M. Ali, H. Mourad, A novel hybrid technique to predict the lithium-ion battery's behavior and estimate the intern impedance, International Journal of Emerging Electric Power Systems 18 (4).

[28] Z. elabadine Dahmane, A. Malek, M. Bouhali, M. Bounabi, K. Kaced, M. S. A. Cheikh, A proposed pulses current method to extract the batteries parameters, in: Systems and Control (ICSC), 2017 6th International Conference on, IEEE, 2017, pp. 555–560.

[29] S. Zhang, K. Xu, T. Jow, Electrochemical impedance study on the low temperature of li-ion batteries, Electrochimica acta 49 (7) (2004) 1057–1061.

[30] T. R. Tanim, C. D. Rahn, C.-Y. Wang, A temperature dependent, single particle, lithium ion cell model including electrolyte diffusion, Journal of Dynamic Systems, Measurement, and Control 137 (1) (2015) 011005.

[31] Y. Hu, S. Yurkovich, Y. Guezennec, B. Yurkovich, Electro-thermal battery model identification for automotive applications, Journal of Power Sources 196 (1) (2011) 449–457.

[32] W. Waag, S. Käbitz, D. U. Sauer, Experimental investigation of the lithium-ion battery impedance characteristic at various conditions and aging states and its influence on the application, Applied Energy 102 (2013) 885–897.

[33] C. Chen, J. Liu, K. Amine, Symmetric cell approach and impedance spectroscopy of high power lithium-ion batteries, Journal of Power Sources 96 (2) (2001) 321–328.

[34] R. E. Williford, V. V. Viswanathan, J.-G. Zhang, Effects of entropy changes in anodes and cathodes on the thermal behavior of lithium ion batteries, Journal of Power Sources 189 (1) (2009) 101–107.

[35] K. K. Parsons, Design and simulation of passive thermal management system for lithium-ion battery packs on an unmanned ground vehicle.

[36] K. K. Parsons, T. J. Mackin, Design and simulation of passive thermal management system for lithium-ion battery packs on an unmanned ground vehicle, Journal of Thermal Science and Engineering Applications 9 (1) (2017) 011012.

[37] W. Gu, C.-Y. Wang, Thermal and electrochemical coupled modeling of a lithium-ion cell, in: Proceedings of the ECS, Vol. 99, 2000, pp. 748–762.

[38] P. Taheri, M. Bahrami, Temperature rise in prismatic polymer lithium-ion batteries: An analytic approach, SAE International Journal of Passenger Cars-Electronic and Electrical Systems 5 (2012-01-0334) (2012) 164–176.

[39] P. Rong, M. Pedram, An analytical model for predicting the remaining battery capacity of lithium-ion batteries, IEEE Transactions on Very Large Scale Integration (VLSI) Systems 14 (5) (2006) 441–451.

[40] Y. Zhang, C.-Y. Wang, X. Tang, Cycling degradation of an automotive lifepo4 lithium-ion battery, Journal of Power Sources 196 (3) (2011) 1513–1520.

[41] E. Prada, D. Di Domenico, Y. Creff, J. Bernard, V. Sauvant-Moynot, F. Huet, A simplified electrochemical and thermal aging model of lifepo4-graphite li-ion batteries: Power and capacity fade simulations, Journal of The Electrochemical Society 160 (4) (2013) A616–A628.

[42] B. Y. Liaw, M. Dubarry, A roadmap to understand battery performance in electric and hybrid vehicle operation, Elsevier, 2010.

[43] V. Klass, M. Behm, G. Lindbergh, Evaluating real-life performance of lithium-ion battery packs in electric vehicles, Journal of The Electrochemical Society 159 (11) (2012) A1856–A1860.

[44] A. Barré, F. Suard, M. Gérard, M. Montaru, D. Riu, Statistical analysis for understanding and predicting battery degradations in real-life electric vehicle use, Journal of Power Sources 245 (2014) 846–856.

[45] H. Khayyam, J. Abawajy, R. N. Jazar, Intelligent energy management control of vehicle air conditioning system coupled with engine, Applied thermal engineering 48 (2012) 211–224.

[46] J. Larminie, J. Lowry, Electric vehicle technology explained, John Wiley & Sons, 2012.

[47] L. Ramroth, Nrel reveals links among climate control, battery life, and electric vehicle range, National Renewable Energy Laboratory, Tech. Rep 6.

[48] B. Scrosati, History of lithium batteries, Journal of solid state electrochemistry 15 (7-8) (2011) 1623–1630.

[49] J.-M. Tarascon, M. Armand, Issues and challenges facing rechargeable lithium batteries, in: Materials For Sustainable Energy: A Collection of Peer-Reviewed Research and Review Articles from Nature Publishing Group, World Scientific, 2011, pp. 171–179.

[50] M. Endo, C. Kim, K. Nishimura, T. Fujino, K. Miyashita, Recent development of carbon materials for li ion batteries, Carbon 38 (2) (2000) 183–197.

[51] C. M. Hayner, X. Zhao, H. H. Kung, Materials for rechargeable lithium-ion batteries, Annual review of chemical and biomolecular engineering 3 (2012) 445–471.

[52] R. Ahmed, Modeling and state of charge estimation of electric vehicle batteries, Ph.D. thesis (2014).

[53] J. W. Fergus, Recent developments in cathode materials for lithium ion batteries, Journal of power sources 195 (4) (2010) 939–954.

[54] R. Marom, S. F. Amalraj, N. Leifer, D. Jacob, D. Aurbach, A review of advanced and practical lithium battery materials, Journal of Materials Chemistry 21 (27) (2011) 9938–9954.

[55] B. L. Ellis, K. T. Lee, L. F. Nazar, Positive electrode materials for li-ion and li-batteries, Chemistry of materials 22 (3) (2010) 691–714.

[56] T. Ohzuku, R. J. Brodd, An overview of positive-electrode materials for advanced lithium-ion batteries, Journal of Power Sources 174 (2) (2007) 449–456.

[57] S. S. Zhang, A review on the separators of liquid electrolyte li-ion batteries, Journal of Power Sources 164 (1) (2007) 351–364.

[58] M. Dubarry, V. Svoboda, R. Hwu, B. Y. Liaw, Capacity loss in rechargeable lithium cells during cycle life testing: The importance of determining state-of-charge, Journal of Power Sources 174 (2) (2007) 1121–1125.

[59] J. R. Belt, Battery test manual for plug-in hybrid electric vehicles, Tech. rep., Idaho National Laboratory (INL) (2010).

[60] M. Dubarry, C. Truchot, B. Y. Liaw, Cell degradation in commercial lifepo4 cells with high-power and high-energy designs, Journal of Power Sources 258 (2014) 408–419.

[61] D. Kim, K. Koo, J. J. Jeong, T. Goh, S. W. Kim, Second-order discrete-time sliding mode observer for state of charge determination based on a dynamic resistance li-ion battery model, Energies 6 (10) (2013) 5538–5551.

[62] S. Piller, M. Perrin, A. Jossen, Methods for state-of-charge determination and their applications, Journal of power sources 96 (1) (2001) 113–120.

[63] W. Tahil, How much lithium does a liion ev battery really need?, Meridian international research.

[64] V. V. Viswanathan, D. Choi, D. Wang, W. Xu, S. Towne, R. E. Williford, J.-G. Zhang, J. Liu, Z. Yang, Effect of entropy change of lithium intercalation in cathodes and anodes on li-ion battery thermal management, Journal of Power Sources 195 (11) (2010) 3720–3729.

[65] B. Saha, C. C. Quach, K. F. Goebel, Exploring the model design space for battery health management.

[66] G.-A. Nazri, G. Pistoia, Lithium batteries: science and technology, Springer Science & Business Media, 2008.

[67] E. Schaltz, Electrical vehicle design and modeling, in: Electric Vehicles-Modelling and Simulations, InTech, 2011.

[68] F. R. Kalhammer, B. M. Kopf, D. H. Swan, V. P. Roan, M. P. Walsh, Status and prospects for zero emissions vehicle technology, Report of the ARB Independent Expert Panel 1 (1) (2007) 12–36.

[69] P. Axmann, M. Wohlfahrt-Mehrens, Electrochemical energy storage systems for car applications, in: Pres. HySA Systems Business Seminar, 2009.

[70] A. Deutsche Bank, Electric cars-plugged in: Batteries must be included, Deutsche Bank AG, London, Tech. Rep.

[71] C. M. Costa, M. M. Silva, S. Lanceros-Mendez, Battery separators based on vinylidene fluoride (vdf) polymers and copolymers for lithium ion battery applications, Rsc Advances 3 (29) (2013) 11404–11417.

[72] J. Tarascon, J.-m. tarascon and m. armand, nature (london) 414, 359 (2001)., Nature (London) 414 (2001) 359.

[73] O. Erdinc, B. Vural, M. Uzunoglu, A dynamic lithium-ion battery model considering the effects of temperature and capacity fading, in: Clean Electrical Power, 2009 International Conference on, IEEE, 2009, pp. 383–386.

[74] L. Lam, P. Bauer, E. Kelder, A practical circuit-based model for li-ion battery cells in electric vehicle applications, in: Telecommunications Energy Conference (INTELEC), 2011 IEEE 33rd International, IEEE, 2011, pp. 1–9.

[75] A. Ostadi, M. Kazerani, S.-K. Chen, Optimal sizing of the energy storage system (ess) in a battery-electric vehicle, in: Transportation Electrification Conference and Expo (ITEC), 2013 IEEE, IEEE, 2013, pp. 1–6.

[76] J. Newman, W. Tiedemann, Porous-electrode theory with battery applications, AIChE Journal 21 (1) (1975) 25–41.

[77] T. F. Fuller, M. Doyle, J. Newman, Simulation and optimization of the dual lithium ion insertion cell, Journal of the Electrochemical Society 141 (1) (1994) 1–10.

[78] P. M. Gomadam, J. W. Weidner, R. A. Dougal, R. E. White, Mathematical modeling of lithium-ion and nickel battery systems, Journal of power sources 110 (2) (2002) 267–284.

[79] H. He, R. Xiong, J. Fan, Evaluation of lithium-ion battery equivalent circuit models for state of charge estimation by an experimental approach, Energies 4 (4) (2011) 582–598.

[80] A. Hentunen, T. Lehmuspelto, J. Suomela, Time-domain parameter extraction method for thévenin-equivalent circuit battery models, ieee transactions on energy conversion 29 (3) (2014) 558–566.

[81] A. Fotouhi, D. J. Auger, K. Propp, S. Longo, M. Wild, A review on electric vehicle battery modelling: From lithium-ion toward lithium–sulphur, Renewable and Sustainable Energy Reviews 56 (2016) 1008–1021.

[82] I. Buchmann, How to store batteries, Battery University.

[83] X. Lin, J. Park, L. Liu, Y. Lee, A. Sastry, W. Lu, A comprehensive capacity fade model and analysis for li-ion batteries, Journal of The Electrochemical Society 160 (10) (2013) A1701–A1710.

[84] A. F. Bower, P. R. Guduru, V. A. Sethuraman, A finite strain model of stress, diffusion, plastic flow, and electrochemical reactions in a lithium-ion half-cell, Journal of the Mechanics and Physics of Solids 59 (4) (2011) 804–828.

[85] S. B. Peterson, J. Apt, J. Whitacre, Lithium-ion battery cell degradation resulting from realistic vehicle and vehicle-to-grid utilization, Journal of Power Sources 195 (8) (2010) 2385–2392.

[86] A. Barré, B. Deguilhem, S. Grolleau, M. Gérard, F. Suard, D. Riu, A review on lithium-ion battery ageing mechanisms and estimations for automotive applications, Journal of Power Sources 241 (2013) 680–689.

[87] A. Pesaran, M. Keyser, G.-H. Kim, S. Santhanagopalan, K. Smith, Tools for designing thermal management of batteries in electric drive vehicles (presentation), Tech. rep., National Renewable Energy Lab.(NREL), Golden, CO (United States) (2013).

[88] T. Waldmann, M. Wilka, M. Kasper, M. Fleischhammer, M. Wohlfahrt-Mehrens, Temperature dependent ageing mechanisms in lithium-ion batteries–a post-mortem study, Journal of Power Sources 262 (2014) 129–135.

[89] P. Arora, R. E. White, M. Doyle, Capacity fade mechanisms and side reactions in lithium-ion batteries, Journal of the Electrochemical Society 145 (10) (1998) 3647–3667.

[90] H. Maleki, J. N. Howard, Effects of overdischarge on performance and thermal stability of a li-ion cell, Journal of power sources 160 (2) (2006) 1395–1402.

[91] C. C. Chan, A. Bouscayrol, K. Chen, Electric, hybrid, and fuel-cell vehicles: Architectures and modeling, IEEE transactions on vehicular technology 59 (2) (2010) 589–598.

[92] S. Buller, M. Thele, R. De Doncker, E. Karden, Impedance-based simulation models of supercapacitors and li-ion batteries for power electronic applications, IEEE Trans. Ind. Appl 41 (3) (2005) 742–747.

[93] D. W. Dees, V. S. Battaglia, A. Bélanger, Electrochemical modeling of lithium polymer batteries, Journal of power sources 110 (2) (2002) 310–320.

[94] H. Dai, X. Wei, Z. Sun, J. Wang, W. Gu, Online cell soc estimation of li-ion battery packs using a dual time-scale kalman filtering for ev applications, Applied Energy 95 (2012) 227–237.

[95] T. Mesbahi, F. Khenfri, N. Rizoug, K. Chaaban, P. Bartholomeüs, P. Le Moigne, Dynamical modeling of li-ion batteries for electric vehicle applications based on hybrid particle swarm–nelder–mead (pso–nm) optimization algorithm, Electric Power Systems Research 131 (2016) 195–204.

[96] N. Devillers, M.-C. Péra, S. Jemei, F. Gustin, D. Bienaimé, Complementary characterization methods for lithium-ion polymer secondary battery modeling, International Journal of Electrical Power & Energy Systems 67 (2015) 168–178.

[97] V. Franco, M. Kousoulidou, M. Muntean, L. Ntziachristos, S. Hausberger, P. Dilara, Road vehicle emission factors development: A review, Atmospheric Environment 70 (2013) 84–97.